INTEGRATED TWO-DIMENSIONAL/THREE-DIMENSIONAL COLLAGEN SCAFFOLDS WITH EMBEDDED CHANNELS

Neda Fakhri

A THESIS SUBMITTED TO THE FACULTY OF GRADUATE STUDIES

IN PARTIAL FULFILLMENT OF THE REQUIREMENTS FOR THE DEGREE OF

MASTER OF APPLIED SCIENCE

GRADUATE PROGRAM IN MECHANICAL ENGINEERING

YORK UNIVERSITY

TORONTO, ONTARIO

July 2022

Graphical Abstract*

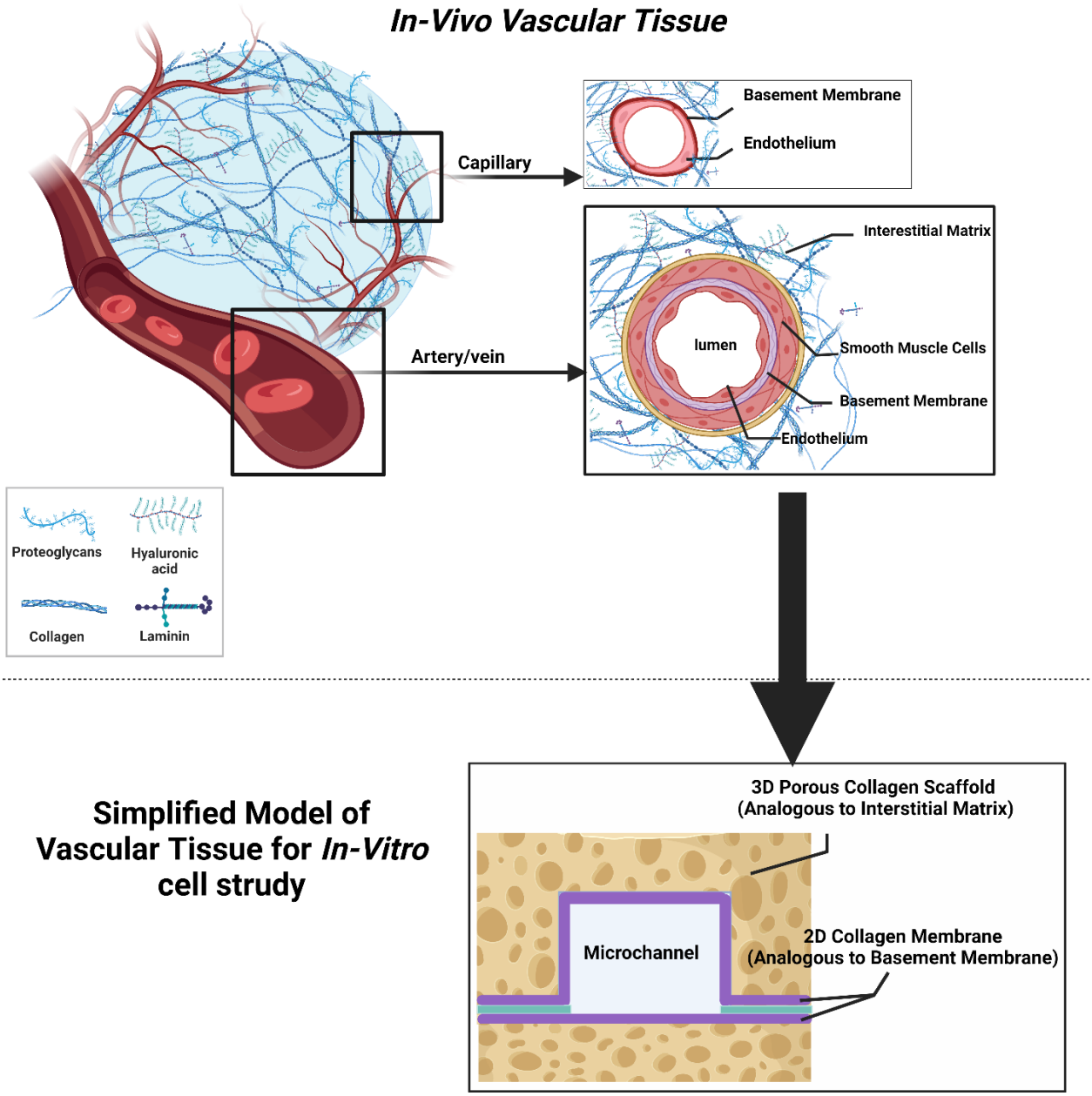

* Created with BioRender.com

Abstract

We developed a two-step method for simple integration of basement membrane (BM) in a 3D porous scaffold (i.e., interstitial matrix (IM)) embedded with channels wherein the 2D BM analog was fabricated by casting collagen on a positive master mold and slowly air-dried at room temperature to replicate the microchannel feature on the mold. Then, collagen slurry was poured over the 2D collagen film while it is still supported by the mold and the whole assembly is freeze-dried. The contact printing method was used to enclose channels with another non-patterned integrated collagen scaffold. The channels with and without the 2D BM were tested for leakage. The results showed no leakage when 2D collagen films were included in the scaffolds, even at flow rates as high as 25 ml/min. The present ECM model can be used in modeling tissues containing large vessels where the membrane restricts the permeation of fluid.

Acknowledgments

I would like to express my sincere gratitude and appreciation to Professor Rezai and Professor Sachlos for their support and guidance throughout my research. I would also like to express my heartfelt thanks to Dr. Khalili for all her helps and kindness throughout this research.

Table of Contents

List of Figures

List of Tables

1. Introduction

1.1. Introduction and Research Motivation

Tissue engineering is an emerging field for repairing and regeneration of injured organs and tissues of the body using a combination of multidisciplinary fields[1]. Recent technological advancements have made tissue engineering a promising field for organ regeneration and transplantation. The healing process in mammals is mainly based on repairing the damaged tissues rather than pure regeneration. The repairing process is usually followed by scar formation, with an exception for minor injuries such as paper cuts. Some tissues such as bone can be self-regenerated and healed; however, there are situations where the body response is insufficient compared to the level of injury[2]. In such circumstances, autografts† and allografts‡ are the primary sources for repairing large tissue defects[3]. However, these methods have several disadvantages, such as limited supply, infection transmission, and risk of rejection[4-6]. As a result, more attention has been drawn to the use of engineered scaffolds in tissue regeneration.

In tissue engineering, a variety of materials including natural-based (e.g., collagen[7], gelatin[8], alginate[8, 9], chitosan[10], chondroitin sulfate[11], hyaluronan[12], and heparin sulfate[13]) and synthetic-based (e.g., polycaprolactone[14], polyglycolic acid[15], poly lactic acid[16], and poly vinyl alcohol[9]) have been used to fabricate engineered tissues. Although synthetic materials cover a wide range of properties and they are adaptable to different fabrication processes, they usually lack biological

† Tissue or organ transferred into a new position in the body of the same person
‡ A graft transplanted between genetically nonidentical individuals of the same species

relevance to corresponding native tissues. Natural materials, however, provide a suitable structure for cell culture. For example, collagen, the most abundant protein in the extracellular matrix (ECM),[§] has been an appropriate candidate for tissue engineering by providing binding sites for cells, but engineering their properties and embedding channels, for vascularization, in them are relatively difficult.

Despite the recent advances in tissue engineering using scaffold-based methods, the FDA-approved clinical trials are still limited. Nevertheless, engineered skin and cartilage tissue have been extensively used in clinical trials. This is because in these tissues, the nutrient can reach the cells from far-distance blood vessels (> 200μm)[17, 18]. However, in other tissues, oxygen and nutrition should be supplied from a neighboring blood source that is no farther than 200 μm from a cell. Otherwise, hypoxia[**] state will occur, giving rise to the death of the cells in the deeper layers. Accordingly, engineering collagen tissues that are vascularized has become of utmost importance.

One of the research motivations of this thesis was to fabricate an engineered tissue containing pre-vascular networks (see **Figure 1-1a**). By doing so, the cells in the deeper layers of the collagen scaffolds can be supplied with oxygen, and nutritious materials before the natural invasion of host vasculature occurs. The early efforts to fabricate synthetic vascular elements date back to the 1980s when Weinberg and Bell used subtractive molding to fabricate the first collagen-based blood vessel *in-vitro*[19]. Since then, more sophisticated microfabrication techniques have been developed, facilitating the fabrication of engineered tissues with more

[§] Three dimensional (3D) porous structure that surround and support cells, also known as connective tissue
[**] Lack of oxygen

complex vascular networks. While some tissue-engineered scaffolds have been presented in the literature (reviewed in chapter 2), there are still some shortcomings to be addressed. For instance, the proposed scaffolds to date do not possess all the tissue elements such as BM[20-26] IM[4, 20, 27-31] of the corresponding *in-vivo* tissues to make them biomimetic, or the materials that have been used and the ultimate structure of the corresponding tissues have not been biologically relevant[32-38].

In this thesis, we aimed to use microfabrication techniques to fabricate a pre-vascularized, collagen-based scaffold comprising both BM and IM (see **Figure 1-1b**). These scaffolds can further be used for studying the underlying cellular mechanisms or investigating the effect of drugs on specific cells. After sufficient study is implemented in fabricating these scaffolds and further development is made in their testing and characterization, they can be used for studying tissues' biology, performing chemical and drug screening on multi-cell tissues, and even implanting them into the human body for tissue repair in the long term (**Figure 1-1c**).

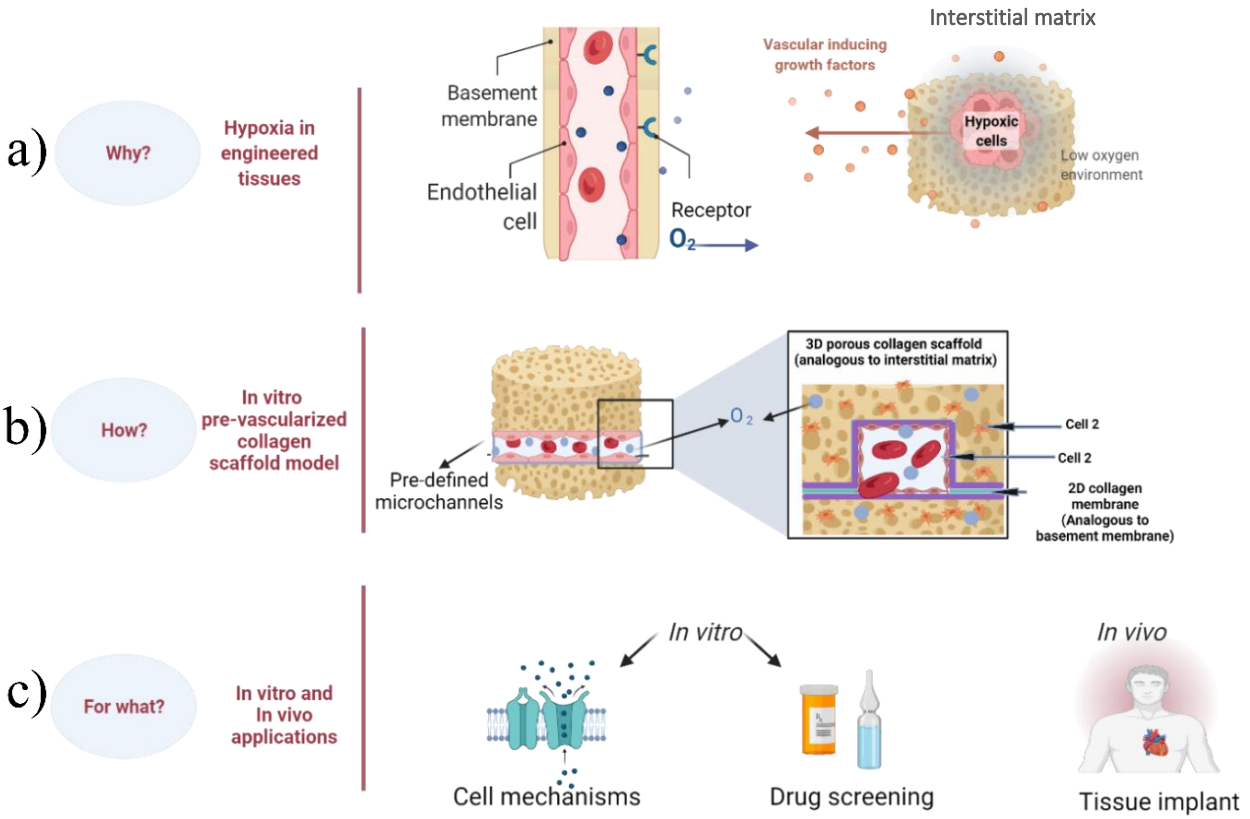

Figure 1-1. Graphical abstract of the motivation behind the proposed research. a) Hypoxia state in engineered tissue where the embedded cells in the engineered tissue will not receive sufficient oxygen. b) To resolve the problems associated with the hypoxia state, pre-defined microchannels should be provided within the engineered scaffolds providing nutrition and oxygen to the cells. c) The resulting engineered tissues can be used for studying the underlying mechanisms of cell behaviors or investigating the effects of different drugs on the cells, or eventually, they can be used for tissue implantation.

1.2. Research Goals and Objectives

The developed collagen-based scaffolds in the literature do not contain all the elements of the corresponding *in-vivo* tissues. A number of vascularized collagen-based tissue-engineered scaffolds have been reported, but they contain either an IM[4, 20, 27-31], or a BM[20-26]. My thesis objective is to develop a more physiologically relevant pre-vascularized collagen-based tissue scaffold. The scaffold comprises an embedded channel representing a vessel, in which the interior surface of the channel is separated from the 3D porous IM by a 2D collagen BM. The proposed scaffold with a 3D porous collagen layer can serve as an ECM in which various types of cells such as endothelial cells[39], mesenchymal stem cells[40], and Keratinocytes[41] can be cultured to model different tissues in the body. The integration of 2D BM and 3D collagen IM in a scaffold not only results in biological relevance but also preserves the integrity of the channels while inhibiting convective leakage of the flowing medium from the microchannel into the ECM. This is important because fluid exchange between the blood vessels and the surrounding tissues is mostly non-convective and based on a selective mechanism controlled by endothelial cells in response to surrounding stimuli. With embedded micro-scaled channels as blood vessels in the engineered tissue structures, the proposed scaffold can have many applications in cell and tissue studies and toxicity assessment in drug discovery.

To achieve the abovementioned goals, the following objectives were investigated:

1. Mimicking the BM function by fabricating a micropatterned 2D collagen membrane (**Figure 1-2a**).

2. Mimicking the IM by integrating a 3D porous collagen matrix onto the 2D collagen membrane (**Figure 1-2b**).

3. Development of a 3D porous collagen matrix with an embedded closed channel lined with a 2D BM (**Figure 1-2c**).

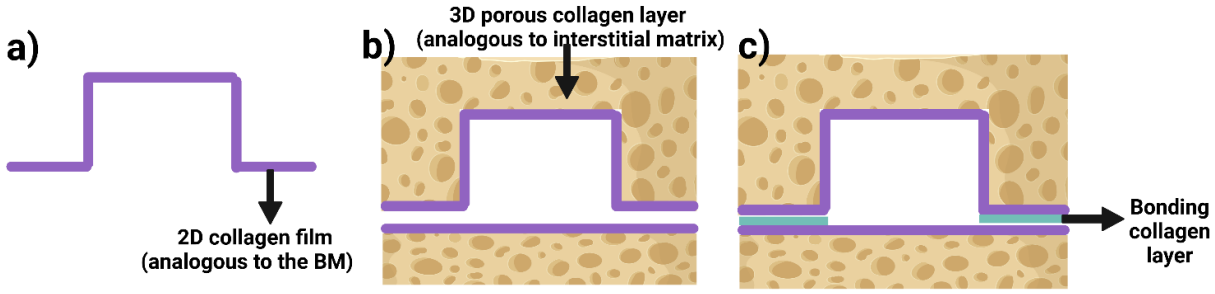

Figure 1-2. Schematic of objectives studied in this thesis; a) Fabrication of a patterned 2D collagen film serving as BM, b) fabrication of a 3D collagen scaffold on the 2D membrane to mimic the IM, and c) development of an embedded channel inside the 2D-3D collagen scaffold

1.3. Thesis Organization

The first chapter of this thesis presents an introduction to the research and the motivation for this study, followed by the defined research objectives

The second chapter of the thesis provides a thorough introduction to the tissue structure and information about important components of *in-vivo* tissues. Then, a detailed literature review is provided for different engineered tissues, and a comparison is provided for all the tissue models studied in the literature. The limitations and research opportunities are also discussed for different tissue models.

In chapter 3, the methodologies used for the fabrication of the collagen scaffolds and the corresponding methods for analyzing the fabricated collagens are described. Microscopy (e.g., optical and scanning electron microscopy (SEM)) and image analysis techniques used to analyze the resulting sizes of the collagen channels are also explained. Image analysis techniques were used to determine the collagen scaffolds and their pore size distribution. Furthermore, the mechanical strength, permeability, and leakage tests are presented for the resulting collagen scaffolds containing microchannels.

In chapter 4, the results and the corresponding discussions are presented. The first section provides the characterization result of the 2D collagen scaffold, including thickness and mechanical properties (thesis objective 1). The second section provides the characteristics of the 3D collagen scaffold (i.e., pore size, mechanical properties, permeability) and the properties of the corresponding collagen-based microchannels (i.e., width, height, and perimeter) (thesis objective 2). The third section presents the characteristics of the integrated 3D/2D scaffold. SEM images are

provided to confirm the bonding between different layers of the integrated collagen scaffolds. Finally, the mechanical strength and leakage test results are provided to assess the performance of the sealed channels (thesis objective 3).

The fifth chapter summarizes the findings of the presented thesis, followed by the recommendations for future research.

2. Literature Review

2.1. Tissue Structure

This section provides a brief introduction to the physiology of *in-vivo* tissues. Almost all tissues have the following contents: ECM and vascular networks. The structure of each of the abovementioned components is elaborated in the following sections.

2.1.1. Extracellular Matrix (ECM)

Almost all tissues and organs have a non-cellular component called ECM which provides physical structure as well as biochemical and biomechanical cues that are required for the cells to function (see **Figure 1-1**). Although all ECMs are composed of proteins, polysaccharides, and water, it has been reported that the composition, mechanical properties, structure, and topology of ECM for each tissue are different. The unique ECM of each tissue evolves by tissue development in a dynamic and reciprocal cross-talk between the cells and their biochemical and biomechanical microenvironment[42].

Mechanical properties of the ECM are important to study to compare the behaviour of the engineered tissues with the behaviour of corresponding *in-vivo* tissues. For example, the J-shaped stress-strain behaviour in the human aorta is an important feature. This behaviour, also known as strain-stiffening, is the key defensive strategy in highly expansive blood vessels against critical damages (e.g., aneurysm and disruption give rise to stroke). When the aorta extends because of blood pressure, it

becomes stiffer. The stored energy of the extended aorta is then released, leading to the movement of the blood whose accumulation extended the blood vessel[43].

The ECM consists of two distinct components, IM and BM[44-47], which are elaborated below.

2.1.1.1. Interstitial Matrix *(IM)*

IMs are 3D porous networks of heterogeneous textures that have both structural and signalling functions[48]. Physical properties of interstitial ECM, such as fibre thickness, orientation, density, stiffness, and pore size impact cellular activities. Furthermore, it serves as a large storage of releasable growth factors, which aids in cell growth and migration[49]. The focal adhesion of cells (e.g., integrins) links the actin cytoskeleton of the cells to the ECM. These focal adhesions can sense the composition, physiological stress, and mechanical stress of the ECM. The cells then respond accordingly through cell growth or death, cell motility, cytoskeleton reorganization, and gene expression. For example, if the cells were exposed to mechanical stress, this mechanical force can be sensed through the focal adhesions, and then the cells go through cytoskeleton reinforcement and reorientation. According to the stimuli, cells would rewire the ECM network by applying forces to the ECM fibres or secreting soluble molecules that weaken or reproduce the ECM fibres. As a result, a reciprocal function exists between cells and their corresponding ECM[50].

The pore size structure and the mechanical properties of the IM are the two important physical properties that affect the cells' behaviour. The optimum pore sizes for the culture of cells vary between 5 to 400 μm according to the tissue type. For example, the optimum pore size for neovascularization was reported $5\mu m$, while for bone regeneration, a pore size of between 100 to

400 μm was considered suitable[51]. The appropriate pore size for liver tissue engineering and vascular smooth muscle cell binding is reported to be 40-150 μm and 60-150 μm, respectively[51]. Further, elasticity of different tissues was reported to be different, which contributes to the behavior of their corresponding cells. For example, muscle elasticity is in the order of 10 KPa, and softer tissues such as brain elasticity is smaller and is between 0.1 to 1 KPa[52].

2.1.1.2. Basement Membrane *(BM)*

BM is a thin dense sheet-like layer of ECM surrounding most animal tissues. BMs have a wide variety of functions for the tissues, such as: i) acting as a substrate for cell adhesion and migration, ii) separating tissues and acting as a barrier to prevent transmigration of most cells (except for leucocytes and stem cells)[53], iii) shaping the tissues by their composition,[54] and iv) acting as a reservoir for growth factors[55].

While shaping the tissue and providing the substrate for cells to adhere to, the BM also provide mechanical strength for the tissues. The elastic (Young's) modulus of the adult BM in various tissues is estimated to be in the 1–4 MPa range, 1000 times larger than that of the overlaying epithelium layer (1–4 kPa) based on the measurements[56]. The sheet-like structure of BM is due to its polymeric networks of laminin and type IV collagen, which are linked together through other ECM proteins, including nidogen and perlecan[54]. The thickness of the BM varies amongst different vasculatures, ranging from 100nm to 500nm[56, 57].

2.1.1.2.1. Vascular Permeability Mechanisms

The BM serves as an interface between blood flow and surrounding tissue in a vascular network (**Figure 2-1a**). The fluid, solutes, and cells flowing in the vascular system are blocked by the walls of blood arteries. This blocking barrier comprises of Endothelial cells and BM. The vascular barrier allows for the controlled transfer of solutes and cells into the extravascular region, known as extravasation. Under healthy circumstances, molecules with a molecular weight of less than 40 kDa can flow through mature arteries, but bigger proteins such as albumin (66 kDa) and transferrin (80 kDa) are blocked. However, under pathological states such as inflammation and allergies, even molecules as large as 2,000 kDa may extravasate[58, 59].

The bulk of extravasation mechanisms, however, are paracellular and involve the opening of cell-cell junctions (**Figure 2-1b**). Adherens junctions and tight junctions are two primary protein complexes that create cell-cell junctions. These cell-cell junctions have poor fluid and solute permeability under normal circumstances. Cell-cell junctions can move away, open, or be internalized under particular conditions to provide space between endothelial cells, allowing fluid or cells to flow into the extravascular space. The number and arrangement of these junctions determine how permeability in the vasculature varies to meet the demands of different organs and tissues[59]. Some of these extravasation processes are transcellular, meaning that solutes or cells are taken up by an endothelial cell and transferred from the luminal to the other side within a vesicle-like structure (see **Figure 2-1c**). The transcellular extravasation can also happen by the endothelial fenestrae, holes in the endothelial structure, through which the solutes/cells can be transferred from the luminal side to the other side (**Figure 2-1d**).

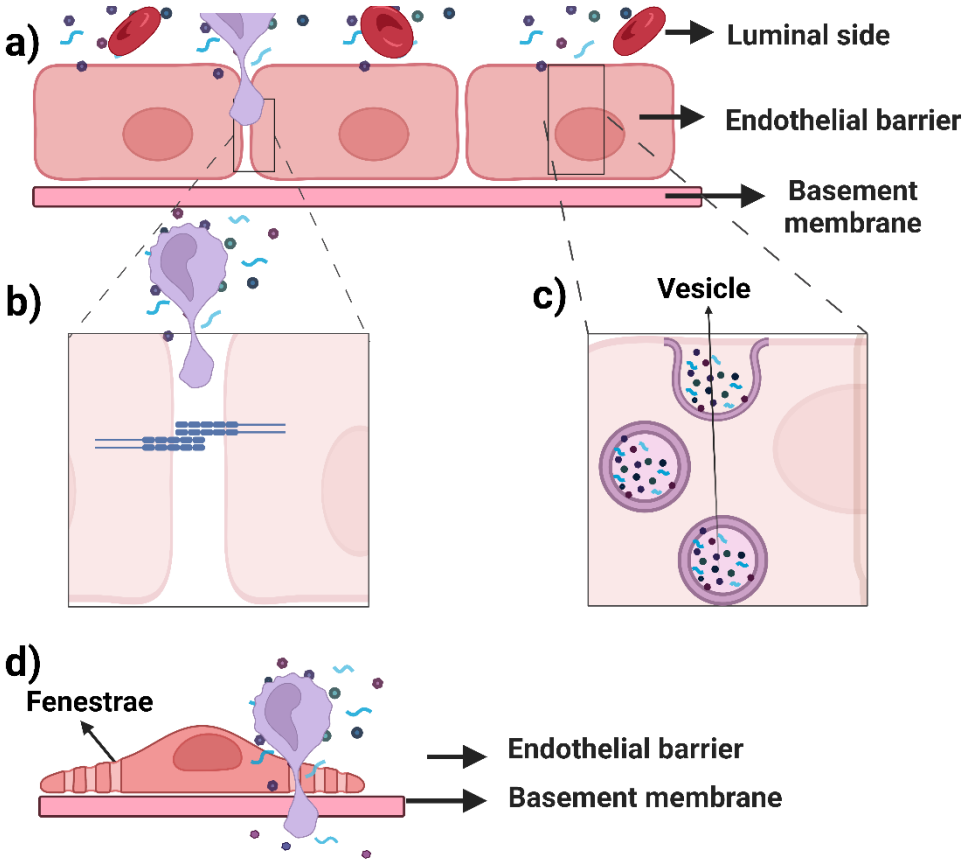

Figure 2-1. Vascular permeability mechanisms: a) Vascular barrier containing endothelial barrier and the BM, b) Paracellular extravasation where the cells/solutes pass the vascular barrier by opening the cell-cell junction, c) transcellular extravasation where the solutes are taken up by vesicle and are transferred through the BM, and d) transcellular extravasation through the fenestrae of endothelial cells (adapted from Wettschureck et al.[60] and created with BioRender.com)

Cells must first pass the endothelium barrier before passing through the BM to transmigrate from the luminal to the abluminal side (i.e., the tissue area outside the lumen). After getting through the endothelial barrier, cells/solutes need to pass the BM to reach the abluminal side. In continuous BMs, the membrane needs to be disintegrated for the solute or cells to pass to the other side. Generally, continuous BMs have pores with diameters ranging from 10 to 130 nm (only very small

molecules pass through)[54, 56, 61]. In these BMs, the local endothelial cells will produce matrix metalloproteinases (MMP), which help disintegrate the BM (**Figure 2-2a**). Additionally, it was believed that endothelial contraction exerts a mechanical force on the underlying BM, promoting disintegration of the BM collagen network and thus increasing the size of the local hole[60].

As seen in **Figure 2-2b**, in lumens with discontinuous BM, the transmigration occurs through the BM breaches (pores). It has been observed that the discontinuous BMs (e.g., the sinusoidal capillaries in the liver) contain pore sizes ranging between 100 nm to 1 μm[62]. It is worth noting that holes in the BM can be formed passively by the space between the fibre networks or actively by cellular degradation processes (MMP)[56].

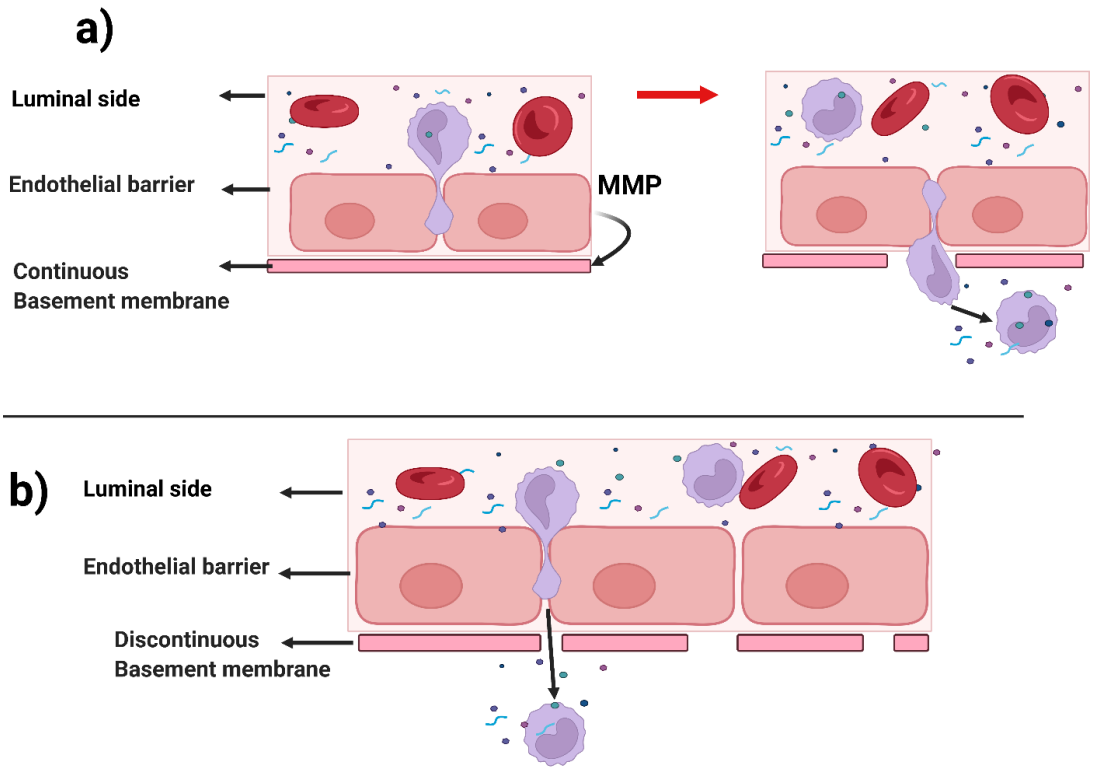

Figure 2-2. Transmigration of cells and solutes through a) continuous BM by dissolving the BM by MMPs, and b) discontinuous capillaries by passing through the holes of BM (adapted from Wettschureck et al.[60] and created with BioRender.com.)

Additionally, changes in BM thickness across vasculature impact the vascular barrier's permeability. The BM thickness varies amongst different vessels, with the aorta having the thickest BM (500 nm), followed by the carotid artery and inferior vena cava having 300 nm thick BMs, and the saphenous vein having the thinnest BM (100 nm)[56, 57].

The endothelial barrier of various organs and vascular beds exhibits considerable structural and functional variation. For example, the endothelial cells of brain capillaries are firmly attached via tight junction complexes and are surrounded by a basal membrane, pericytes, and the end-feet of astrocyte processes, all of which contribute to the formation of the blood-brain barrier. By contrast, the endothelial cell layer of microvessels in the liver or bone marrow is discontinuous, allowing cells and solutes to flow more freely. Other endothelia, such as those found in exocrine and endocrine glands, renal glomeruli, and the intestinal mucosa, contain fenestrae that promote transport. However, under normal conditions, the permeability of the majority of microvessels is restricted due to a continuous endothelium barrier surrounded by a basal membrane and some pericytes[60]. Therefore, as mentioned above, vascular permeability strongly depends on the endothelial barrier activity and the production of the MMPs.

2.1.1.2.2. BM Dysfunctionality

The irregular remodeling of the vascular wall is linked to several vascular disorders, including atherosclerosis and hypertension[60]. The most common BM abnormality observed in vascular disorders is BM thickness. According to Siperstein and colleagues 1968[63], a 2-fold increase in capillary BM thickness was initially seen in diabetics, and further studies have validated this finding throughout the years[64-66]. In atherosclerosis, the same phenomena appear to be the cause, as indicated by the increased BM thickness of intramyocardial capillaries in individuals who have

suffered an acute myocardial infarction[67,68]. Similarly, endothelial BM thickening has been observed in Alzheimer's disease resulting in the accumulation of β-amyloid peptides inside the cerebral blood vessels in the brain, which in turn disrupts cognition (See **Figure 2-3**)[54,69-71]. Although the processes behind vascular BM thickening are unknown, they may entail an imbalance in the synthesis and/or degradation of BM components or a shift in their relative abundance[56].

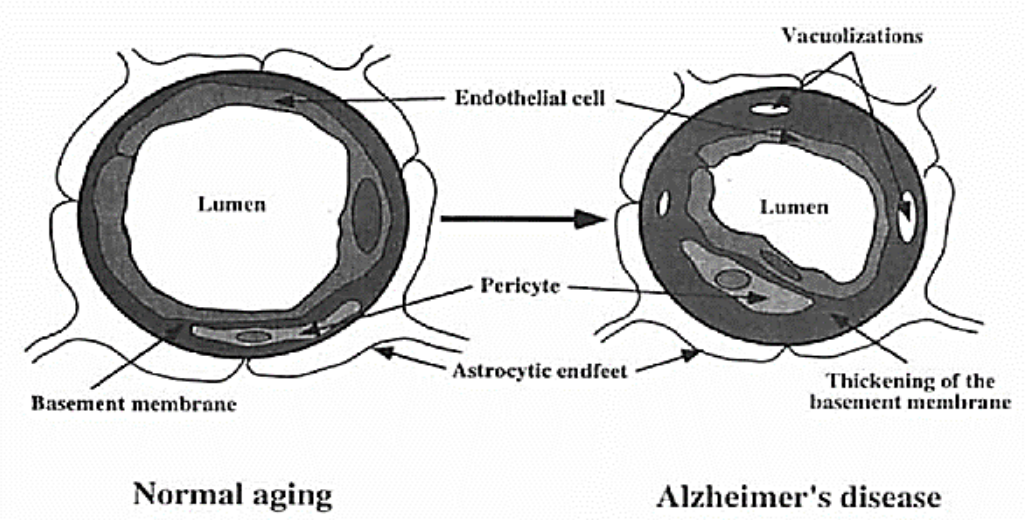

Figure 2-3. The BM in healthy and Alzheimer's brain[70]. Figure was reproduced with permission from Wiley.

The physical and chemical properties of BM play an important role in cells' function[72]. Changing the structure and composition of BM (e.g., the mutation in laminin or collagen deficiency) results in serious defects in tissue formation and cell adhesion, viability, and migration[73]. In Alport's syndrome, the abnormal distribution of laminin changes the BM's morphology and permeability,

resulting in plasma protein leakage into the urine[74, 75]. In diabetic patients, the BMs of the kidney are irregularly thickened, causing reduced filtration and kidney failure[71, 76, 77]. Gene mutations in the BM is another dysfunction that occurs in different tissues such as kidney, eye, and skin resulting in autoimmune responses such as blistering[78].

Changes in vascular permeability are another issue that is associated with BM dysfunction. For example, acute myeloid leukemia cells alter their microenvironment and cause a severe functional abnormality. In addition, acute myeloid leukemia cause increased permeability of vascular wall barriers, resulting in increased reactive oxygen species and nitric oxide[79]. The consequences of vascular barrier dysfunction in disease are also dependent on the afflicted organ. In the brain, disruption of the blood-brain-barrier can result in cerebral edema, increased intracranial pressure, impaired cognitive or motor function, and even death. In the lung, leakage can impair gas exchange and lead to hypoxia, hypercapnia, and fatal outcome[59].

2.1.2. Vascular Networks *In-vivo*

Most tissues rely on vascular networks for nutrient delivery and waste removal. The artery, arteriole, capillary, venule, and vein are all part of the vascular network, which is a single-linked vascular system. The blood circulation starts from the heart, where blood is pumped out into the aorta with a mean velocity of 23 cm/s [78]. Next, blood goes into arteries from which the vasculatures are subdivided into smaller microvessels (i.e., arterioles) and finally into capillaries. Capillaries have a wall thickness of 1 μm, and they only consist of a single layer of endothelial cells supported by BM, where the distance of the tissue cells from adjacent capillaries is less than 200μm[80, 81]. The total

cross-sectional area for the vascular network (the sum of all the cross-sections of a specific vessel type) varies between 4 cm^2 in aorta to more than 1000 cm^2 in capillaries.[82, 83] Ranges for diameters of various blood vessels are shown in **Figure 2-4**.

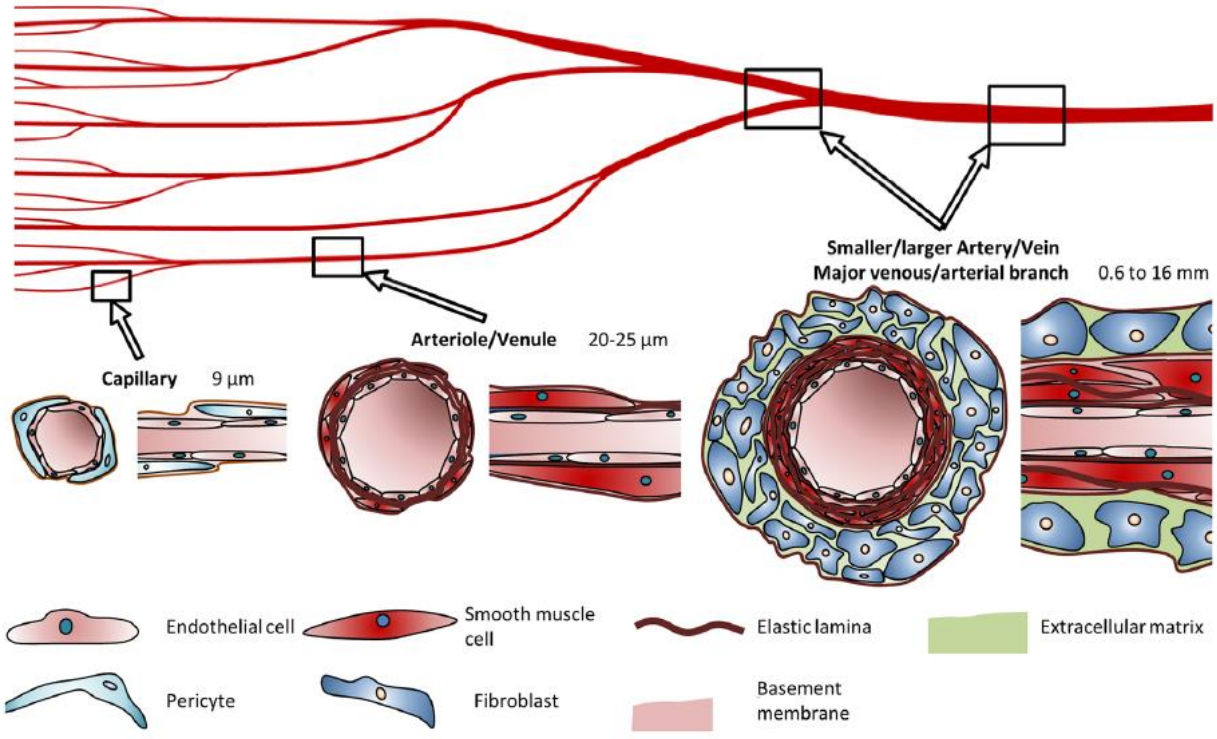

Figure 2-4. Properties of different blood vessels in the body, including large blood vessels such as the aorta and smaller blood vessels such as capillaries and venules[84]

In-vivo, blood vessels can be generated via vasculogenesis, angiogenesis, and arteriogenesis[85]. Vasculogenesis is the process by which endothelial cells differentiate from their progenitor cells and proliferate inside previously avascular[††] tissue to establish a primitive capillary network during early embryonic development[86, 87].

Angiogenesis occurs after vasculogenesis when the original vascular network is transformed into more complicated networks. During this process, endothelial cells are activated upon receiving the secreted vascular growth factors (e.g., VEGF[‡‡], FGF[§§], and TGF[***]- **Figure 2-5a**) and begin to destroy their surrounding matrix via the release of matrix metalloproteinases (MMPs, **Figure 2-5b**) [86]. Endothelial cells then move into the gaps, producing capillary buds and sprouts (**Figure 2-5c**). Endothelial cells proliferate following the migrating endothelium, lengthening the newly formed blood artery. Also, the endothelial progenitor cells differentiate and migrate into the newly formed capillaries to further assist in lumen formation (**Figure 2-5d**). Finally, arteriogenesis is the process through which pre-existing tiny arterioles are structurally enlarged and remodeled into bigger arteries (**Figure 2-5e**) [87].

[††] Without blood vessel
[‡‡] Vascular endothelial growth factor
[§§] Fibroblast growth factor
[***] Transforming growth factor

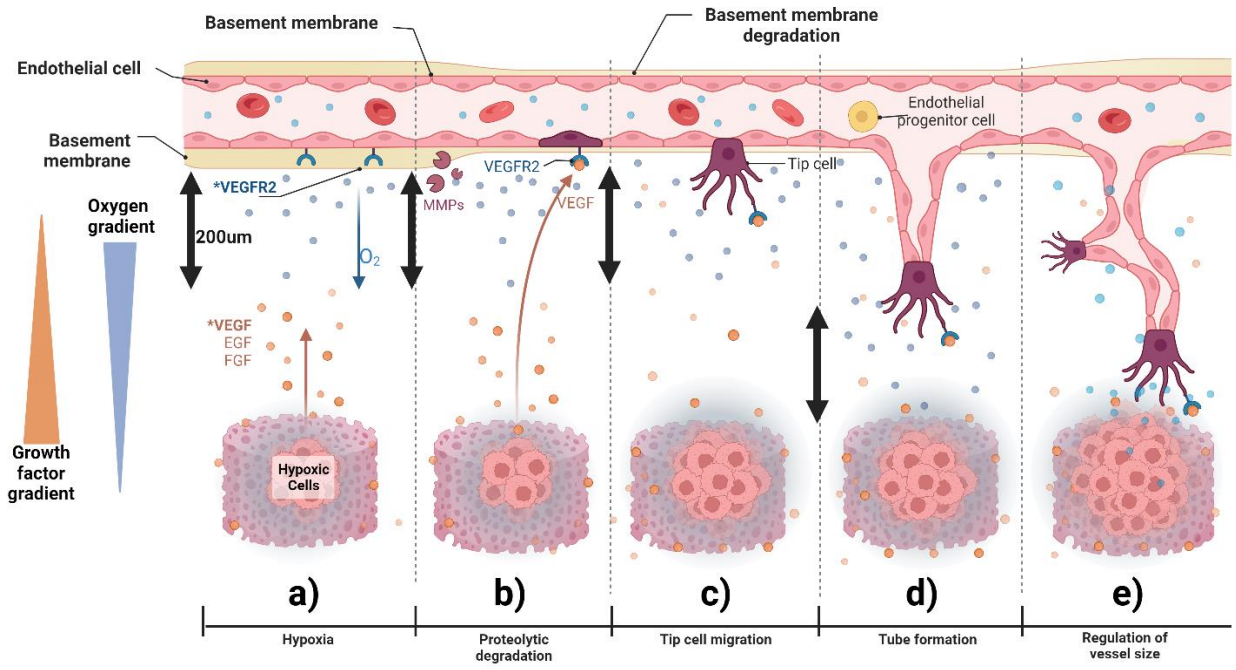

Figure 2-5. *In-vivo* vascularization schematic: a) vascular growth factors are secreted by hypoxic cells, b) the endothelial cells are activated upon receiving the secreted vascular growth factors and release of matrix metalloproteinases degrading BM as well as the ECM, c) tip cells are grown towards the hypoxic areas, d) endothelial progenitor cells differentiate into mature endothelial cells to participate into vascular generation combined with cell proliferation of the available endothelial cells, and e) This process is further developed to regulate the vessel sizes based on required oxygen and nutrition (adapted from Bridges et al.[88] and from "Tumor vascularization", by BioRender.com (2020). Retrieved from https://app.biorender.com/biorender-templates.).

Numerous studies have sought to replicate the native tissue environment for cell culture by mimicking the properties of the native tissue environment, i.e., the IM, the BM, and the vasculatures. The following section provides an overview of the engineered scaffold fabrication processes.

2.2. Engineered Tissue Scaffolds

As described in chapter 1, reciprocating communication exists between cells and their ECM microenvironment. Thus, by tailoring the chemical composition of the scaffold (e.g., adding hydroxyapatite)[89, 90], it would be possible to control cell-ECM interaction, which consequently controls cell signaling pathways[91]. Several materials have been used to fabricate engineered tissue scaffolds (**Figure 2-6**). The scaffold composition falls into two major categories: a) natural materials and b) synthetic materials.

The natural materials that have been reported in scaffold fabrication are collagen[7], gelatin[8], alginate[8, 9], chitosan[10], chondroitin sulfate[11], hyaluronan[12], and heparin sulfate[13]. Although natural materials have physiological relevance, their fabrication methods are limited because these materials are not compatible with harsh fabricating methods. For example, collagen contains proteins that cannot tolerate high temperatures. Therefore, the usage of any fabrication method that involve high temperature will not be applicable to collagen.

In the case of synthetic materials, their physical properties can be easily modified, making them more flexible in selecting the fabrication method. The synthetic materials used in the literature are polycaprolactone (PCL)[14], poly glycolic acid (PGA)[15], poly lactic acid (PLA)[16], and poly vinyl alcohol (PVA)[9].

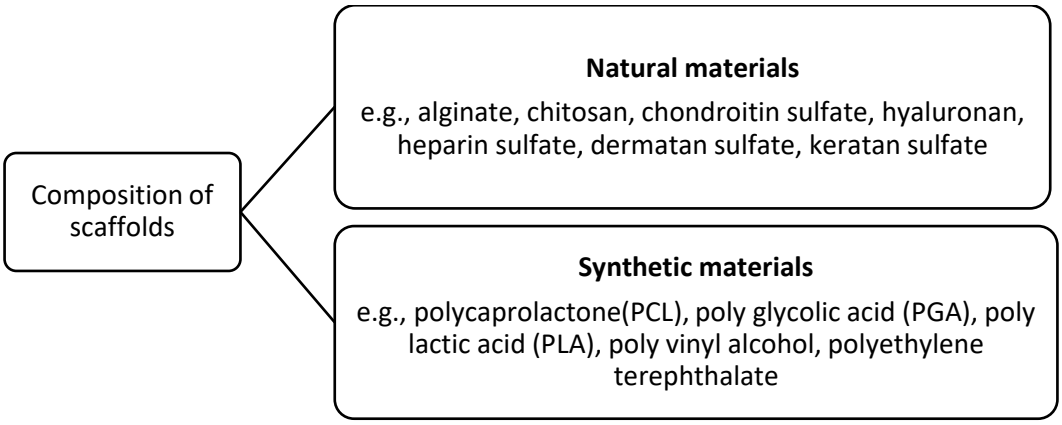

Figure 2-6. A diagram for the materials used in tissue engineering

Collagens are the building blocks of connective tissue. Rope-like proteins are found in high concentrations in load-bearing tissues such as tendon, bone, skin, and cartilage[92]. As Collagen is a natural polymer that is the main component of ECMs, it makes an appropriate candidate for fabricating tissues mimicking *in-vivo* environments for cells[93]. In most tissue engineering studies, collagen is proved to be a promising material because cells can adhere to the specific motifs on collagen, and also it has unique biological properties such as biocompatibility, biodegradation, and hydrophilicity[80, 94].

The mechanical properties of the engineered tissues have a significant effect on cell behavior. Thus, it is of utmost importance to simulate the mechanical behavior of the desired tissues. For example, the stress-strain curves in soft tissues have a j-shaped trend which is due to the structure of the tissue (e.g., pore structure, thickness) and the composition of the tissue (e.g., collagen and elastin). Tissues with j-shaped stress-strain curves show a strain stiffening behavior in which their corresponding stiffness increases at higher strains. For example, blood vessels have small stiffness at lower strains. However, the stiffness increases several orders of magnitudes in higher strains

which is attributed to the collagen contents of blood vessels[43]. This nonlinear behavior is essential because it can protect the tissues or the vessels against aneurysm formation[43].

The following section discusses the techniques used to create collagen tissue scaffolds composed of IM, BM, and vascular networks.

2.2.1. Interstitial Matrix in Engineered Tissues

To understand the cell-ECM interplay, most investigations have focused on 3D hydrogels or 2D collagen films. Although these materials have answered many of our questions regarding cell function, they are not realistic candidates to mimic the *in-vivo* tissue structures. 3D porous scaffolds, however, are better models as they allow the cells to grow in the 3D environment where the interstitial flow can easily pass through the scaffold. Also, the porous scaffold can provide cells with wider cellular activities (i.e., cell migration, cell-cell, and cell-ECM interactions), as opposed to hydrogels which not only hinder cell activity but also exert unnecessary forces on cells which might, in turn, affect their function[95].

To fabricate 3D porous structures for tissue engineering applications, several methods have been introduced, such as foaming[96], leaching[97], electrospinning[98, 99], and freeze-drying[10, 100-102]. Freeze-dying is a rather simple technique to fabricate 3D porous scaffolds where a suspension (i.e., collagen and acetic acid) is frozen to trap the collagen fibers between growing ice crystals. This produces a continuous network of ice crystals surrounded by collagen fibers. Subsequent sublimation of the ice crystals during the drying phase leads to the formation of a highly porous collagen scaffold. As the porous structure of the resulting scaffold mirrors the ice crystal structure formed during freezing, the structure of the pores can be effectively controlled by altering the

freezing process used during freeze-drying. Accordingly, modifications to this process are the key to creating a range of scaffolds with different pore structures[101]. The porosity and pore sizes of the scaffolds fabricated are largely dependent on parameters such as collagen concentration[7, 102], final freezing temperature[101,103], cooling rate[100], annealing step[101], directional freezing[104], and crosslinking method[101].

2.2.2. Basement Membrane in Engineered Tissues

Incorporation of BM in regenerated tissues and engineering its properties make the corresponding tissues more physiologically relevant to the *in-vivo* tissues and eventually the organs[105-107]. Further, fabrication of *in-vitro* tissues containing BM can shed light on the vasculature-related biological processes such as blood-brain barrier function[72], angiogenesis[108], tumour growth, and metastasis.[109] Transwell inserts are the most-common tools used to study the function of BM in co-culture systems. It contains two compartments that are separated by a membrane (see **Figure 2-7**). It can be used for both anchorage-dependant and anchorage-independent cells. Transwell inserts can also be used to study chemical gradients in cell culture (**Figure 2-7c**). By using Transwell inserts, cells may be cultured in a manner that allows them to communicate with one another while physically isolated[110, 111].

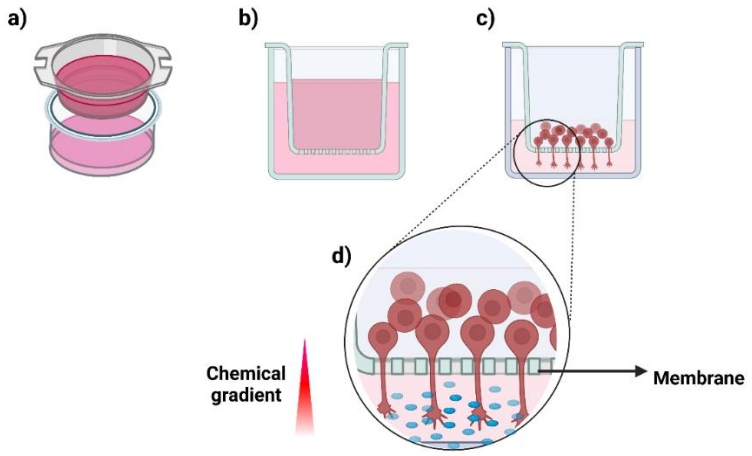

Figure 2-7. Schematic of Transwell inserts; a) overall view, b) side-view, c) culture of neuron cells on the inner compartment, d) the outgrowth of axons towards the chemicals while the soma is isolated in the inner compartment (adapted from Gonzales et al.[112] and created with BioRender.com)

As mentioned in chapter 2, one of the roles of BM is to keep the cells apart and give structure to tissues. BM acts as a membrane that prevents the transmigration of cells. Although not directly claimed in the literature, several studies have been conducted in the co-culturing of different types of cells in which they implement the BM function by separating the cells and culturing them in separate compartments[112-114]. Some microfluidic-based co-culture systems have been designed with a centrally positioned membrane that divides two cell culture compartments[22,115,116]. These microfluidic-based designs enabled flowing media in cell-culture compartments mimicking the blood flow *in-vivo* in which the cells in the upper and lower compartments are indirectly in contact through the membrane (**Figure 2-8a**). The advantage of this method is that by cultivating the two cell types on either side of this membrane, the distances between the two cell types can be reduced, and improved cell-cell interactions can be achieved. Although this method is suitable for co-culturing, it is not an appropriate model for microscopy since it is challenging to image the cells

through the membrane. The imaging becomes even more challenging when the device contains more than two layers. Then the middle compartments cannot be imaged without cutting the device (which hinders the real-time monitoring of the cells during the experiments)[117]. Also, since the cells are vertically positioned in this model, even if the device allows us to observe the cells from the top and the bottom compartment, taking pictures will be difficult because the other cells would cause interference in the form of noise in the background. The separate compartments for each cell types enable the user to feed the cells with their specific media and analyse the secreting factors from each compartment separately. However, being cultured on a membrane, this system lacks the 3D porous structure of ECM, and therefore the result might night accurately resemble the *in-vivo* tissue structure. Further, due to its multilayer design, microfabrication steps are more difficult, and also reliable sealing of this sandwich structure is difficult [117].

The horizontally positioned microchannels, however, have resolved the microscopy issues with vertically positioned microchannels (**Figure 2-8b**). In these horizontal microfluidic devices, microgrooves are exceedingly small (less than 10μm), thereby hindering the transmigration of cells between compartments while they communicate through microgrooves by their secreting molecules. As the cell compartments are horizontally placed, the interface of the two compartments can be monitored constantly during the experiments. Also, the cells in this device are not stacked. Therefore, the co-culturing of several cells in parallel channels would not hinder the real-time imaging of each compartment during the experiments [117]. This method's disadvantage is the relatively large distance between the cells, which affects their crosstalk.

In vertically positioned microfluidics, the cells are in close contact, but in horizontally positioned microfluidic devices, there is a distance between cells where distance results in the formation of

chemical concentration gradients between compartments[117]. The microgrooves in these models are claimed to play the role of BM in the *in-vitro* cell co-culture models[118-120]. Note that cells have weak adhesion to the corresponding compartments on the substrate, mostly made of an elastomer called polydimethylsiloxane (PDMS) [121]. As a result, surface treatment methods are needed to improve the cell adhesion to the microfluidic walls. Also, the fabrication of microgrooves requires sophisticated microfabrication instruments with high precision, which can be quite expensive.

To omit the need of microgrooves, cell compartments can be separated by micropillars (**Figure 2-8c**). Micropillars' height can be as small as 100 μm, and in contrast to microgrooves, they do not require the alignment of microfabricated layers (as the height of cell compartments and the pillars are equal). However, the gaps between these micropillars are large, and the cells can pass through. For this reason, usually, a middle compartment is designed in these devices, which contains either ECM gel[122, 123] or ECM composite scaffold[124], thus prohibiting the transmigration of cells between side compartments. The design shown in **Figure 2-8c** has been used to study the effect of different chemicals on cell behaviour, wherein the cells are confined in the middle compartment containing ECM, and the media with different factors are flown in the side compartments[85].

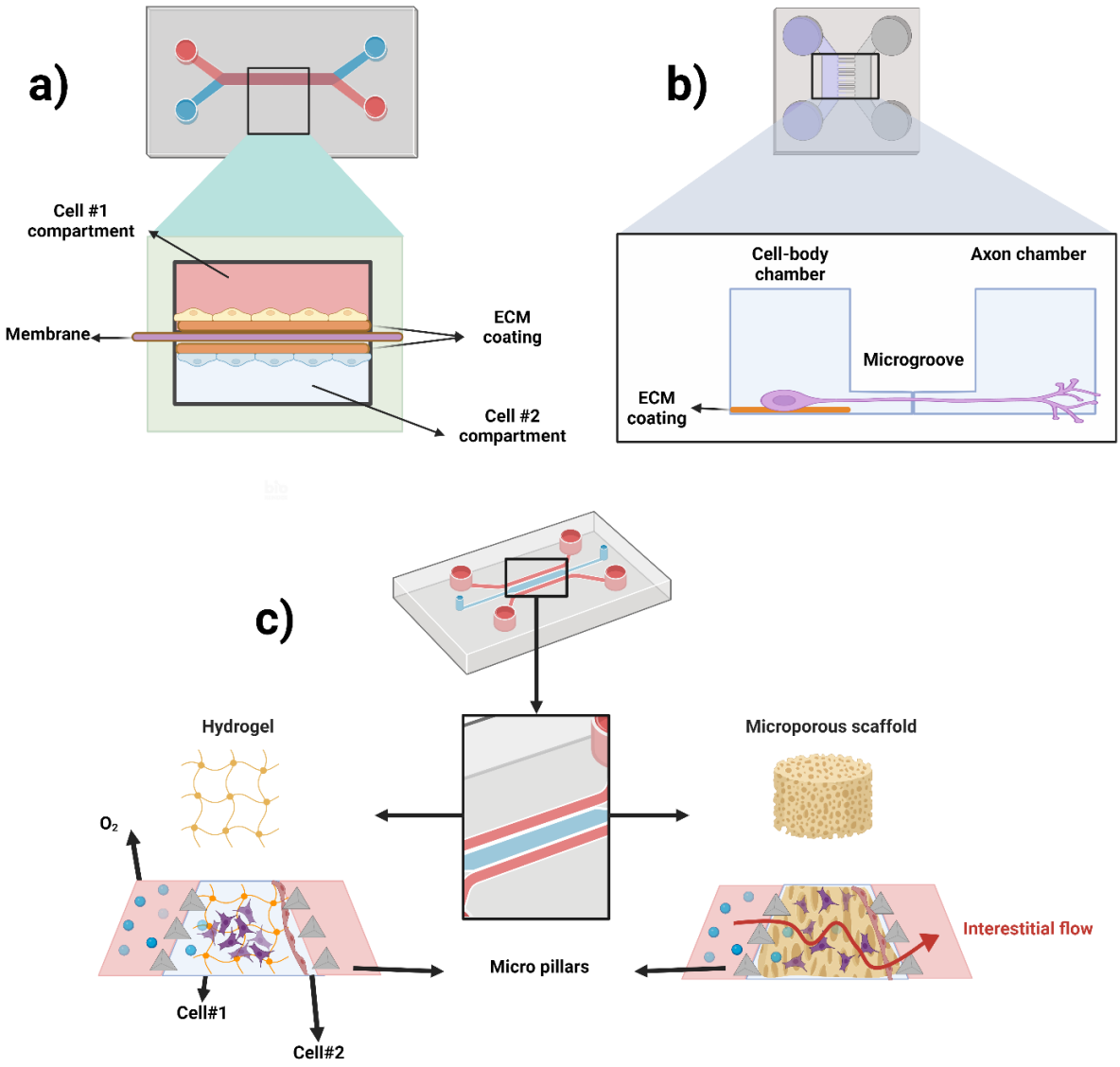

Figure 2-8. Microfluidic cell study models; a) Vertical compartment microfluidics (adapted from Wong et al.[125] and created with BioRender.com), b) Horizontal compartment microfluidics containing microgrooves (adapted from Lee et al.[126] and created with BioRender.com), and c) Horizontal compartment microfluidics containing micropillars (adapted from Ahn et al. [127] and created with BioRender.com)

In an attempt to make more physiologically relevant models involving BM, some two-layered micropatterned scaffolds composed of 2D films attached to 3D scaffolds have also been

developed (**Figure 2-9**) [128-130]. The 2D layer was formed by casting collagen on the mold, then air-dried. Following the 2D collagen film formation, the film was laminated to a 3D collagen scaffold. The lamination was carried out by placing the patterned collagen film on the collagen slurry and then freeze-drying the sample. Since the patterns on the membrane are now soaked in collagen slurry, the membrane will take up water. Thus, in the freeze-drying step, a huge deformation was observed. The final patterns on collagen formed by this method were 120-300μm in width and 60-240μm in depth. As shown in **Figure 2-9a**, these micropatterned structures were fabricated as skin equivalents comprising a basal lamina used to study the effect of membrane topography on keratinocyte cell proliferation and differentiation. Another study presented an integrated 2D/3D silk-based scaffold providing a pre-vascularized network for the engineered tissues (**Figure 2-9b**) [107]. However, since they used a stainless-steel rod to form the conduit-shaped microchannels, only straight channels could be fabricated. The fabricated silk-based channels had circular cross-sections, and their diameter ranged from 150μm-780μm. To fabricate the 2D silk layer as the BM analogue, the molds were dipped inside the silk solution to form a layer by letting the thin layer to dry. The thicknesses of the BMs were reported to be between 2-20μm. Further, they used silk to fabricate the channels, which were reported to have poor cell adhesion properties[105, 106]. In another patent application[131], channels were formed using a sacrificial layer, and then the sacrificial mold was removed by a solvent to form the patterns in the bulk material. Then, a membrane was used to seal and stack the channel compartments used for cell culture. However, the membrane did not line the whole interior surfaces of the corresponding channels, so it cannot be considered a physiologically relevant vasculature (**Figure 2-9c**).

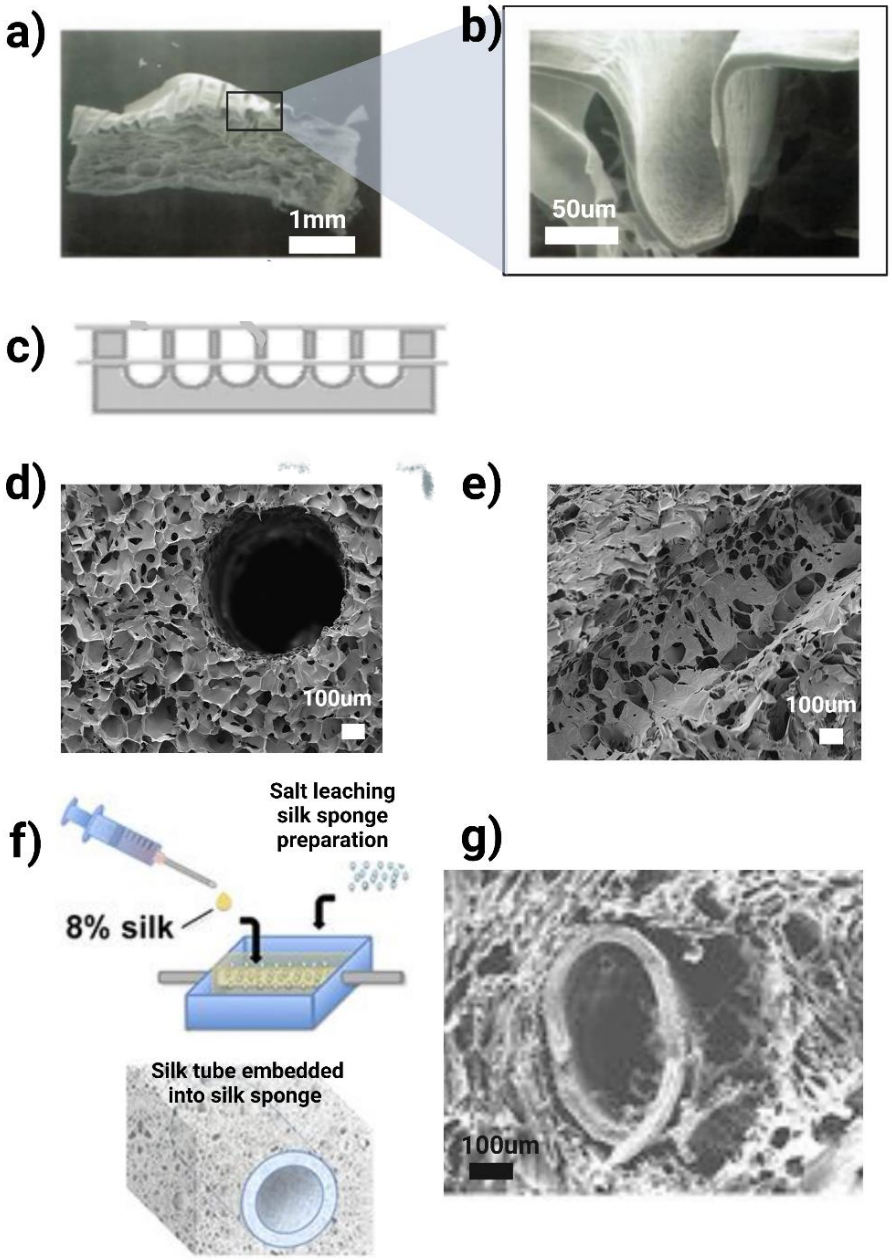

Figure 2-9. 3D scaffold comprising IM and BM; a) and b) Composite dermal equivalent with a microfabricated membrane[128] (Permission was obtained from Wiley) c) Stack of scaffolds with channels compartments that uses membrane for sealing channels[131], 3D silk-based scaffold with an embedded channel d) cross-section view (Permission was obtained from Wiley) e) top view of the fabricated silk-based channel[132] (Permission was obtained from Wiley), f) schematic view for 3D silk-based scaffolds with embedded channels having BM (Permission was obtained from Wiley) and g) the SEM image of the corresponding silk-based scaffold (Permission was obtained from Wiley)[133]

2.2.3. Vascularization of the Engineered Tissues

Originally, the engineered tissues were fabricated without pre-vascularization and then implanted in patients' bodies[134, 135]. By doing so, they relied on the natural invasion of vascular networks within engineered tissues (**Figure 2-10**). However, it is revealed that natural invasion after implantation is less than 1 mm per day[136]. As such, the generated vascular networks could not provide sufficient blood supplies, resulting in the death of cells in regions away from the capillaries ($>200\mu m$) [137].

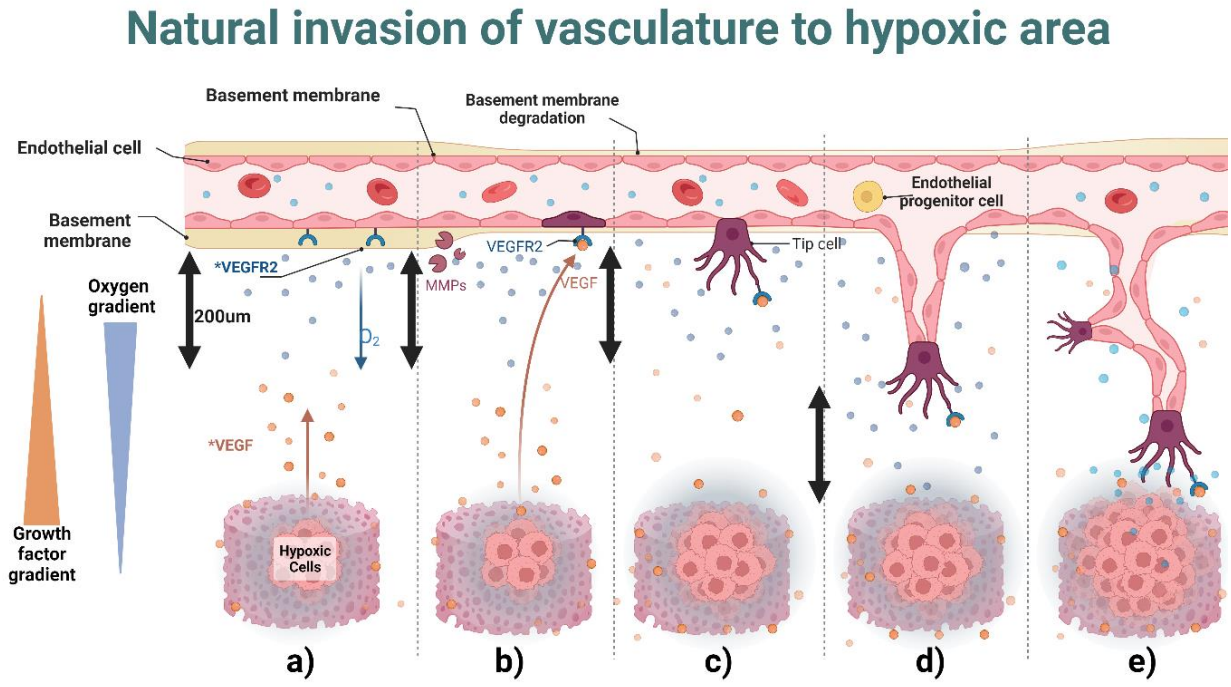

Figure 2-10. Schematic of natural invasion of the vasculature to a hypoxic area (adapted from Bridges et al.[88] and from "Tumor vascularization", by BioRender.com (2020). Retrieved from https://app.biorender.com/biorender-templates).

To resolve the above challenge, pre-vascularization was introduced. **Figure 2-11** shows two general categories for studies involving pre-vascularization of the engineered tissues: i) a bottom-up approach where the pre-vascularization is implemented by culturing the proangiogenic cells on the engineered scaffolds and using proangiogenic factors in the surrounding media, and ii) a top-down approach where the pre-defined channel networks are initially embedded within the engineered tissues, followed by the invasion of the networks based on an *in-vivo* mimicking vascularization[138].

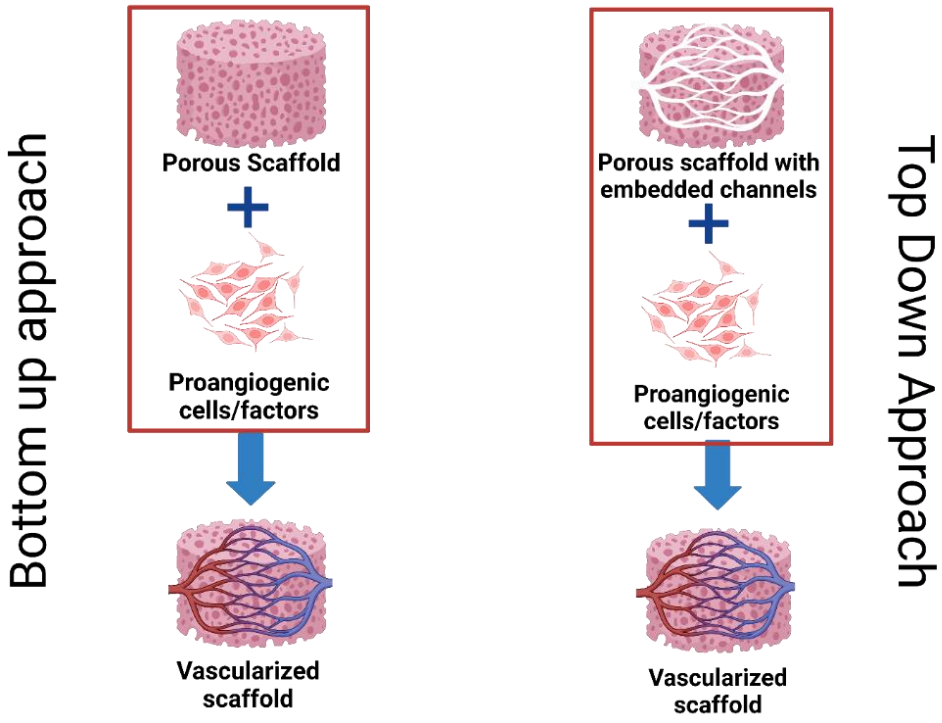

Figure 2-11. Different approaches for vascularization of engineered tissues: Left) the bottom-up approaches where the vascularized networks were formed by the cultured cells inside the scaffold, and Right) the top-down approach where the primitive networks are generated during scaffold fabrication followed by *in-vivo* mimicking vascularization using proangiogenic cells. Figure is created with BioRender.com

Table 2-1 summarizes studies involving the bottom-up and top-down pre-vascularization techniques. In the following section, these approaches are explained in more detail, and a literature review is provided.

Table 2-1. A summary of tissue engineering studies involving pre-vascularization using angiogenic factors and/or proangiogenic cells

Method	Pre-vascularization technique	ECM composition	ECM fabrication method	*IM*	Cell type	Ref
Bottom-Up	Pre-seeding the scaffold with angiogenic factor releasing cells	Silk fibroin gel	Freeze-drying	Yes	Co-culture of endothelial cells and osteoblast	139
Bottom-Up	Co-culturing proangiogenic cells with EC	Fibrin hydrogel and HA nanocrystals	Gelation	Yes (No pores)	Lung fibroblasts-human umbilical vein endothelial cell	140
Bottom-Up	Pro-angiogenic factor	Collagen type I	Freeze-Drying	Yes	Human endothelial cells, human adipose-derived stem cells. (It is not a co-culture)	141
Top-down	Proangiogenic growth factor	Collagen type I	Freeze-drying	Yes	Epithelial cells	142
Top-down	Proangiogenic growth factors	Type I collagen and Matrigel gel	Gelation	Yes (No pores)	Co-culture of Endothelial cells and Mouse smooth muscle cells	143
Top-down	Proangiogenic growth factors	Type I collagen	Gelation	Yes (No pores)	Co-culture of Human endothelial cells, Human pericytes /human smooth muscle cells	33
Top-down	Angiogenic growth factor and co-culturing with pro-angiogenic releasing cells	Calcium silicate/β-tricalcium phosphate	3D printing	Solid Matrix (not porous)	Co-culture of human bone marrow-derived monocytes and human umbilical vein endothelial cells	144

2.2.3.1. Bottom-up Pre-vascularization

The first common method which has been used to pre-vascularize tissues is culturing endothelial, endothelial progenitor, or epithelial cells in engineered tissues along with the use of proangiogenic

growth factors (i.e., vascular inducing factors) such as vascular endothelial growth factors (VEGF).

One of the difficulties involved with pre-vascularization based on proangiogenic cells is the random spread of newly formed vascular networks within the engineered tissue. This is because it is hard to control the position of initial endothelial cells lining the inner vascular network[4]. Further, there are some restrictions concerned with using proangiogenic factors, such as their instability[145], high cost[146], and short half-life[147], as well as the risk of tumorigenesis[148].

2.2.3.2. Top-down Pre-vascularization: Microfabrication Techniques

A recent method to generate vascular networks is the use of microfabrication techniques to form pre-vascularized tissues. By doing so, by the time that natural invasion of the vascular network to the implant occurs, the nutrient and oxygen can be supplied to the cells through the pre-vascularized networks. Weinberg and Bell used the microfabrication subtractive molding technique to fabricate the first collagen-based blood vessel *in-vitro*[19]. Since then, the invention of new microfabrication techniques has facilitated pre-vascularized network fabrications.

Previously, some sophisticated microfabrication techniques were used to develop synthetic polymer-based co-culturing systems in which cells can communicate through microchannels while being physically apart[20, 149-158]. The polymeric materials which were used to fabricate these tissue models were usually non-biomimetic (e.g., PLA). As a result, cells were not able to directly anchor to the interior of the cell culture area. The culturing area in the polymeric microchannels was usually coated with proteins such as fibronectin or collagen (analogous to BM) to enable the anchorage of cells[159], making them semi-biomimetic. However, the IM was not included in these microfluidic cell culture

models. Fabrication of pre-vascularized tissues from more biologically relevant materials was proposed. Table 2-2 shows a list of studies where a variety of microfabrication techniques have been used for the microfabrication of embedded pre-vascularized networks. These microfabrication techniques are laser patterning[160], subtractive molding[34], sacrificial molding[161-163], injection molding[33], extrusion-based and laser-assisted bioprinting, 3D printing, micropatterning[164] based on soft lithography, and microfluidic-flow-based fabrication methods. As an example in **Figure 2-12**, José A., et al.[165] used subtractive molding to produce a channel inside a hydrogel scaffold. This scaffold only consisted of IM (cells were cultured inside the hydrogel), and it did not have any BM. Subtractive molding is usually based on using wire rod templates, so it can only produce straight channels. Also, since the scaffold is hydrogel-based, it is not porous. As such, it cannot provide interstitial flow while the cells are also exposed to unnecessary forces exerted by the hydrogel.

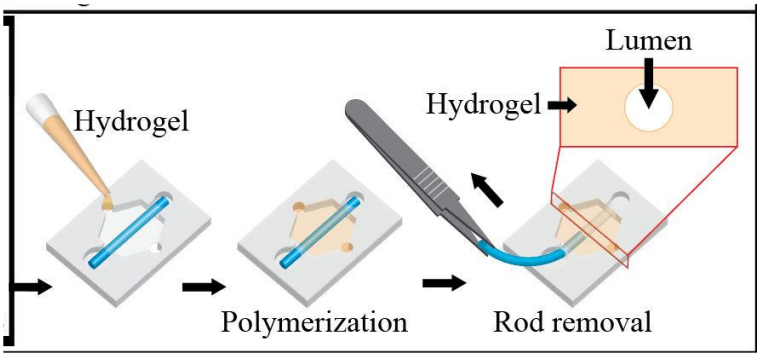

Figure 2-12. Fabrication of pre-vascularized ECM channel in hydrogel using subtractive molding method; José A., et al. fabricated PDMS patterned to produce lumens inside the hydrogel [165]. Permission was obtained from Wiley.

Moreover, the cells cannot have their natural phenotype as they cannot spread as they would in *in-vivo* tissues[166]. The use of these microfabrication techniques in producing a pre-vascularized scaffold resulted in the emergence of more biologically relevant engineered tissues.

Table 2-2. Summary of studies involving scaffolds with pre-defined microchannels

Pre-vascularization technique	ECM Material	ECM fabrication method	IM	BM	Cell type	Disadvantages	Ref
Laser patterning	Collagen type I	Freeze-drying	☑	☒	Human fibroblasts	-Short wavelengths (<400 nm) can be damaging to cellular content due to higher light absorption by water. -Collagen denaturation due to thermal damage	160
Laser patterning	Gold nanorods, cell encapsulating collagen, hydrogel	Gelation	☑	☒	Endothelial cells	-Short wavelengths (<400 nm) can be damaging to cellular content due to higher light absorption by water. -Collagen denaturation due to thermal damage -Gold nanoparticles are cytotoxic	167
Subtractive molding	Silk Fibroin	Freeze-drying	☑	☒	Implanted in the groin of Sprague Dawley rats	-Only straight pattens can be fabricated, as the mold needs to be removed. -Existence of wire rods affects the pore structure inside the scaffold as the scaffold undergo the freezing process.	168
Injection molding	Collagen gel	Gelation	☑ - Not porous	☒	Co-culture of human umbilical vein endothelial cells with three different stromal fibroblasts cell lines	NA	169
Co-axial microfluidic	Polyether Sulfone	Air drying	☒	☑	No cell culture	-Limited patterns are feasible -The core flow needs to be removed, which usually is done by harsh solvents. Also, the residue of the core material remains in the mold, which could be cytotoxic	170
Core flow-sheath flow-based fabrication	Chondroitin Sulfate/Chitosan	Layer by layer assembly of air-dried layers	☒	☑	Co-culture of Mouse embryonic fibroblasts and human-bone marrow-derived mesenchymal stem cells	-limited patterns are feasible -The core flow needs to be removed, which usually is done by harsh solvents. Also, the residue of the core material remains in the mold, which could be cytotoxic	171
Sacrificial molding	poly-3-hydroxybutyrate-co-3-hydroxyvalerate (PHBV)	Electrospinning	☑- Not porous	☒	Co-culture of human dermal microvascular endothelial cells and human dermal fibroblasts	-The sacrificial mold needs to be removed, which usually is done by harsh solvents. Also, the residue of the core material remains in the mold, which could be cytotoxic	172
Sacrificial molding	Chitosan and Collagen	Freeze-drying	☑	☒	Cardiomyocytes and endothelial cells	The sacrificial mold needs to be removed, which usually is done by harsh solvents. Also, the	[161]

						residue of the core material remains in the mold, which could be cytotoxic	
Micropatterning on PDMS mold made by photolithography and soft lithography	Silk scaffold	Air drying	☒	☑	Hepatocyte carcinoma cells	-Shrinkage of collagen due to either high evaporation rate or surface tension effects of residual solvents during the solvent evaporation process	[173]
Bioprinting (Extrusion based)	Gelatin, hyaluronic acid, and Methacrylic Anhydride	Gelation	☑- Not porous	☒	Human adipose-derived stem cells and endothelial cells	-Limited to specific materials with printability properties -Higher cell densities but lower speed and resolution (In comparison with inkjet bioprinting) -Bio-inks viscosity= in the range of 30-6 $\times 10^7$mPa s -Resolution =200-1000µm - Potential nozzle clogging - Decreased cell viability due to shear stress - Not all biomaterials are printable: bio-ink formulations having adequate mechanical properties for fabrication of stable 3D constructs at good bioprinting accuracy often presents a suboptimal environment for cell migration and spreading[174]	[175]
Bioprinting (Laser-assisted bioprinting)	Alginate and EDTA blood plasma	Gelation and laser bioprinting	☑- Not porous	☒	Human adipose-derived stem cells	-Although cell transfer using the LIFT technique has been successful, the cell survival rate is often below 85%. -Thermal damage of ECM proteins -bio-ink viscosity=1-300 mPa s[174]	[175]
Bioprinting (Inkjet bioprinting)	Thrombin and fibrinogen	Gelation	☑- Not porous	☒	Endothelial cells	- The inherent inability of the printing head to provide a continuous flow. - Bio-inks viscosity= lower than 10 mPa s[174] - Low cell densities in comparison with other bioprinting methods - Thermal inkjet printing will cause activity loss resulting from very high temperatures, which may reach above 200 ℃	[176]

According to **Table 2-2**, BM has only been included in three of the presented studies. However, in none of these three studies the pores of IM have been considered. Owing to the fact that they do

not have porous IM, they could not have interstitial fluid for delivering the fresh nutrient and removing the wastes, so they all lack biological similarity to their corresponding *in-vivo* tissues.

In a study conducted by Pin et al., microfabrication was used for patterning the mold, which was then used to pattern the collagen scaffold. The resulting two-layered micropatterned collagen scaffold, comprising 2D collagen films attached to 3D collagen scaffolds, was used as skin equivalent[118–120]. However, these micropatterned structures were only at the surface. They were fabricated as skin equivalent comprising a basal lamina and were used for studying the effect of membrane topography on keratinocyte cells' proliferation and differentiation.

In **Table 2-3,** a brief overview of the micropatterned scaffolds formed on negative molds is provided. Note that these micropatterns were not sealed, meaning that the patterns were only at the surface of the scaffold, so their corresponding scaffold did not contain any pre-defined microchannels inside them. However, a promising bonding method can integrate them into pre-vascularized scaffolds.

Table 2-3. Summary of studies involving fabrication of micropatterns on scaffolds with no predefined microchannels

Micropatterning techniques – Mold fabrication	ECM Material	ECM fabrication method	IM	BM	Cell type	ref
Micropatterning: Photolithography is used to form a Positive SU-8 mold, followed by casting the alginate on the SU-8 mold to fabricate a negative alginate mold.	Collagen hydrogel	Gelation	☑-Not Porous	☑-PET membrane	Epithelial cells	[177]
Micropatterning: PDMS negative mold was fabricated by standard photolithography followed by soft lithography.	Chondroitin Sulfate and type I Collagen from fish scale	Gelation	☑- No Porous	☒	Oral keratinocytes	[178]
Micropatterning: PDMS negative mold was fabricated by standard photolithography followed by soft lithography.	Gelatin, Chondroitin-6-sulfate, Hyaluronic acid	Freeze-drying of hydrogel	☑	☒	Human fibroblasts	[179]
Micropatterning: laser patterning of polyimide chip to be used as a mold	Collagen type I		☑	☑	Human keratinocyte	[180]
Micropatterning: PDMS negative mold was fabricated by standard photolithography followed by soft lithography.	Collagen type I	IM fabrication: Freeze-drying BM fabrication: Air drying	☑	☑	Keratinocytes	[130]
Micropatterning: PDMS negative mold was fabricated by standard photolithography followed by soft lithography.	Collagen–GAG	IM fabrication: Freeze-drying BM fabrication: Air drying	☑	☑	Human keratinocytes	[129]
Micropatterning: PDMS negative mold was fabricated by standard photolithography followed by soft lithography.	Collagen-fibronectin coating	IM fabrication: Freeze-drying BM fabrication: Air drying	☑	☑	Keratinocytes	[180]
Liquid dispensing: A micropatterned ice line template was prepared by dispensing pure water droplets onto the pre-cooled copper plate as follows to be used as a mold	Collagen type I	Freeze-drying	☑	☒	Endothelial cells and skeletal muscle myoblasts	[27]
Liquid dispensing: A micropatterned ice line template was prepared by dispensing pure water droplets onto the pre-cooled copper plate as follows to be used as a mold	Collagen type I	Freeze-drying	☑	☒	Skeletal muscle myoblasts	[181]
Liquid dispensing: A micropatterned ice line template was prepared by dispensing pure water droplets onto the pre-cooled copper plate as follows to be used as a mold	Dexamethasone-loaded calcium phosphate nanoparticles/collagen composite	Freeze-drying	☑	☒	Human mesenchymal stem cells HUVECs	[4]

2.2.4. Bonding and Enclosure of ECM Scaffolds

After defining vascular networks on a tissue scaffold using one of the planar fabrication methods described in the previous section, these layers should be bonded to other flat or structured layers to enclose the engineered vessels. Various bonding techniques such as bonding by high temperature[182], adhesive medical sealants[183], contact printing by gel[184], or collagen slurry[128-130] have been developed. Price et al. used micropatterning to pattern the surface of hydrogel using a positive PDMS replica[182]. Then, they used hot embossing (high temperature) to bond the gel-based patterned substrate to a plain substrate to seal and form closed microchannels. However, high temperature will lead to denaturation of the substrate, and thus, it has adverse effects on the scaffold.

In another study, to have a scaffold comprising both high mechanical strength and porosity, a porous collagen-based material was bonded to a non-porous collagen material. This was carried out by applying a controlled amount of a bonding layer of a collagen gel to the bonding surface of the non-porous collagen material. Then, it was contacted to the surface of the porous collagen material with the gel applied to the bonding surface to partially hydrate a section of the porous material at the interface between the materials. Next, the gel bonding layer was dried at room temperature to bond the layers[184]. Although collagen gel is considered a biocompatible material for cell study, it does not provide the characteristics of the native collagen, and thus it does not have the appropriate motifs for cell adhesion. Also, by manually applying the collagen gel to the desired layers, there would be no control over the bonding layer in terms of its thickness or the precision in the application.

Medical adhesives and sealants have been used in bonding tissues. For example, collagen-based compositions were introduced as medical adhesives for bonding soft tissues in which the collagen monomers were polymerized after being chemically changed using an acylating agent, a sulfonating agent, or a mixture of the two[183]. The medical adhesives, however, are normally used for sealing the wound, and it is usually for preventing the wound from contamination.

2.2.5. Research Gaps

In an attempt to produce a multilayered biomimetic scaffold comprising porous IM and BM, the micropatterning technique was used. In micropatterning, the scaffold material (e.g., collagen slurry) is cast on a negative microfabricated mold. Unlike the bioprinting method, micropatterning does not require a specific viscosity for the materials, and thus, a wide range of materials can be fabricated with this method. Further, in the microfabrication technique, the materials will not be exposed to high temperatures or harsh solvents during the fabrication process. Thus, it makes micropatterning an ideal fabrication method for natural polymers such as collagen or laminin, which are prone to denaturation. Further, micropatterning allows the layer-by-layer fabrication of the materials; therefore, a combination of biomaterials can be implemented in the scaffold. For example, as mentioned in section 2.1.1, BM is composed of different materials. It has been observed that the inner side of the lumen usually has more collagen content where as the abluminal layer of the BM is mostly from laminin. In fact, the sidedness of BMs derives from the patterns of protein in the BM (laminin being in the inner epithelial face and Type IV collagen on the IM face). Having these features, the *BM* separates the cells from the interior surface of the vessel from the surrounding cells in the 3D porous *IM*. According to the aforementioned reasoning, the producing

multilayer BM helps to develop a more biomimetic membrane. The layer-by-layer fabrication in the micropatterning can provide these patterns, which makes it an appropriate method of fabrication.

Most of the tissue engineering studies with pre-vascularized scaffold rely on methods that form the channel without the need for bonding, such as subtractive molding, in which the channels are formed by removing the mold after the fabrication. Also, there are limited studies on bonding the collagen layer and the channels with collagen film lining inside the channel (i.e., to function as BM). It is worth mentioning that the patterning techniques presented in **Table 2-3,** which have been limited to the surface of the scaffolds, can be integrated into an encapsulated channel by the aforementioned bonding methods. By sealing these patterns with a layer of scaffold (i.e., bonding them using an appropriate technique), one can embed microchannels in a tissue-engineered scaffold. Using a promising bonding method, these patterning techniques could be used for the fabrication of vasculatures in a scaffold.

3. Designs and Experimental Methodologies

3.1. Collagen Scaffold

3.1.1. Design Principle of Collagen Scaffold

In this study, we fabricated collagen scaffolds with embedded microchannels. The scaffold contained three main components: i) 3D porous collagen foam resembling the IM, ii) 2D collagen film resembling the BM, and iii) a microchannel embedded within the scaffold to be used in the future as a blood vessel (see **Figure 3-1**).

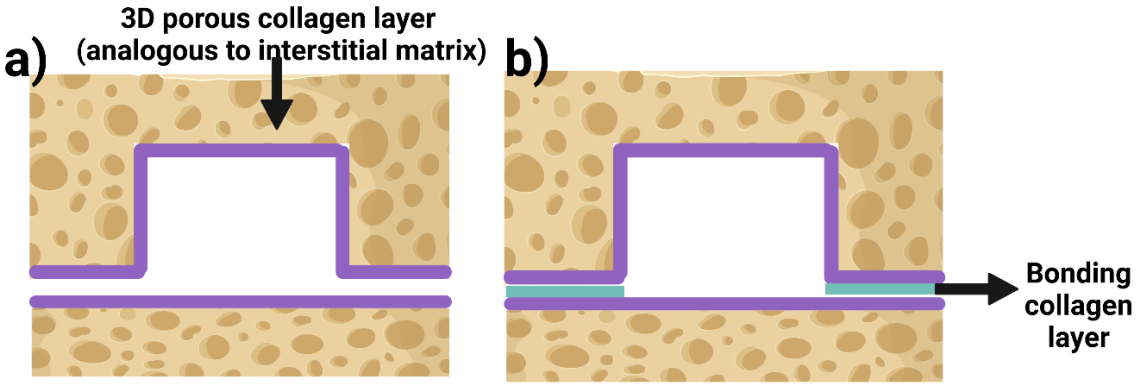

Figure 3-1. The novel scaffold devised in this thesis simulated tissues with embedded microchannels, as shown from the cross-sectional orientation: a) Schematic representation of the collagen layers with 3D IM and 2D BM, and b) forming the enclosed embedded microchannel by bonding the two layers. (Created with BioRendenr.Com)

The microchannels in this design were thoroughly lined with 2D collagen films and were fabricated in a way to be in the middle of the 3D porous scaffold. In the fabrication process, we aimed for channels with a square-shaped cross-section in which the width and height of the

channels varied in the range of 300μm -1500μm, which falls in the range of medium arteries and veins.[83]

Our fabricated scaffold (**Figure 3-1**) was made from pure collagen. Collagen was chosen for the scaffold as it comprises desired motifs for cell attachment, as discussed in chapter 2. Unlike techniques like sacrificial molding[185], our fabrication technique for microstructures (i.e., freeze-drying of collagen slurry to form porous scaffold) and macrostructures (i.e., micropatterning the collagen by casting the slurry on a patterned mold and forming the channels) is not prone to contaminate the scaffold. In addition, freeze-drying was chosen as the fabrication method so that the final scaffold contains micro-pores. The interconnected pores of the scaffold were designed to work as means of molecule/fluid transmigration. Further, the interconnected pores were devised to provide interstitial fluid inside the scaffold so that later it can deliver nutrients to the cells and remove the waste from the scaffold. The BM integrated into the current design of the scaffold was developed to provide a physical barrier at the interface of the channel and the 3D collagen scaffold. The BM was designed to improve the integrity of the microchannels in terms of structure and to prevent excessive leakage from the channel while potentially allowing the diffusion of gases and transmigration of signaling molecules in future applications. The integration and enclosure of the microchannel were implemented so that these channels can simulate the artery/vein structure where the convective leakage is negligible and a high fluid velocity exists in the blood vessels. This collagen-based microfluidic system has the potential for testing cells in dynamic modes under a specific flow rate simulating the flow of blood in vessels.

3.1.2. Mold Fabrication

Two types of replication molds were fabricated for casting and freeze-drying of collagen. One was 3D-printed plastic molds, and the other was a PDMS replica. The PDMS replica was used for fabricating the test structure as the collagen does not attach to the surface of the PDMS, and it is easy to fabricate several replicate molds. For this purpose, a positive master mold was fabricated using PDMS elastomer and curing agent (Dow Corning, USA) mixed at a 10:1 ratio. The mixture was degassed and poured on a 3D-printed negative mold to make the positive PDMS replica. Next, the degassed PDMS mixture was cured for 2 hours at 80°C. After the polymerization was completed, the PDMS layer was detached from the mold. The positive PDMS replica was then washed thoroughly for further usage.

For the single-channel collagens, used for studying the effect of neighboring channels on deformation and also for fabricating the channel lined with 2D collagen film, a positive 3D printed mold was used based on a CAD model. **Figure 3-2** shows the PDMS and 3D printed molds with square cross-section channels of 800μm in width.

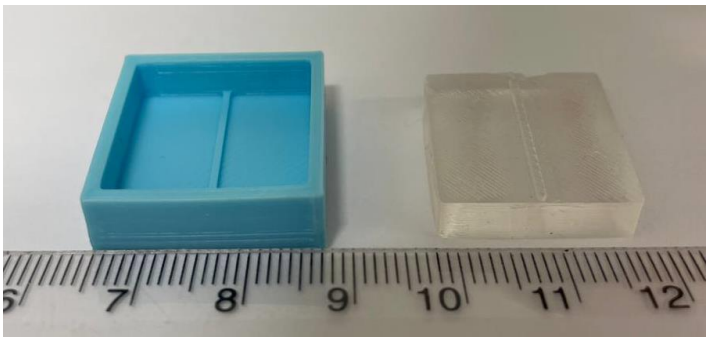

Figure 3-2. positive molds with a square cross-section channel of 800µm in width. Left is the 3D printed mold, and right is the PDMS mold

3.1.3. Collagen Layers Fabrication

The prepared PDMS replica was used for the fabrication of collagen-based microchannels with test structure patterns as explained in Scheme shown in **Figure 3-3**. In step, a, a suspension of 1 w/v concentration collagen was prepared by mixing 1 g of fibrillar collagen type I from bovine Achilles tendon (Sigma Aldrich) with 0.05 mol/L acetic acid. The resulting collagen slurry was then incubated overnight at 4℃ and agitated by a conventional blender (on an ice bath to keep the temperature low) to become homogenous (i.e., in step b). The resulting bubbles of the collagen slurry were eliminated in the next step by centrifuging with the speed of $400 \times g$[†††] (i.e., in step c). In the next step, the collagen slurry was poured over the patterned microfabricated mold and was left at room temperature so that the water in the collagen slurry evaporated and a 2D collagen film was formed. In step e, we poured a freshly prepared collagen slurry on top of the 2D collagen film while the 2D was supported by the mold and froze it at a fixed temperature (i.e., either -20 or -80 ℃). In step f, the frozen collagen was freeze-dried, resulting in an integrated 3D porous collagen scaffold attached to a dense, 2D collagen (see **Figure 3-3j**).

[†††] Relative centrifugal force (g)

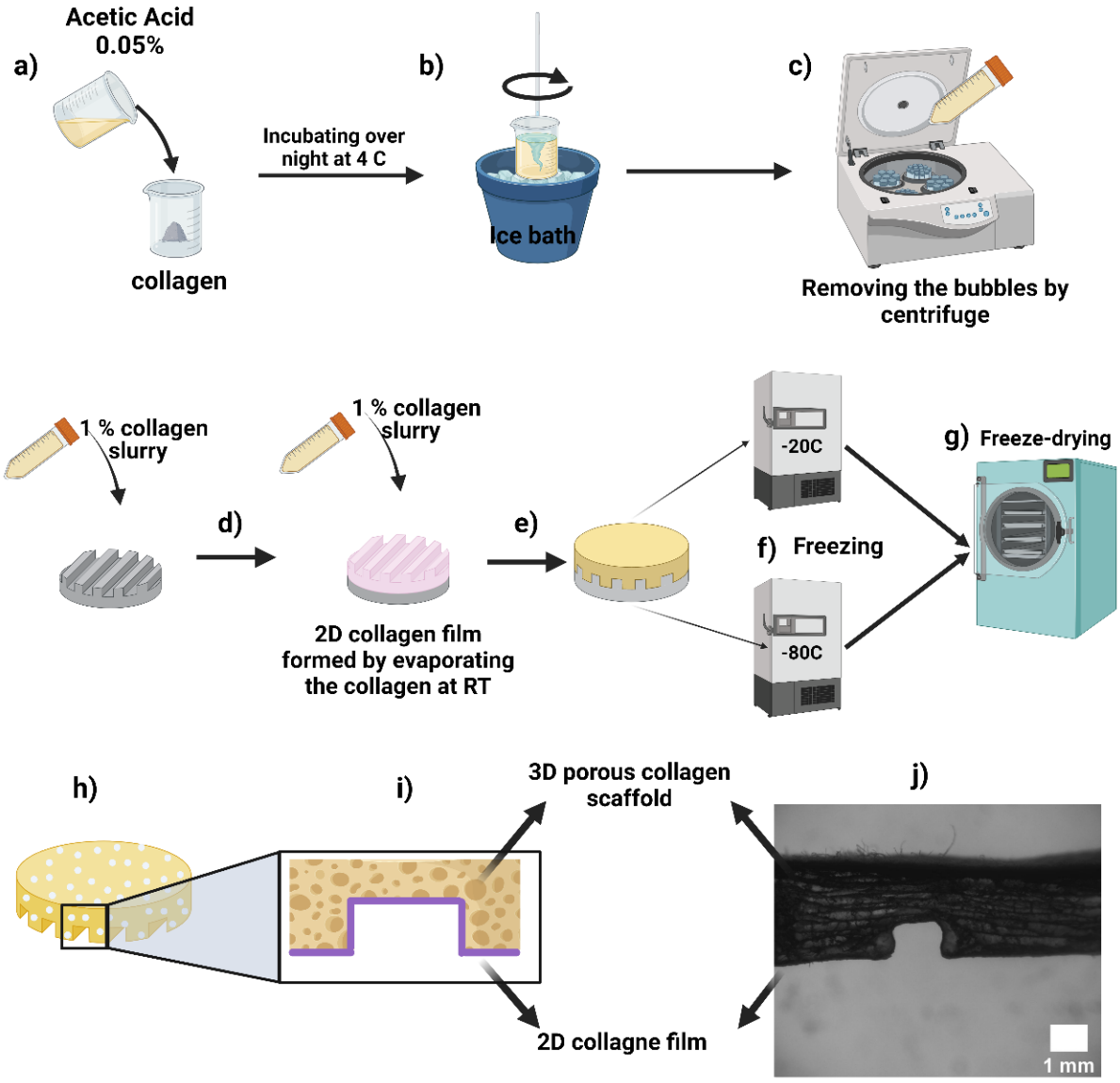

Figure 3-3. Steps for fabrication of collagen microchannels (Created with BioRender.com)

Once the collagen-based microchannels with 3D/2D structures were fabricated, a second substrate without any pattern was needed to seal the patterned channels. Similar steps were followed to fabricate a non-patterned 3D scaffold over a flat 2D collagen layer. The bonding method for these two substrates is elaborated in the next section.

3.1.4. Bonding of Collagen Layers

We used the contact printing method to form closed channels by bonding a patterned collagen scaffold (in **Figure 3-4a**) with a second non-patterned collagen scaffold (in **Figure 3-4b**). A layer of 2% collagen slurry was spin-coated at 1500rpm for 15s to form a uniform layer of collagen on a glass substrate (see **Figure 3-4c**). Next, the scaffold containing patterns was contacted with the layer of spin-coated collagen, and it was bonded to the non-patterned collagen layer to seal the channel (**Figure 3-4d**). Finally, the bonded assembly was left at room temperature so that water would evaporate (**Figure 3-4e**). Two needles are used at the inlet and outlet of the channels for flowing the media through the scaffolds. **Figure 3-5** shows one of the fabricated collagen scaffolds with needles for the inlet and outlet.

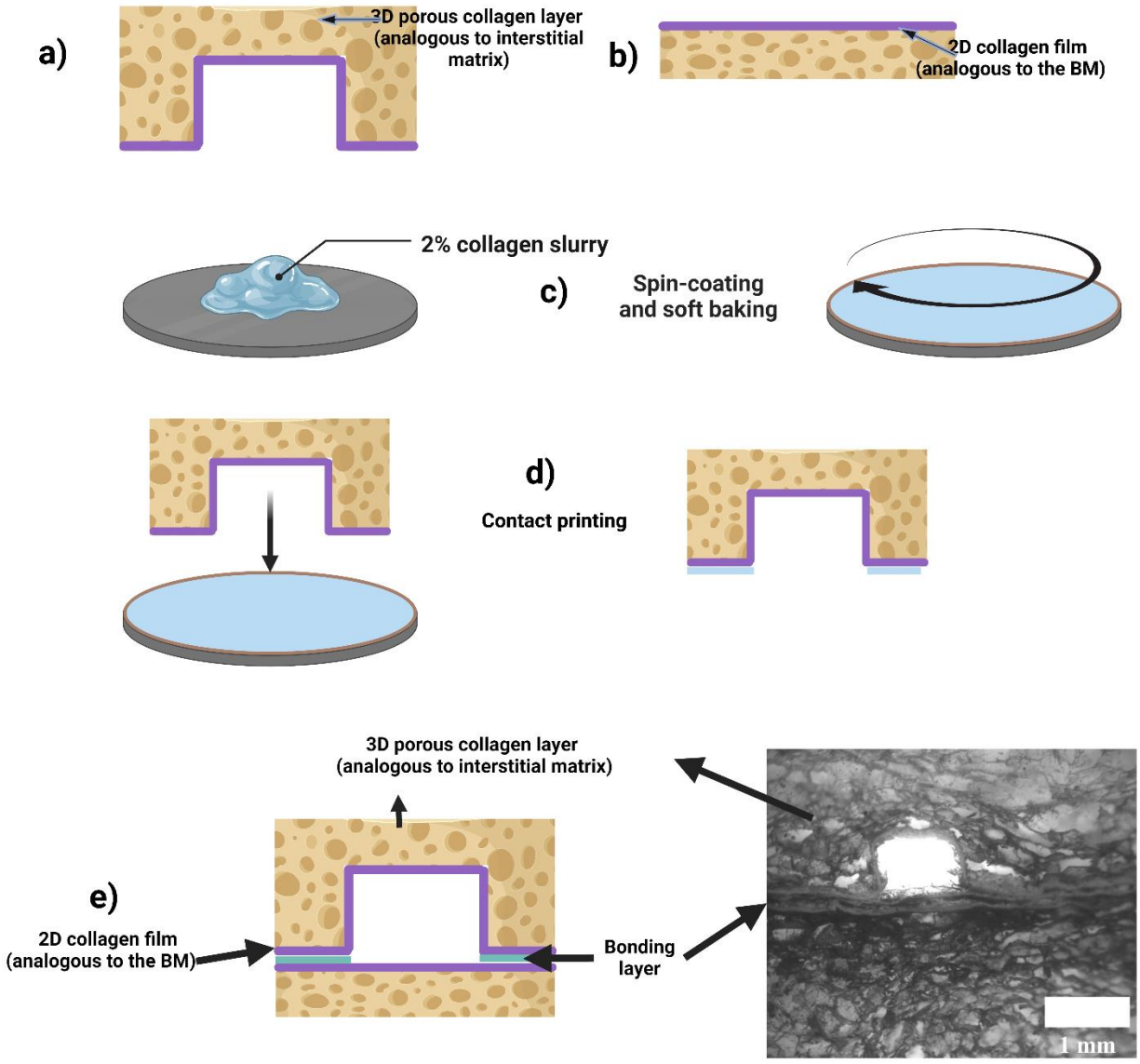

Figure 3-4. Contact printing method for bonding patterned collagen with a second collagen scaffold (Panels a to e were created with BioRender.com)

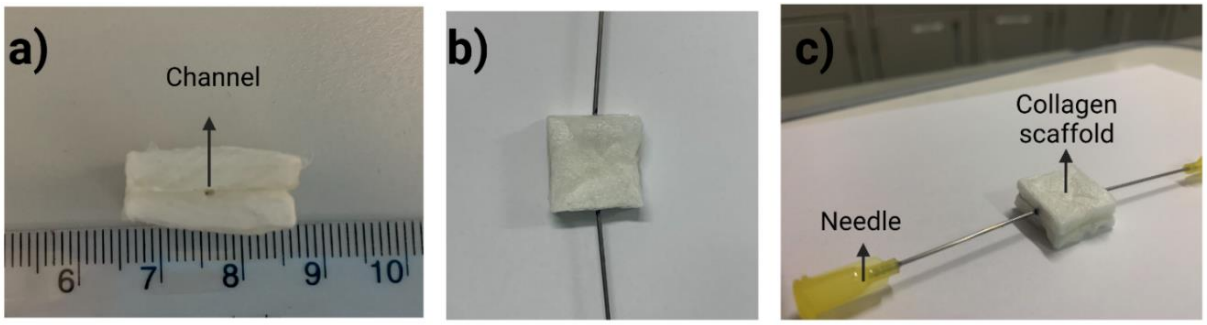

Figure 3-5. Image of final collage scaffold, a) cross-section view of the embedded channel, b) top view of the channel with needles for the inlet and outlet, c) side view of the collagen channel

3.2.Channel Test Structure Fabrication

A PDMS mold containing six parallel microchannels was fabricated according to section 3.1.3. The test structures had square cross-sections with sizes ranging between $300\mu m$ to $1.5mm$ in height and width. This PDMS replica was then used for the fabrication of collagen-based microchannels with test structure patterns according to the method explained in section 3.1.3. To obtain a cross-sectional view of the fabricated test structures (**Figure 3-6**), the fabricated collagen scaffold containing test structures was cut using a diamond wire saw (DWS 100, Diamond Wire Tec, Weinheim).

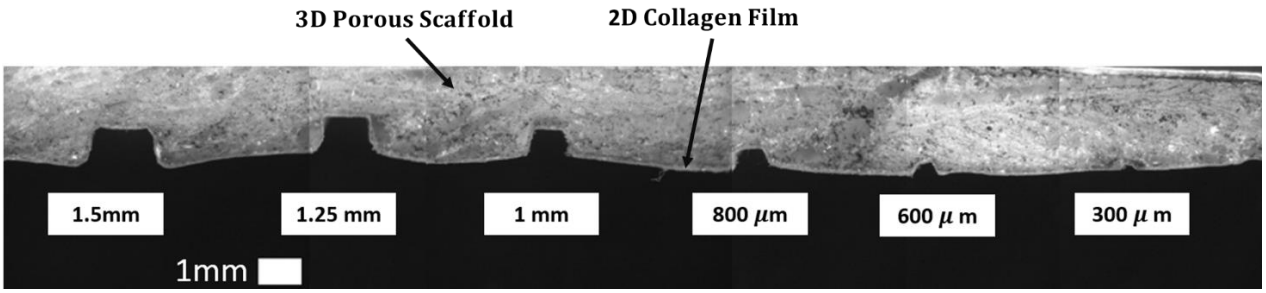

Figure 3-6. The fabricated collagen scaffold comprising the integrated 2D and 3D collagen scaffold with six parallel test structures (the numbers inside white boxes denote the targeted size of the microchannels ranging from 300μm to 1.5 mm).

3.3.Characterization of Collagen Layers

3.3.1. Micro and Macro Structural Properties

In this thesis, the properties of the scaffold were divided into two major categories. The macroscopic structure of the scaffold (e.g., width and height of channels, the perimeter of the channel, and cross-section area) and the microscopic structure of the scaffold (e.g., pore size).

To measure the macroscopic structure of the scaffold, optical images of the collagen scaffolds were taken using an upright Leica microscope with a CMOS monochrome camera (GS3-U3-51S5M-C, Point Grey, Canada). Then, MATLAB codes were developed to measure the above-mentioned macroscopic properties of the scaffold.

The microscopic structure of the scaffold (i.e., pore size) was investigated using Scanning Electron Microscopy (SEM) images. Then, the pore size image analysis algorithm from Rabbani et al.[186] was used to characterize and quantify pore size and the pore distribution in the scaffolds.

3.3.2. Mechanical Properties

To determine the mechanical properties of the 3D collagen scaffold and 2D collagen film, a tensile test was implemented by a TA Discovery HR-2 hybrid rheometer (see **Figures 3-7a and 3-7b**). To evaluate the mechanical behavior of the 3D collagen scaffold and 2D collagen film, the tensile stress vs. strain curves were obtained at two different states: i) when the collagen was dry and ii) when the collagen was hydrated. A strain rate of 0.005 s^{-1} was used for all the tensile tests. Tensile stress vs. strain curves were obtained for the fabricated collagen films and 3D scaffolds to evaluate whether the resulting stress-strain curves are j-shaped, similar to the soft tissues in the body, and to evaluate the stiffness of the resulting engineered tissues compared to different tissues in the human's body. Also, the slope of the curve was measured to determine the stiffness of the samples at desired strain ranges.

In this thesis, we were also interested in quantifying the bond strength between the 2D film and the 3D collagen scaffold (see **Figure 3-7c**) and the bond strength between two substrates of integrated 2D/3D collagen scaffolds (see **Figure 3-7d**). To do so, we measure the required forces to separate the 2D collagen film from the 3D collagen scaffold or separate two integrated 3D/2D scaffolds bonded with collagen glue as the bonding layer. Using this experiment, we can quantify the average stress required to separate a specific surface of bonded materials (i.e., either 2D collagen film bonded to a 3D collagen scaffold or two integrated 2D/3D scaffolds bonded by contact printing method).

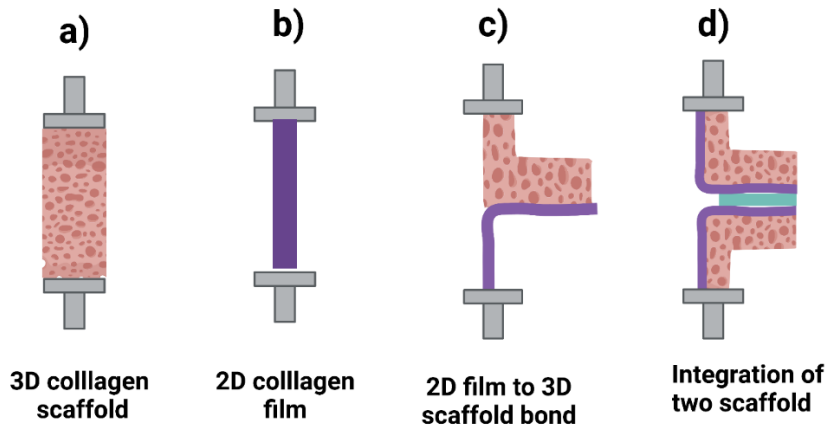

Figure 3-7. Mechanical tests were used to quantify mechanical properties for a) 3D collagen scaffold, b) 2D collagen film, c) required forces for separation of 2D collagen film from 3D collagen scaffold, and d) required forces for separation of two layers of integrated collagens. Created with BioRender.com

3.3.3. Water Permeability

To investigate whether the fabricated 3D collagen scaffolds and 2D collagen films around the microchannels are permeable to the flow inside the channel, the permeability test was conducted as follows. The 3D scaffold (1% w/v) was fabricated at -20℃, and the diameter and thickness were 11mm and 10 mm, respectively. As for 2D collagen film, it was fabricated by air drying at room temperature, and the thickness and the diameter of the 2D collagen were 50μm and 11mm, respectively. We added 2 ml of water over the collagen (either the 3D scaffold or the 2D film), as shown in **Figure 3-8**. We then measured the time spent until all the water passed through the collagen scaffold or 2D collagen films. Prior to performing the experiments, we sufficiently hydrated the collagen scaffolds so that almost all of the waters passed through the collagen.

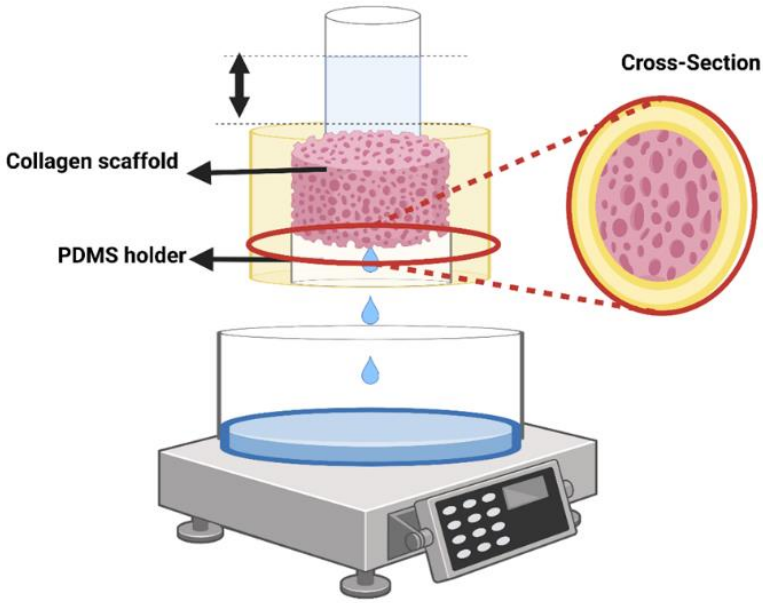

Figure 3-8. Schematic of the setup employed for permeability measurement of 3D porous collagen (Created with BioRender.com)

3.3.4. Leak Test of Embedded Channels in Collagen Layers

A leak test was performed to evaluate the performance of the fabricated collagen scaffold. As shown in **Figure 3-9a**, collagen scaffolds were submerged in water prior to the experiment to mimic the *in-vivo* condition. For performing the experiments, two needles were attached to the fabricated collagen scaffolds with microchannels to enable flowing water into the channels (see **Figure 3-9b**). The test was conducted in two different models where the scaffold comprised: i) a channel lined with 2D collagen film (see **Figure 3-9c**) and ii) a channel without 2D collagen film (see **Figure 3-9d**).

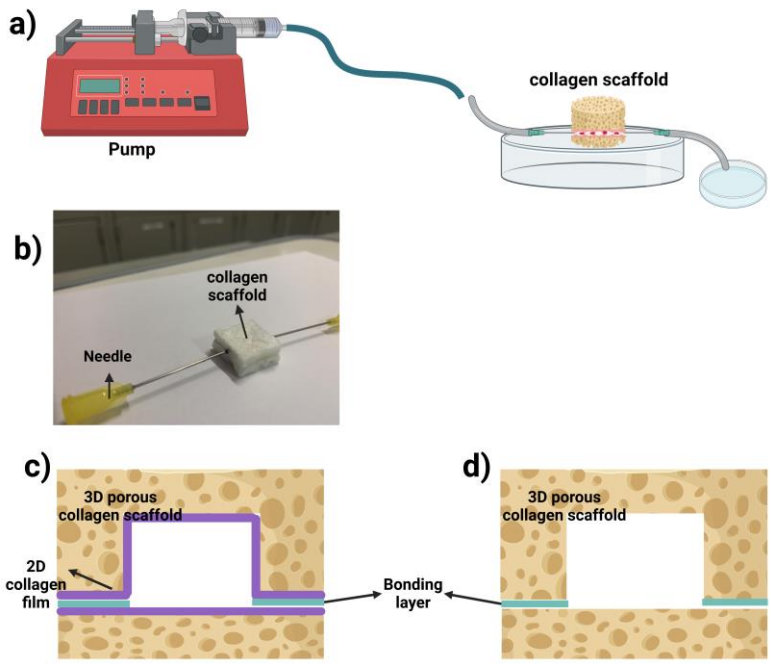

Figure 3-9. Leak test for evaluating the performance of the fabricated microchannels: a) the schematic representation of the leak test, b) the actual collagen scaffold used for the leak test with the inlet and outlet, c) the collagen scaffold comprising channels that are lined with 2D collagen film, and d) the scaffold comprising a channel without 2D collagen film. Panels a, c, and d are created with BioRender.com.

To quantify if there is any leakage of media flowing through the scaffold, we compared the volumetric flow rate of water at the inlet and the corresponding volumetric flow rates at the outlet. To investigate the effect of using 2D collagen film as a BM, we repeated this leak test for the situation where the microchannel is fabricated without collagen film. In this situation, it was hypothesized that some of the flowing media would penetrate through the porous structure of the 3D collagen scaffold. This could be especially important when the flow rates are relatively low,

so the average residence time[‡‡‡] of the media in the channel would be relatively large. To perform the leak test, we passed 10 mL of water through the microchannel at different flow rates (5, 10, 100, 500, 1000, 5000, 10000, 25000$\mu l/\min$). We then measured the collected volume of water at the outlet at the end of each experiment. Finally, we could calculate the flow rate of water that penetrated collagen scaffolds.

To simulate the flow of blood in the veins, it is important to implement conditions where there is a dynamic similarity between the flow in the engineered collagen-based scaffold and the flow in the veins and arteries. To achieve dynamic similarity, Reynold's number should be adjusted to be the same[187]. Reynolds number is the ratio of inertial forces to the viscous forces and can be obtained as follows:

$$Re = \frac{U_m D_h}{\nu} \tag{3-2}$$

where ν is the kinematic viscosity of the media, U_m is the average velocity of the flowing media and D_h is the hydrodynamic diameter:

$$D_h = \frac{4A}{P} \tag{3-3}$$

where A and P are the area and the perimeter of the microfluidic channel, respectively.

[‡‡‡] The residence time of a fluid particle is the total time that the particle spends inside the channel from the inlet to the outlet. It can be defined as the channel length divided by the fluid average velocity (i.e., volumetric flow rate divided by the cross-sectional area of the channel).

3.4. Image Processing

To obtain the pore size distribution and the mean pore size, we used a MATLAB code developed by Rabbani et al.[186]. Another MATLAB code was developed to calculate the width of the corresponding collagen-based test structures (**Figure 3-10a**).

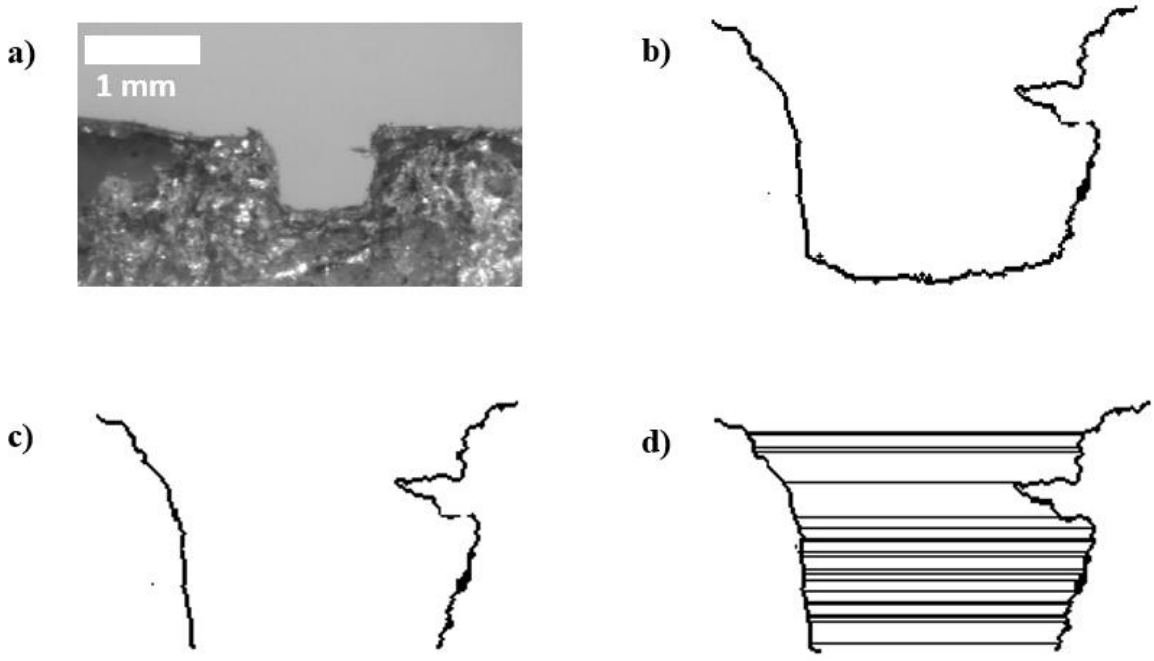

Figure 3-10. Steps required to obtain the average width of the collagen-based microchannels. a) the optical image from the cross-sectional view of a collagen channel, b) the edges of the microchannel are detected, c) the edges corresponding to the side walls of the microchannel are kept, and the rest of the edges in the image are removed, and d) horizontal lines are drawn by the MATLAB routine, and the mean of their lengths is determined.

To do so, the built-in MATLAB function "edge.m" was used for edge detection (see **Figure 3-10b**). Then, the edges corresponding to the side walls of the microchannels were selected by the user, and the remaining edges corresponding to the bottom of the microchannel were removed (see **Figure 3-10c**). Finally, a sufficient number of horizontal lines were drawn by the developed code between the detected edges of vertical microchannel walls (see **Figure 3-10d**), and their average length was reported as the width of the microchannel. A similar procedure was followed to determine the height of the microchannels (see **Figure 3-11**). The additional required step was to add a baseline from which the height of the microchannels could be calculated (see **Figure 3-11d**).

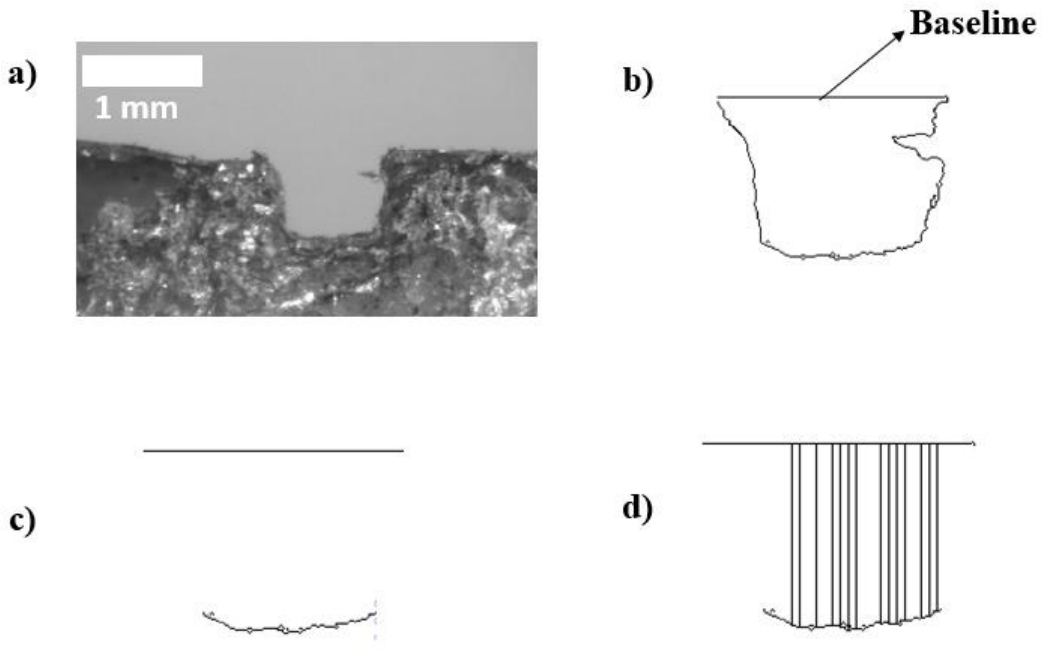

Figure 3-11. Steps required to obtain the average height of the collagen-based microchannels: a) the optical image from the cross-sectional view of the collagen channel, b) the edges of the microchannel are detected, and the baseline from which the height is calculated is added to the image of edges by the user, c) the edges corresponding to the baseline and the bottom of the channel is kept, and the rest of edges in the image are removed, and d) the vertical lines are drawn by the MATLAB routine, and the mean of their length is determined.

The thickness of the 2D collagen films was also determined by a similar method as the height determination algorithm, whose intermediate steps were shown in Figure 3-11, except that a baseline is not required to be specified (see **Figure 3-12**).

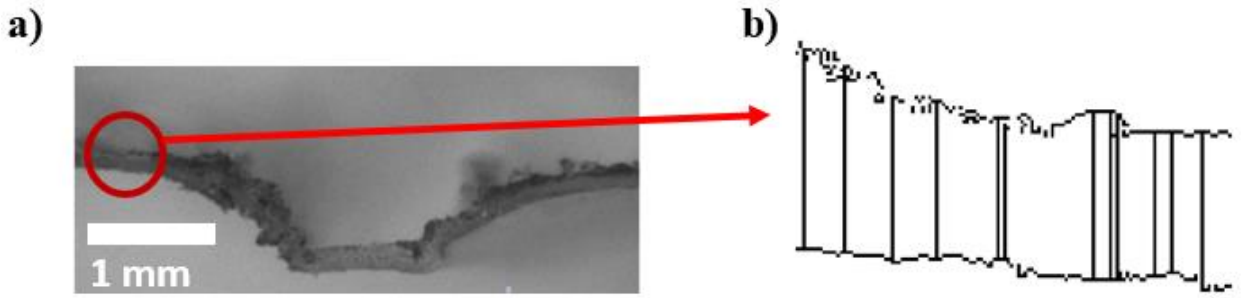

Figure 3-12. Image analysis to obtain the thickness of the 2D collagen film, a) an optical image obtained from the side view of a 2D collagen film, and b) vertical lines which were drawn between the boundaries of the 2D layer whose corresponding length mean represents the 2D film thickness

Another image analysis algorithm was used to obtain the perimeter of the channels (see **Figure 3-13a**). In this algorithm, the edges of the microchannels are initially detected. Next, the MATLAB-developed algorithm determines some representative points from the subsequent edge points. Afterward, the perimeter is approximated by adding the lengths of all connecting lines passing through the representative points (i.e., green lines in **Figure 3-13b**).

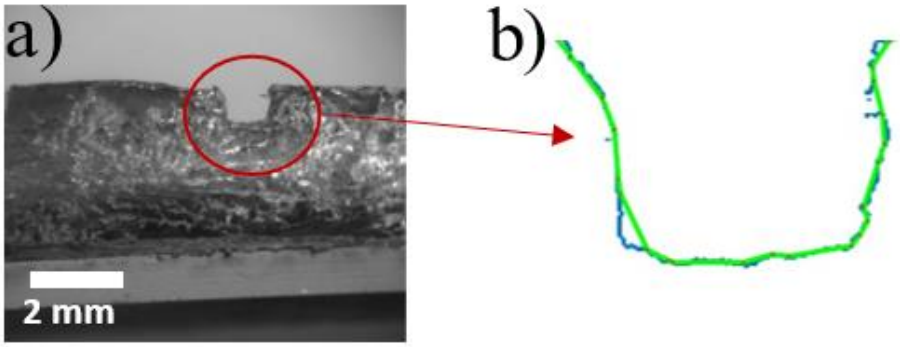

Figure 3-13. Edge detection and perimeter calculation using image analysis: a) the cross-sectional view of the original image and b) the edges of the microchannel walls (shown in blue) and the connecting lines (shown in green) between the subsequent edge points

The cross-sectional area for the final collagen-based microchannels was also obtained using image analysis. As shown in **Figure 3-14a,** the image containing a cross-sectional view of the channels was converted into a binary image. The number of resulting white pixels (see **Figure 3-14b**) in the binary image is proportional to the cross-sectional area and can be obtained by multiplying the number of pixels by the area-to-pixel ratio.

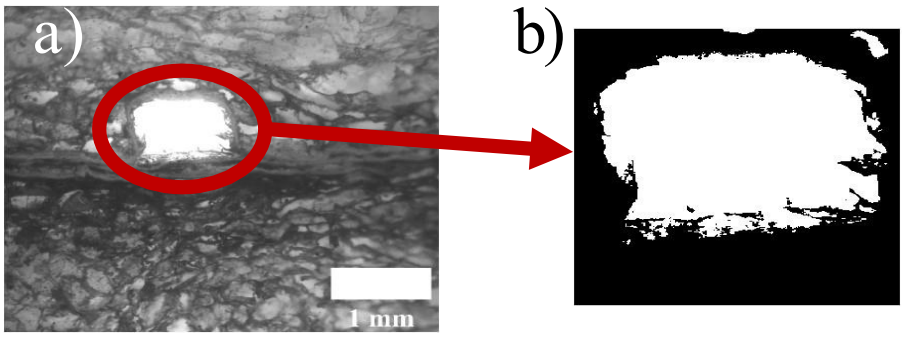

Figure 3-14. Channel area determination using image analysis: a) cross-sectional view of a 3D/2D integrated collagen scaffold with an embedded microchannel, and b) the filtered image whose number of white pixels corresponds to the cross-sectional area of the collagen microchannel.

4. Result and Discussion

As indicated in chapter one, the objective of this thesis was to simulate the three main components of *in-vivo* tissues, including IM, BM, and vascular channel. For doing so, we fabricated collagen scaffolds with embedded microchannels. The scaffold contained three main components: i) a 3D porous collagen scaffold, ii) a 2D collagen film, and iii) a microchannel embedded within the scaffold. The microchannels in this design were thoroughly lined with the 2D collagen film and were fabricated in a way to be in the middle of the 3D-porous scaffold. In the fabrication process, we aimed for channels with a square-shaped cross-section in which the channel width and height vary in the range of 300μm -1500μm.

In this section, the results for the characterization of properties for different components involved in the fabrication of the engineered tissue are explained. Important properties were: i) pore size distribution and pore walls thickness of the collagen scaffolds, ii) stiffness of the collagen scaffolds in dry and wet conditions, iii) thickness of the collagen films when different amounts of collagens are used, iv) stiffness of the 2D collagen film for dry and hydrated states, v) width, height, and perimeter of the resulting collagen scaffolds vs. the corresponding values in the test structure molds, and vi) shrinkage in the resulting microchannels. Following the characterization of the properties, we implemented a leak test for various flow rates to evaluate the performance of the fabricated microchannel.

4.1. 3D Collagen Layer Characterization

4.1.1. Pore Size Distribution and Wall Thicknesses of Collagen Pores

To determine the microscopic structure of the collagen scaffolds fabricated using freezing temperatures of -20 and -80 ℃, collagen samples (1% concentration) were cut, and SEM images were obtained from the collagen scaffolds cross-sections. **Figures 4-1a** and **4-1b** show the SEM images for 3D collagen scaffolds fabricated using freezing temperatures of -80℃ and -20 ℃, respectively. **Figures 4-1c** and **4-1d** show close-up images of the samples above. As shown, using a freezing temperature of -20 ℃ resulted in larger pore sizes which can be attributed to the formation of larger ice crystals at the freezing temperature of -20 ℃ compared to -80 ℃. This result is in agreement with the literature reporting that by decreasing the freezing temperature, the average size of the scaffold pores is expected to decrease[100, 188].

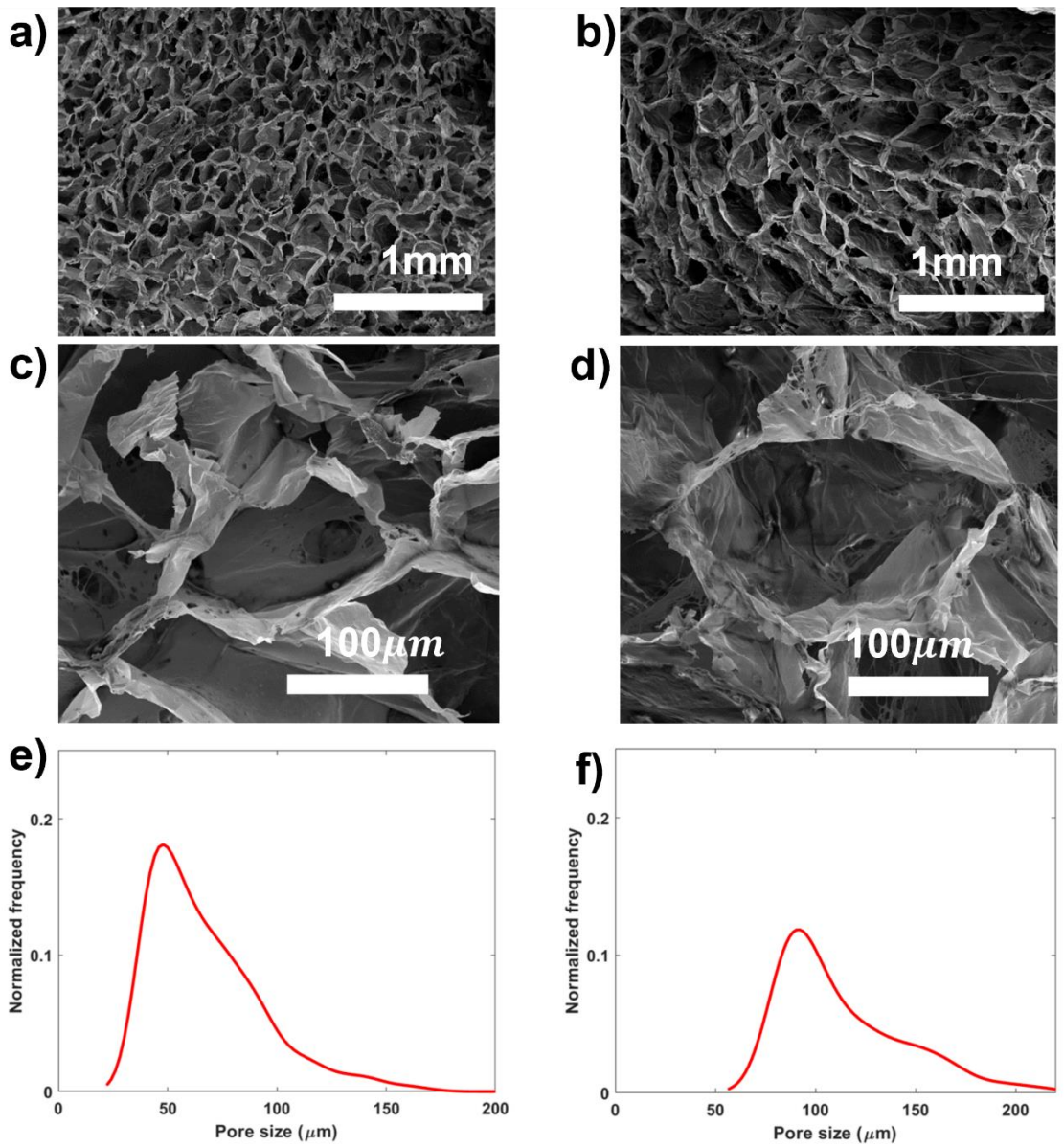

Figure 4-1. SEM images of porous 3D collagen scaffolds and the corresponding pore size distributions: a) porous collagen scaffold fabricated using a freezing temperature of -20 ℃, b) porous collagen scaffold fabricated using a freezing temperature of -80 ℃, c) SEM image of a single pore in porous collagen fabricated using a freezing temperature of -20 ℃, d) SEM image of a single pore in porous collagen fabricated using a freezing temperature of -20 ℃ and -80 ℃, e) pore size distribution for collagen scaffolds fabricated using a freezing temperature of -80 ℃, and f) pore size distribution for a porous scaffold fabricated using a freezing temperature of -20 ℃ temperatures.

From SEM images, image analysis was conducted to measure pore sizes, pore distribution, and pore wall thickness of the corresponding collagen scaffold. **Figures 4-1d** and **4-1e** show the corresponding pore size distributions of the collagen scaffolds fabricated using freezing temperatures of -80 ℃ and -20 ℃, respectively. The average pore size for the collagen fabricated using the freezing temperature of -80 ℃ is 67.9 μm which is less than the corresponding value for collagen fabricated using the freezing temperature of -20 ℃, which is 113.1 μm.

The larger pore sizes for the fabricated collagen scaffolds using the freezing temperature of -20 ℃ have been reported to be suitable for cell culture in terms of cell seeding efficiency and spatial cell distribution within the scaffold[189], so we used a freezing temperature of -20 ℃ for the rest of this study for 3D scaffold fabrications. O'Brien et al. obtained the pore size of 121 μm for their scaffolds using a freezing temperature of -20 ℃ at a lower concentration of collagen slurry (i.e., 0.5%)[100]. Faraj et al. obtained an average 89 μm pore size for their collagen scaffolds using a freezing temperature of -20 ℃ and a similar concentration of collage slurry (i.e., 0.9 %) compared to the concentration of our collagen slurry (i.e., 1%). Further, they obtained the average pore size of 42μ for their collagen scaffolds fabricated using a freezing temperature of -80 ℃. Difference between the pore sizes of the scaffolds in different studies can be attributed to protocols which were slightly different.

Further, it is reported that the thickness of the fibers in the structure of implanted tissues influences the adhesion properties of the mesenchymal stem cells[190]. We measured the thickness of the collagen fibers (pore walls) for collagens fabricated using two freezing temperatures. Collagen fibers thickness is expected to be higher in collagens with a freezing temperature of -20 ℃[190]. The average thickness of the collagen fibers was obtained using ten different pore walls for each of the

SEM images in **Figure 4-1**. As shown in **Figure 4-2**, the average collagen fiber thicknesses fabricated using a freezing temperature of -20 ℃ is larger than the corresponding average wall thickness of collagen pores generated using a freezing temperature of -80 ℃. Wahl et al. obtained the wall thickness of the collagen-hydroxyapatite fibrils to be 20 μm and 10 μm for -20 ℃ and -80 ℃ freezing temperatures, respectively[190]. So, our result is consistent with the reported literature.

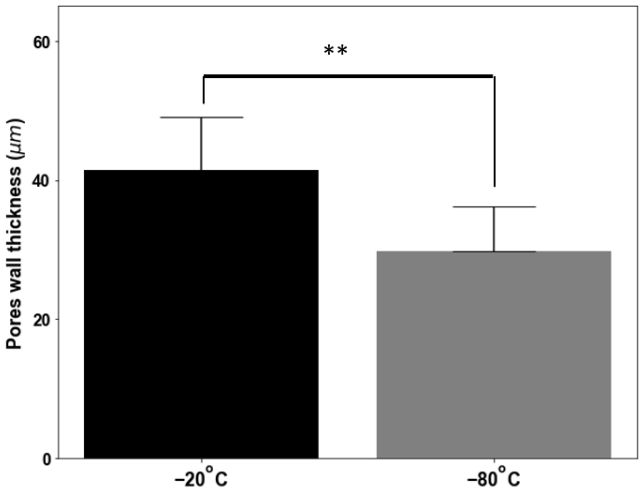

Figure 4.2. The average thickness of pore walls from 3D porous collagens fabricated using freezing temperatures of -20 ℃ and -80℃. The p-value is 0.0011 (**) for n=10 data in each group.

4.1.2. Mechanical Properties of 3D Collagen Layers

To determine the mechanical properties of the porous collagen scaffold, tensile stress-strain curves were obtained for two different scaffolds (1%w/v) fabricated using freezing temperatures of -20 ℃ and -80 ℃. According to the literature, stiffness for the collagens fabricated using a freezing temperature of -80 ℃ is less than for collagens fabricated using a freezing temperature of -80 ℃[190]. This is mainly attributed to the larger collagen fiber thicknesses of collagen scaffolds at -20 ℃

freezing temperature. At higher freezing temperatures, more collagen is expelled into the interstices, and thicker collage walls are created, leading to a higher Young's modulus[190]. **Figure 4-3** shows a comparison between Young's modulus of collagen scaffolds fabricated using two different freezing temperatures (-20 ℃ and -80 ℃). The stiffness of the collagen scaffold was significantly higher at -20 ℃ than the stiffness of the collagen scaffolds fabricated at a freezing temperature of -80 ℃.

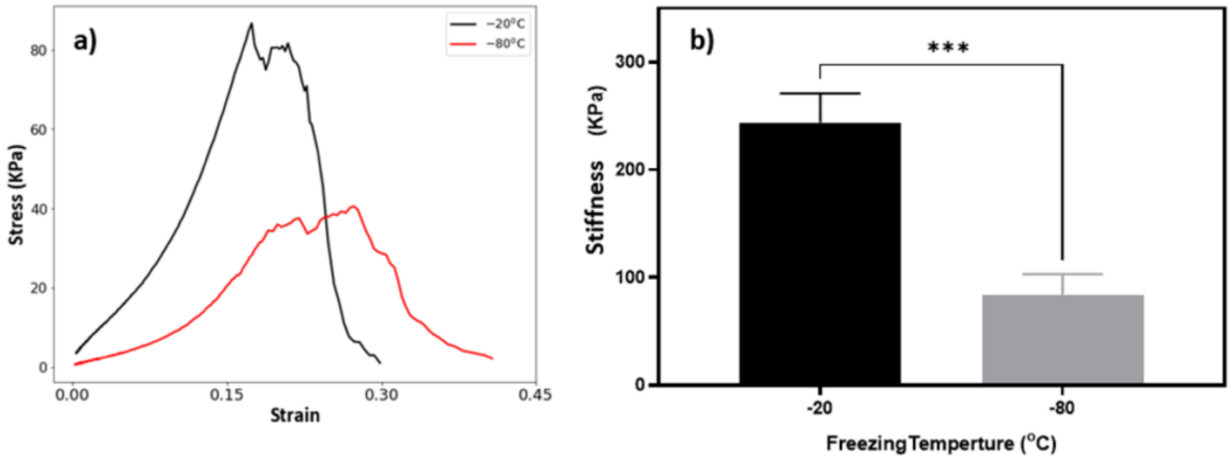

Figure 4-3. Mechanical properties of dry collagen scaffolds fabricated using freezing temperatures of -20 and -80 ℃: a) tensile stress vs. strain curves for the corresponding scaffolds, and b) stiffness in low strains. The p-value is 0.00021 (***) for n=3 data in each group.

Since the collagen scaffold will eventually be used for cell culture purposes and it will be hydrated, it is of utmost importance to determine the properties of the collagen in the actual cell-based tests. According to the previous studies, stiffness should decrease when the collagen gets hydrated[191]. As shown in **Figure 4-4**, the stiffness of the collagen scaffolds fabricated using a freezing

temperature of -20 ℃ decreases significantly when it is hydrated as compared to situations where collagen scaffolds are dry.

This is attributed to the existence of water molecules among the collagen fibrils decreasing the required stresses for collagen to stretch[191] (see **Figure 4-4b**). As shown in Figure 4-4a, hydrated collagen scaffold fracture occurs at higher strains (i.e., more ductility). This increase in ductility can be attributed to the existence of water molecules providing additional space for collagen fibrils to elongate[191].

According to Ryan and O'Brien, Young's modulus of the pure collagen in a hydrated situation was 41 KPa using a freezing temperature of -30 ℃[192].

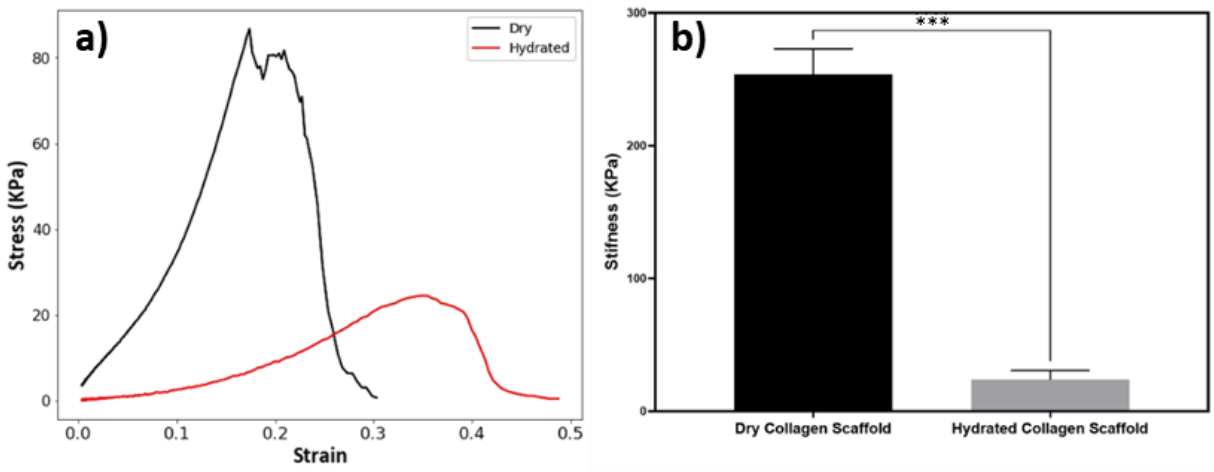

Figure 4-4. Mechanical properties of collagen scaffolds under tensile stress fabricated using a freezing temperature of -20 ℃ when the scaffold is dry or hydrated: a) tensile stress vs. strain curve, and b) stiffness in low strains. The p-value is 0.000392 (***) for n=3 data in each group.

As shown in **Figure 4-4**, collagen scaffolds in both dry and hydrated states show hyper-elastic behaviors, and the slope of the tensile stress vs. strain curves changes as strain increases. This J-shaped trend of the stress-strain curve is similar to what was observed in *in-vivo* soft tissues[193]. The stress-strain curve for the tissues is j-shaped because of their composition (i.e., collagen and elastin) and porous structure[43]. For example, the corresponding stress-strain curve for the blood vessels is J-shaped, protecting blood vessels against aneurysm formation[43]. In the J-shaped stress-strain curves, three major regions exist: i) the plateau region where the sample is not thoroughly straightened, ii) the elastic region where the resistance of tissue increased against the applied stress, and iii) the region of rupture where the tissue starts to tear[193].

4.1.3. Permeability of 3D Collagen Layers

The permeability of the 3D collagen scaffold is important because it affects cell penetration into the scaffold after culturing. Further, we are interested to see the difference between the permeability of 3D collagen scaffolds and 2D collagen films. This study will help us assess how using an integrated collagen-based microchannel containing 2D collagen film affects the penetration of flowing media into the 3D scaffolds (reported later in section 4.1.3.3). Performing the experiment explained in section 3.3.3, an average time of 11.88 ± 7.2 (n=3) minutes took so that 2 ml of water passed through the 3D collagen scaffold. Assuming that the flowrates were constant during the experiment, the permeability of our collagen scaffold was calculated to be $7.04 \times 10^{-12} \pm 4.5 \times 10^{-12} m^2$ based on Darcy's equation[194], which is in agreement with the literature. For instance, Varley et al. reported the permeability of their collagen-GAG scaffold

to be $5 \times 10^{-10}\ m^2$ (they fabricated their scaffolds using a collagen concentration of 0.5% and freezing temperature of -40 ℃)[194].

4.2. 2D Collagen Film Characterization

The 2D collagen film was characterized to investigate the thickness, stiffness, and permeability of the membrane. **Figure 4-5** shows the SEM images of the 2D collagen film inside the channel from the top and side view. As can be seen, the 2D film is a dense layer of collagen with few or no visible pores. Leclech et al. performed a thorough study on BM characteristics of the native tissues and reported very small pores in the orders of nanometers for BMs[56]. Therefore, one cannot expect to detect small pores similar to those in BMs using these SEM images (the BM pore size of the porcine aortic valve is about 30nm)[56].

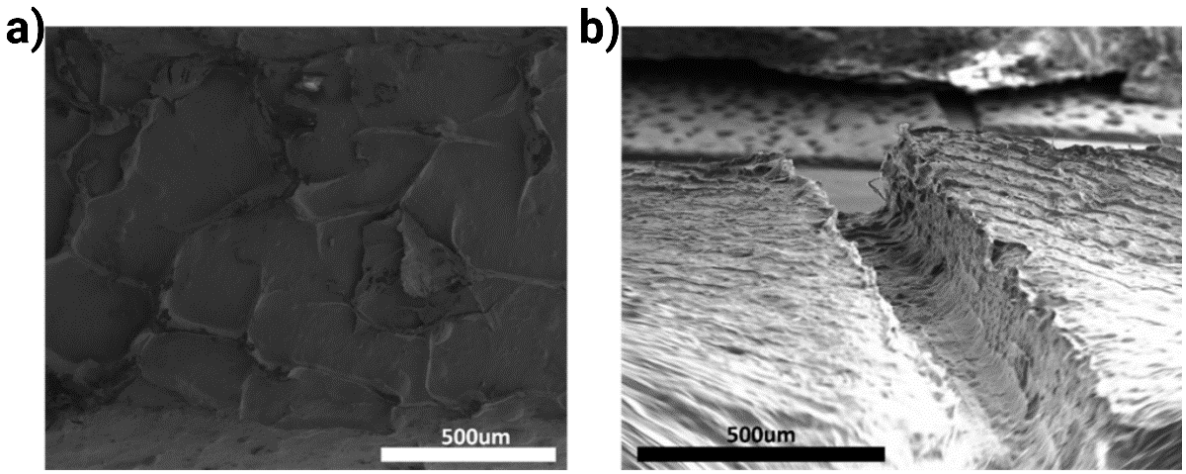

Figure 4-5. SEM images for a) the top surface view of the 2D collagen film and b) the side view of the 2D collagen film.

4.2.1. Film Thickness Measurement

Figure 4-6 shows the thickness of fabricated 2D collagen films using different amounts of collagen per surface area of the master mold. As shown, membranes in the range of 56.2 ± 21 to 209.5 ± 31 μm thickness could be fabricated, and a linear relationship between the amount of collagen used and the resulting film thickness was obtained.

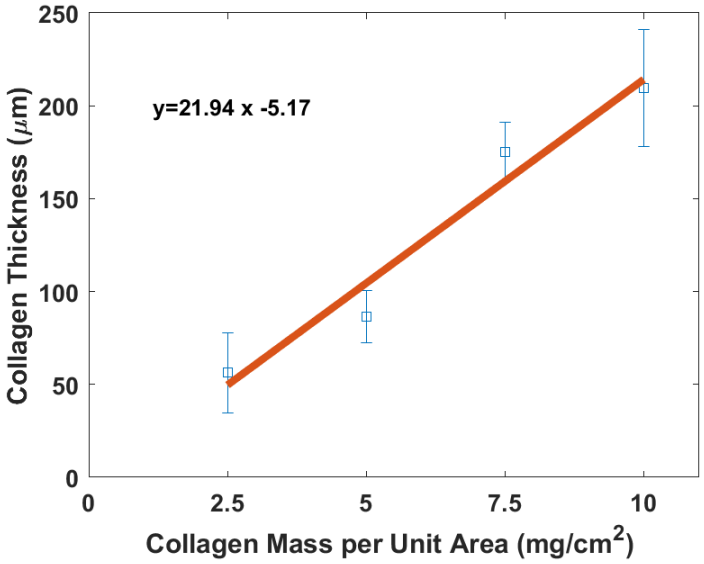

Figure 4-6. 2D collagen film thicknesses for different amounts of collagen consumed. The error bars correspond to the standard deviation of the measured thickness from three different replicates. The fitted line for the experimental run is shown in red.

Liu et al. obtained the collagen thickness of 5 μm to 25 μm, but they did not specify the amount of collagen that they used per unit area[195]. Further, Wolf et al. fabricated collagen-based films with

thickness values ranging from ~35μm to 180 μm when different collagen contents of collagen fibres and/or collagen powder were used (i.e., different collagen masses per unit area ranging from ~6.7 to 23.5 mg/cm^2)[196]. Although our thickness is far larger than the native BM (the thickness of the BM for the aorta is about 500nm [56]), due to the handling issues of the thinner films (having low mechanical properties and being very brittle), we could not reach a thinner film. For fabrication of the collagen microchannels, we used a volume of 5 mg/cm^2, because it was more straight-forward to handle during fabrication process.

4.2.2. Mechanical Properties of Collagen-based 2D Films

The mechanical properties of the collagen film as an analog to the BM can play an important role in the behavior of the cultured cells. Cells can behave in a different manner when cultured on collagen films with different stiffness values. Stress-strain curves for two series of experiments involving dry collagen film and wet collagen film are shown in **Figure 4-7a**. The 2D collagen film shows a brittle behavior in the dry state, meaning that they do not show plasticity (deformation) before rupture. However, when the collagen is hydrated, it shows entirely different behavior. The stiffness of the hydrated collagen is significantly smaller than that of the dry film (**Figure 4-7b**), but the hydrated scaffold shows ductile behavior meaning that it plasticizes and elongates before the rupture, which is attributed to the presence of water inside the hydrated film[191].

The reported stiffness values in **Figure 4-7b** are the slope of the stress-strain curves in Figure 4-7a at low strains. The corresponding stiffness of the *in-vivo* BMs at low strains is reported to be

between 2-5 MPa for renal tubules and venules[197], which is similar to the stiffness of the hydrated collagen films at small strains.

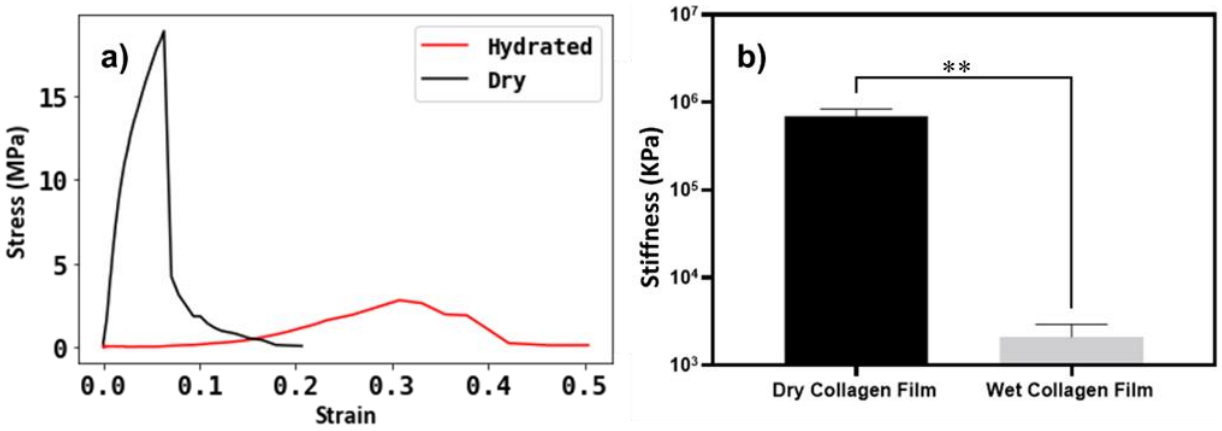

Figure 4-7. Mechanical properties for the 2D collagen film: a) The tensile stress vs. strain curves for 2D collagen films in dry and hydrated states, b) the stiffness of the 2D collagen films in low strains for the dry and the hydrated state. The p-value is 0.0047 (**) for n=3 data in each group.

Aizawa obtained Young's modulus of their dry collagen film with a thickness of 20 μm to be 500 MPa and 1250 MPa when 2D collagen films were fabricated based on nonparallel and parallel fibers, respectively [198]. These Young's modulus values were comparable to those we obtained for our collagen film, with a thickness of around 60 to 70 μm. Chen et al. reported the Young's modulus of their collagen-based membrane in a hydrated state with a thickness of 60 μm to be approximately 2 MPa, which is comparable to our measurements. However, their study did not disclose the weight of pure collagen used per unit area of their membrane [199].

4.2.3. Permeability of 2D Collagen Films

Similar to the test reported for permeability of the 3D collagen layer (section 4.1.1.3), hydraulic pressure was exerted on 2D films using liquid heights. No water passed through the 2D collagen film after one day when 2 ml of water was stored over the BM for two days. The impermeable behavior of the collagen film is similar to BMs in veins and blood arteries [200]. Artery walls are equipped with a water permeation barrier to enable the flowing of blood at high pressures without a noticeable amount of leak[200]. Although the extravasation (i.e., controlled transfer of solute and cells into the extravascular region) is partly blocked by BMs, the endothelial barriers play a more important role in controlling the permeability of vasculature (see section 2.1.1.2.1). In our collagen film, we were able to build an impermeable BM barrier that lines the interior surface of a microchannel with a square-shaped cross-section as a model for veins and small arteries.

4.3. Characterization of Integrated 3D/2D Collagen Layers

Once the 2D BM was fabricated and characterized, a 3D porous collagen scaffold with desired properties was constructed on top of the 2D collagen film to integrate the membrane into the 3D porous scaffold. **Figure 4-8a** and **4-8b** show the SEM images of the integrated 3D/2D collagen scaffolds. Further, **Figure 4-8c** and **4-8d** show the SEM images for collagen-based microchannels when no 2D BM is used.

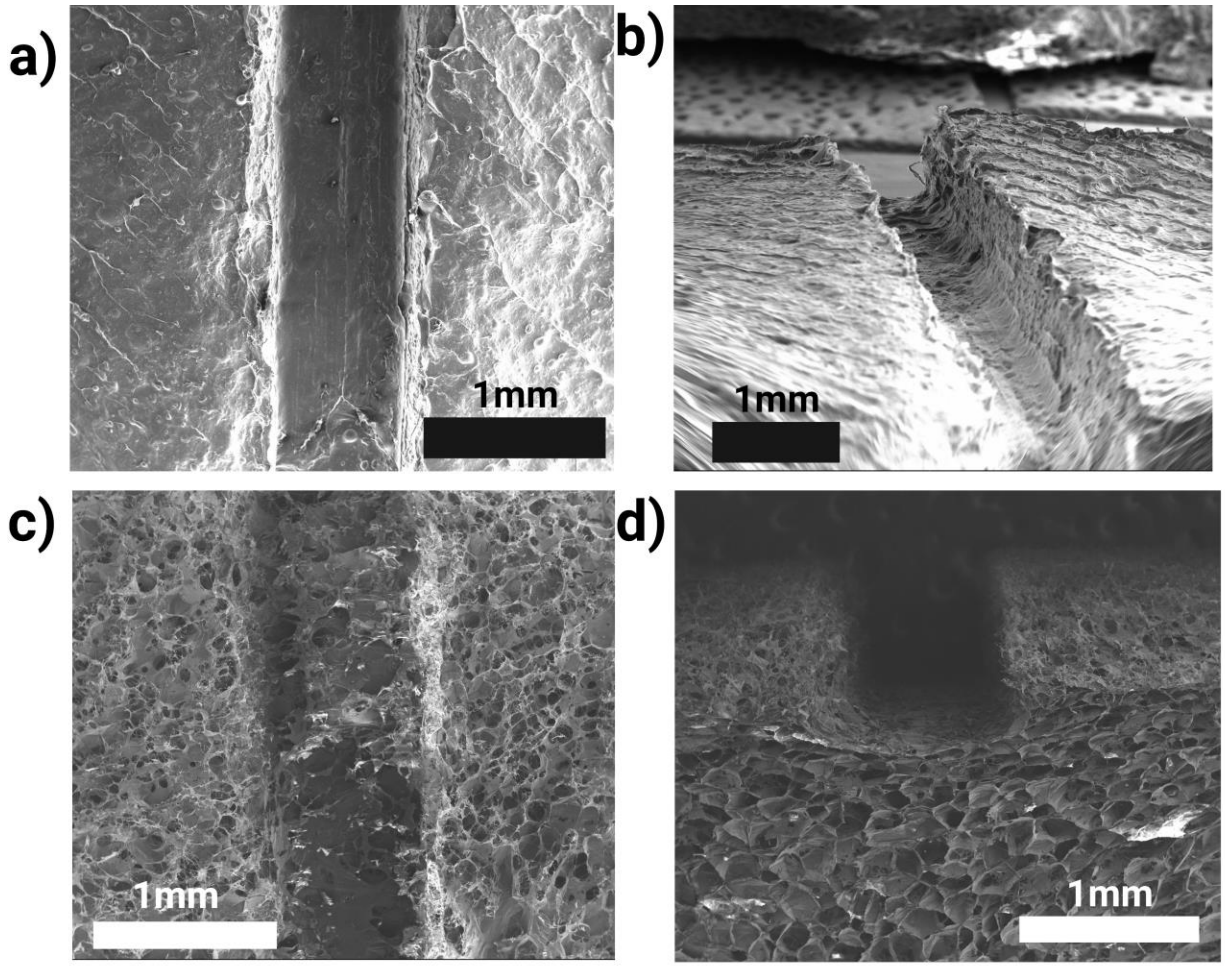

Figure 4-8. The SEM images from fabricated collagen scaffold containing microchannels and without integrating 2D collagen film and with integrating 2D collagen film: a) the top view when 2D collagen film is used, b) side view when 2D collagen film is used, c) the top view when 2D collagen film is not used, and d) side view when 2D collagen film is not used

As shown, the pores on the microchannels without 2D collagen films can result in the penetration of flowing media through the scaffold but using 2D BM can inhibit the permeation of flowing media from the collagen pores.

4.3.1. Test Structure Analysis

In fabricating channels within collagen, it is necessary to study the dimensions of the resulting structure against their corresponding molds to investigate the reliability of the fabrication method. This analysis helps to find a correlation between channel size in the mold vs. the corresponding microchannel sizes in the collagen scaffold (see **Figure 4-9**).

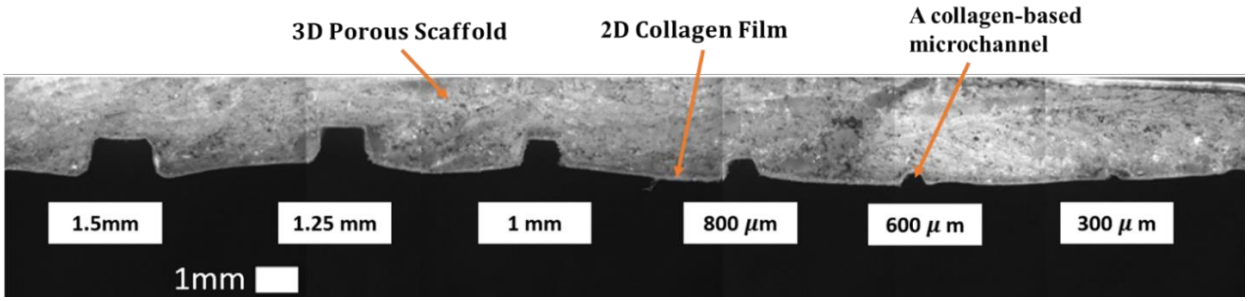

Figure 4-9. Microchannel test structures in 3D/2D integrated collagen scaffolds. The values in the white boxes correspond to the size of the designed square-shaped test structures in CAD design

Figure 4-10a and **4-10b** show the resulting width and height of the fabricated collagen-based microchannels for a variety of sizes vs. the respective width and height sizes of the corresponding molds. The error bars shown over the experimental data correspond to the standard deviation of measurement errors which were obtained by implementing three replicate experiments. As shown, lines were fitted on the collected data for microchannel widths and heights (i.e., red lines in **Figure 4-10**). As shown in **Figure 4-10a**, the fitted line almost matches the diagonal line $y = x$. As a result, the width of collagen microchannels is almost similar to the width of the corresponding molds.

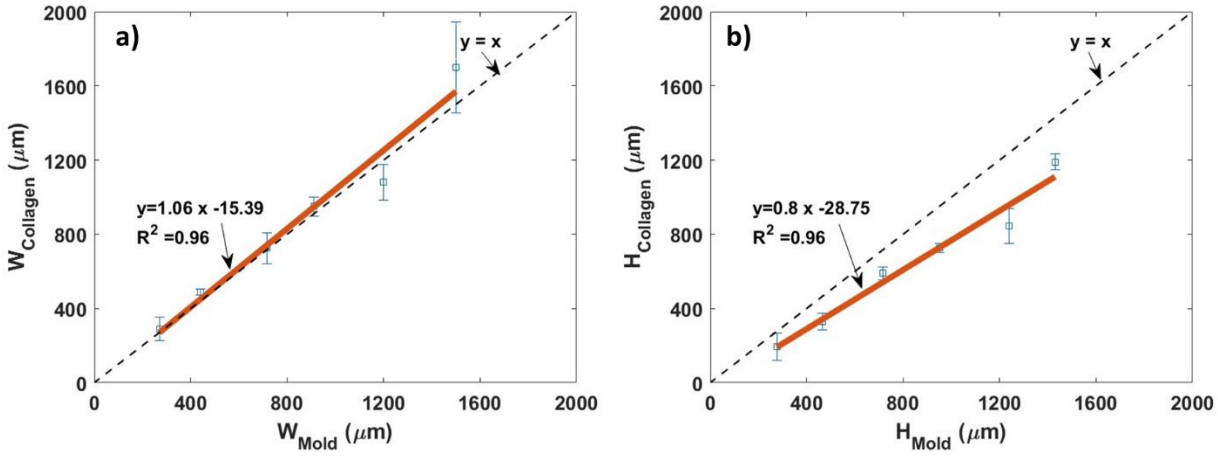

Figure 4-10. The resulting size of collagen microfluidic channels vs. the size of their corresponding molds: a) for the width measurements and b) for the height measurements.

As shown in **Figure 4-10b**, the slope of the line representing the relationship between the collagen microchannel height and the replica height is less than unity. We attributed this to the shrinkage of the collagen-based microchannels during the freeze-drying process. We obtained the shrinkage of the fabricated collagen microchannels in the structure by comparing the perimeter of the collagen-based microchannels and the perimeter of their corresponding molds. The perimeters also are important because they are related to the effective surface area of the corresponding collagen microchannels. **Figures 4-11a** and **4-11b** show a microchannel and its corresponding edges for the perimeter measurement based on the image analysis technique, respectively. The resulting perimeter plot for the collagen microchannels vs. the mold perimeters is shown in **Figure 4-11c.**

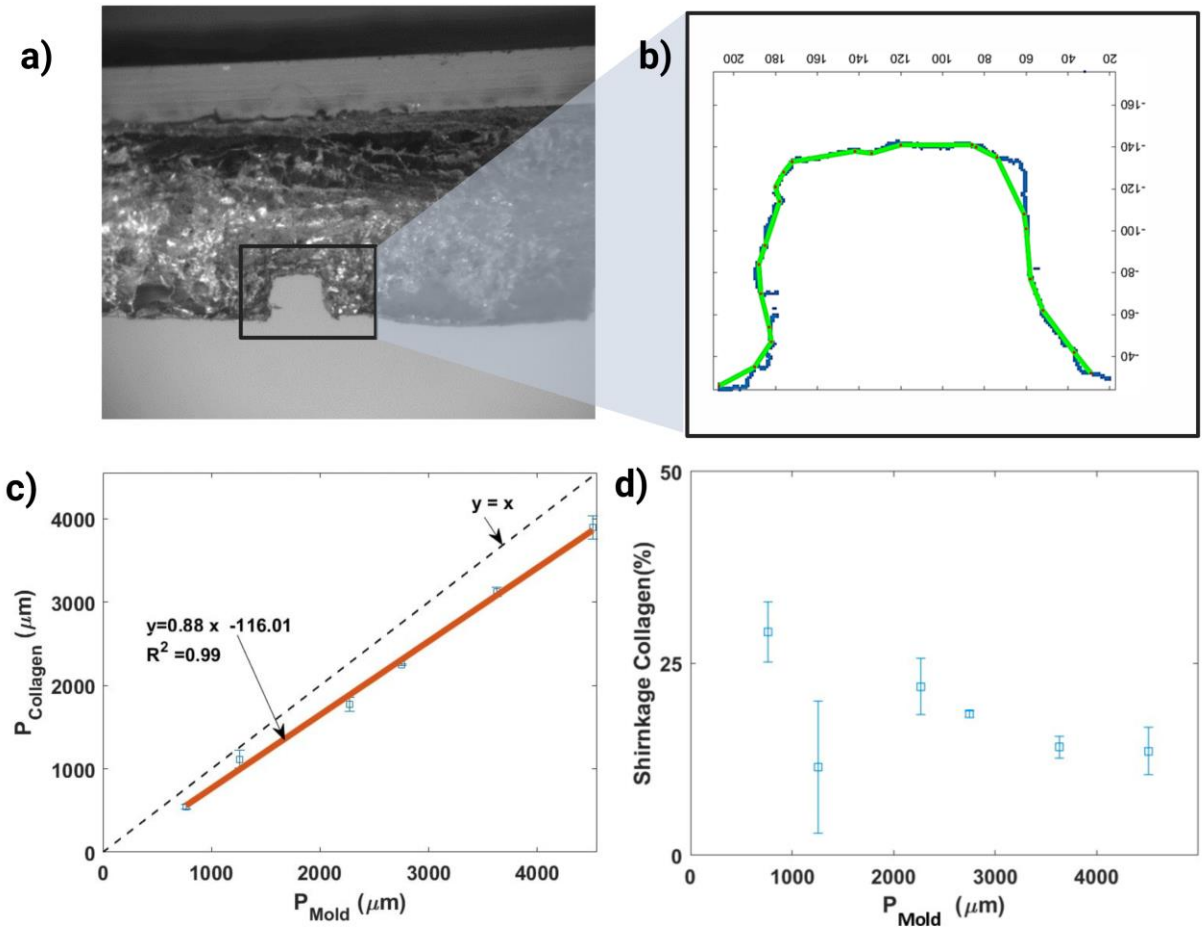

Figure 4-11. Shrinkage of the collagen microchannels in different test structures with different sizes. A) microscopic image of a microchannel (800μm width), b) image analysis from the corresponding channel, c) perimeter of the collagen channel compared to the PDMS master mold, and d) shrinkage of the collagen channels in each test structure size. Error bars show standard deviations of the experiments in three replicates.

As shown, the perimeters of the collagen scaffold microchannels are less than the corresponding perimeter of the molds. **Figure 4-11d** shows the shrinkage of the fabricated microchannels in the test structure patterns. The shrinkage values were calculated based on the percentage of change in the size of the collagen channels perimeters compared to their corresponding replica mold perimeters. As shown, the perimeter of the microchannels shrinks between 15-30% of their target

size. The shrinkage of collagen depends on the fabrication protocol which is used. According to Yeong et al., the shrinkage of the freeze-dried collagen (using 1% collagen slurry and a freezing temperature of -20 ℃) is about 17%[163]. Sachlos et al. reported the shrinkage of collagen scaffolds fabricated based on critical point drying to be ~70% when collagen slurry with a concentration of 1% is used. This shrinkage value decreased to ~55% when they used collagen slurry with higher collagen contents (≥2%w/v)[201].

4.3.2. Tensile Test: Bond Strength

As shown in **Figure 4-12a** and **4-12b,** the tensile test was carried out according to section 3.3.2 for the bond between two collagen substrates (i.e., 3D/2D substrate with an embedded microchannel bonded to a non-patterned 3D/2D substrate) and for the bond between 3D porous collagen scaffold and the 2D collagen film. As shown in **Figure 4-12c,** the bond strength between two substrates is significantly stronger than the bond between the 3D collagen scaffold and the 2D collagen film. The bond strength between two integrated substrates is ~1700 Pa, and the bond strength between the 3D scaffold and the 2D membrane is ~500 Pa. When bonding two different collagen substrates, each substrate is an integrated 3D/2D scaffold that has been bonded together via their 2D films. We used a 2% collagen slurry for bonding two substrates, which resulted in a relatively strong bond. The bond between 2D film and 3D scaffold, however, is not as strong as the bond between two substrates which could be due to: i) bonding between a collagen film and a porous surface having a less effective contact surface for bonding (see the SEM image in **Figure 4-13**), and ii) the bond between 2D and 3D scaffold is based on the 1% collagen slurry poured

over an already cured 2D film which has less collagen content and therefore results in the formation of collagen fibers with less density.

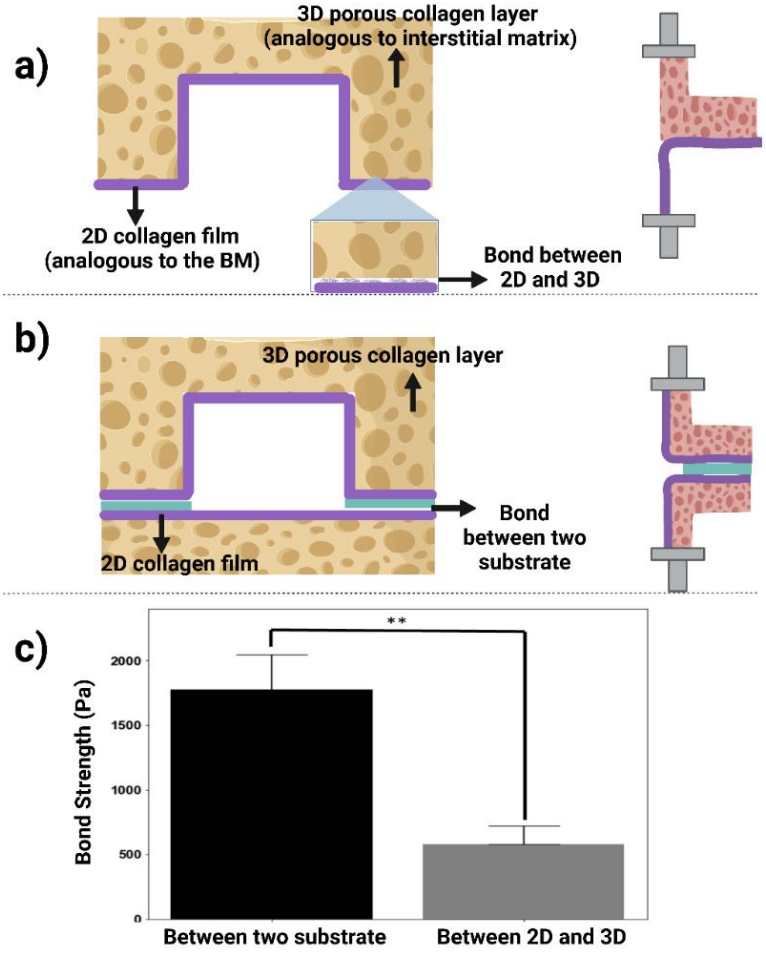

Figure 4-12. Measuring the strengths of the bonds between 3D collagen scaffold and 2D collagen film and between two integrated 2D/3D substrates. a) schematic representation of the bond between 3D and 2D collagen film and its corresponding measurement method, b) schematic representation of the bond between two collagen substrates and method used for bond strength quantification, and c) the quantified strengths of the bonds between panels *shown in a and b. The p-value is 0.0057 based on n=3 data in each group. (Panels a and b are created with BioRender.com)*

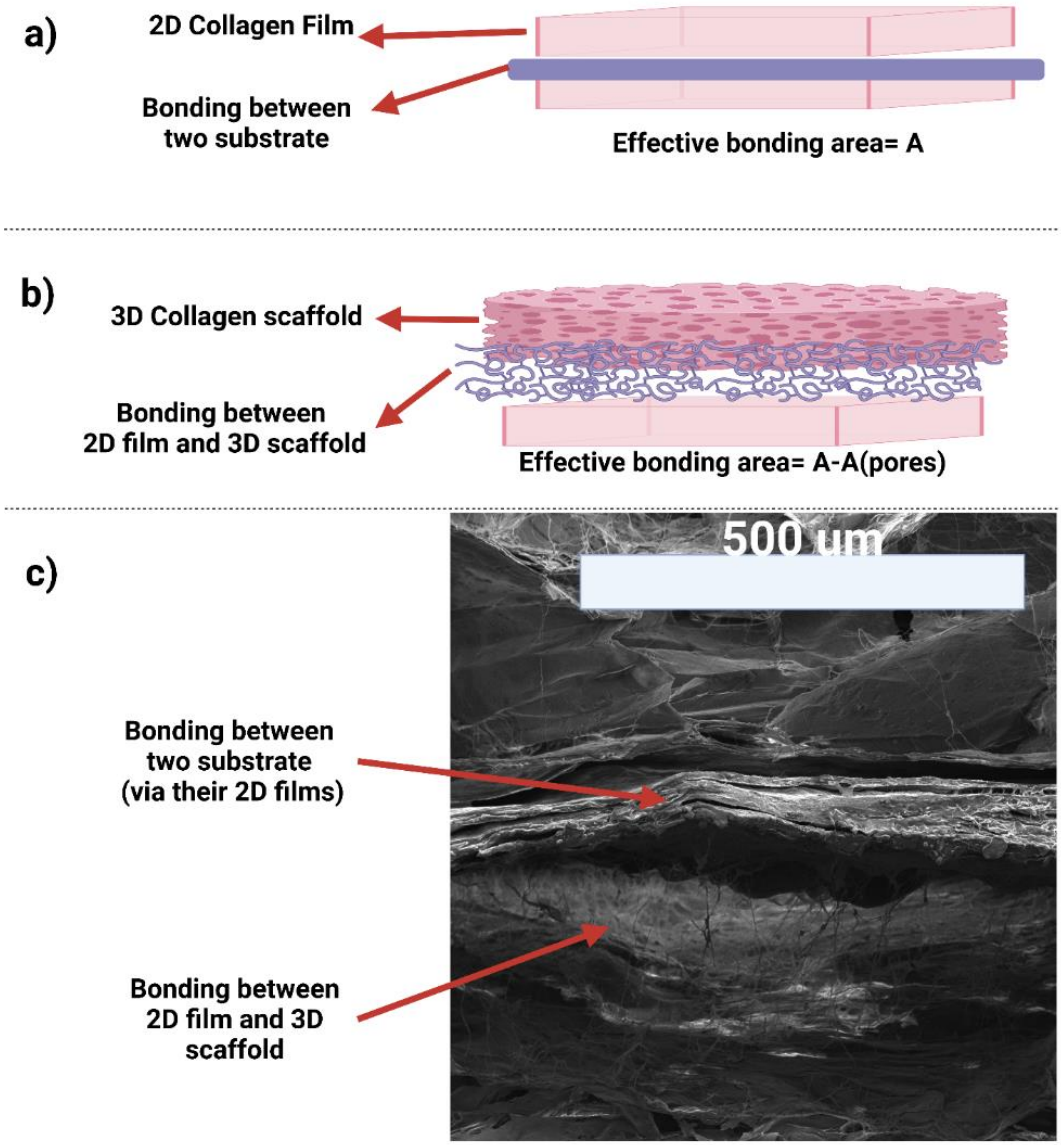

Figure 4-13. SEM image illustrating the bonds between two substrates and between 3D collagen scaffold and 2D collagen film. Each substrate is an integrated 3D/2D scaffold that has been bonded together via its 2D films. (Panels a and b are created with BioRender.com)

4.3.3. Leak Test

The result of the leak test for the final fabricated collagen-based microchannel is shown in **Figure 4-14**. As shown, for a channel lining with 2D film (integrated 3D/2D scaffold), the

corresponding volumetric inflow rates and outflow rates are similar in all of the inflow rates. When a 2D collagen scaffold is used during microfabrication, outflow rates are the same as the corresponding inflow rates regardless of the flow rate or residence time. This can be attributed to the existence of the 2D collagen film, which is not permeable. The same test was repeated for a situation where 2D collagen film was not used. As shown in **Figure 4-14**, in larger flow rates, the corresponding outflow rates for the media are the same as the corresponding inflow rates. This can be attributed to the relatively small fraction of flow rates that penetrated into the pores. In lower flow rates, the orders of magnitudes for the flow rate values of penetrated water were relatively similar to the corresponding inflow rates. The flow rates of penetrated water into the porous collagen were $0.48\pm0.1\ \frac{\mu l}{min}, 0.73 \pm 0.25 \frac{\mu l}{min}$, and $4.67\pm2.08\ \frac{\mu l}{min}$ for the corresponding inflow rates of $5\ \frac{\mu l}{min}$, $10\ \frac{\mu l}{min}$ and $100\ \frac{\mu l}{min}$, respectively. For the higher inflow rates, the penetrated flow rates of the fluid into the porous collagen could not be measured significantly. More accurate methods for quantifying flow rates should be used in the future to obtain the penetration flow rates appropriately.

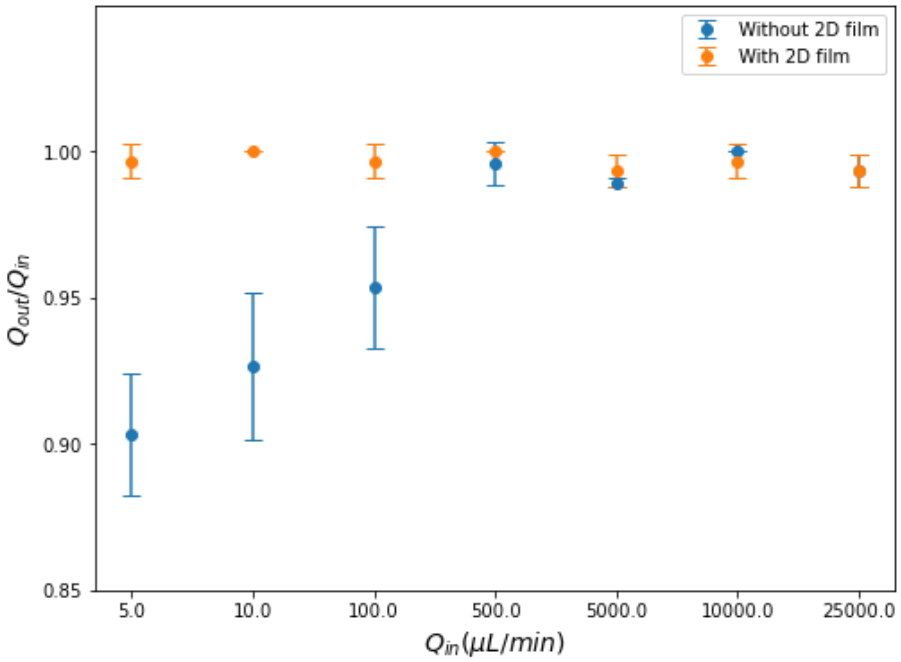

Figure 4-14. The ratio of outflow rates to the inflow rates, when the 2D collagen membrane was used (shown in orange color) and when no 2D BM was used (shown in blue color), in different inflow rates.

In our experiments, Reynold's number corresponding to the lowest flow rate that was tested (i.e., 5 $\mu l/min$) is 0.114. The Reynold's number corresponding to the largest values of tested flow rate (i.e., 25 ml/min) was calculated to be 567.

In the literature, a wide range of Reynold's numbers were reported for the veins. For example, Jayalalitha et al.[202] reported a Reynold's number of 7.28 in the veins, but a higher value was reported by Ostadfar[203] (i.e., Re=150). Further, Reynold's number for blood flows in arteries were reported to be between 110-850[203]. In our experiments, a flow rate of 5 ml/min (with corresponding Reynold's number of 110) could result in a similar dynamic condition as the flow of blood in the veins. Also, the flow rate values of 10 ml/min and 25 $\mu l/min$ with the

corresponding Reynold's number values of 226 and 567 can simulate the flow of blood in the arteries.

4.4. Closing Remarks

Our fabricated scaffold is made from pure collagen. Unlike techniques such as sacrificial molding[174], our fabrication technique for microstructures (i.e., freeze-drying of collagen slurry to form porous scaffold) and macrostructures (i.e., micropatterning the collagen by casting the slurry on a patterned mold and forming the channels) is not prone to contaminate the scaffold. Second, integration of 2D and 3D collagen layers is a novel aspect, simulating the structure of BMs in natural tissues, where the 2D collagen film act as a BM to preserve the integrity of channels while inhibiting leakage of flowing medium through the microchannel. Third, the integration and enclosure of microchannel is another novel aspect in the present thesis, allowing to test cells in the dynamic mode under a specific flow rate simulating the flow of blood in vessels.

Previous microfabrication techniques were mainly based on polymer-based systems, which needed surface modification to enable the anchorage of the cells[20,137,146,147,138–145]. However, our fabricated scaffold is completely made of natural biomimetic collagen. Thus, our collagen-based scaffold may serve as a more biologically relevant and more efficient biocompatible co-culture system for disease studies and drug discovery. To the best of our knowledge, this is the first study where enclosed microchannels were fabricated in a 3D porous collagen scaffold containing an integrated 2D collagen BM. The impermeability of the 2D collagen film makes it a great candidate as a BM analog for larger blood vessels such as veins and arteries, wherein the extent of the permeability is determined by the cultured cells rather than the corresponding BMs[200].

5. Thesis Summary and Future Works

5.1. Thesis summary

I have designed and developed a collagen-based engineered tissue containing microfluidic channels comprising a 3D porous scaffold and a 2D film. The 3D collagen scaffold act as an analog to the IM *in-vivo* environment, and the 2D collagen film acts as a BM analog. Channels with square-shaped cross-sections were fabricated with target sizes ranging from 300 μm to 1500 μm. The analysis of the corresponding collagen-based channels showed that the width of the final collagen channels is similar to their corresponding mold, but the height of the collagen microchannels was less than the height of the corresponding mold, which can be attributed to the height-wise shrinkage. The corresponding collagen microchannel's total perimeter (which is proportional to the area to which cells can anchor) was also measured for different channels. The perimeter of the collagen-based microchannels ranging from 600 μm to 4000 μm corresponded to a surface area between 0.06 m^2 to 0.4 m^2 (i.e., the effective surface area for cell culture). The perimeter of the corresponding collagen scaffolds was between 13% to 30% less than the perimeter of their corresponding molds. Similarly, this can be attributed to the shrinkage of collagen during the microfabrication of collagen-based microchannel.

The pore size distribution of the collagen scaffolds was obtained from SEM images for freezing temperatures of -20 ℃ and -80 ℃. The average pore size for the collagen scaffolds fabricated at -80 ℃ was smaller than the corresponding average pore size of fabricated collagen scaffolds at -20 ℃. Further, the stiffness for the collagen scaffolds fabricated using the freezing temperature of -20 ℃ was obtained more than the stiffness of the corresponding scaffolds fabricated using a

freezing temperature of -80 ℃. This is attributed to the thicker walls of the pores in collagen scaffolds fabricated using a freezing temperature of -80 ℃.

The integrated collagen-based scaffolds were then bonded to fabricate close microchannels. The fabricated microchannels were tested for leakage using a variety of flow rates (between 5 μL/min to 25 mL/min). The results showed that the volumetric outflow rates are similar to the corresponding inflow rates for all of the tested flow rates. This is because the 2D collagen film is not permeable. To investigate the effect of the 2D collagen film, we repeated the test against leakage when no 2D collagen films were used. Water permeation only could be measured for smaller inflow rates (i.e., flowrates$\leq 100\mu l/min$). When the inflow rate increased from $5\mu l/min$ to 100 μl/min, The flow rates of penetrated water into the porous collagen increased from 0.48 ± 0.1 $\mu l/min$ to 4.67 ± 2.08 $\mu l/min$, respectively.

5.2. Limitations and Future Works

My developed scaffold contained a straight microchannel wherein the interior surface of the microchannel was lined with 2D collagen film. In this thesis, I fabricated continuous 2D BMs mimicking the blood flow in the large veins. The continuous BMs do not allow the penetrations of fluid as they do not have pores, and the permeability is entirely governed by endothelial cells. *In-vivo*, the permeability of the BM varies in different blood vessel types (i.e., continuous and discontinuous BM). In future work, however, branched embedded microchannels can be designed wherein the 2D BM analogs have different permeability. By doing so, the permeability of the 2D

BMs can be engineered so that a similar permeability to the corresponding *in-vivo* BMs can be achieved.

BMs *in-vivo* mainly contains collagen type IV and laminin. Laminin accounts for initial BM formation and regulation of cell differentiation, whereas collagen type IV protects BMs against mechanical stresses. In the current study, I used collagen type I for the fabrication of BMs as this type of collagen is the most abundant collagen. In the future, laminin, in addition to collagen type IV, can be used in BM analog fabrication to mimic the composition of BMs *in-vivo* more precisely. Further, the composition of the 3D collagen scaffolds and 2D BMs can be designed so that their properties match the properties of the target tissue *in-vivo*.

The BM used in the current design of the scaffold enables future studying of co-culture cell systems since it provides a physical barrier between different cell types while potentially allowing the diffusion of gases and transmigration of signaling molecules. The porous collagen scaffold comprised micro-structured pores to which cells can adhere. The interconnected pores of our 3D scaffold served as pathways through which the transmigration of molecules could be implemented. Further, my final design containing the 3D porous scaffold and the 2D collagen film can be used as *in-vitro* analogs to study different vasculatures.

Last but not least, cell culture can be done in future studies to study the effect of shear stress on the cell behavior and interaction of different cells when they are co-cultured. Using engineered tissues containing 2D collagen film can be used for co-culture studies wherein a minimum interaction between the cells is desired. Further, collagen microchannels without BMs can be used for co-culture studies where the direct interaction of the cells is needed.

6. References

1. Dzobo, K.; Thomford, N. E.; Senthebane, D. A.; Shipanga, H.; Rowe, A.; Dandara, C.; Pillay, M.; Motaung, K. S. C. M., Advances in regenerative medicine and tissue engineering: innovation and transformation of medicine. *Stem cells international* **2018,** 2018.
2. Krafts, K. P., Tissue repair: The hidden drama. *Organogenesis* **2010,** 6, (4), 225-233.
3. Giannoudis, P. V.; Dinopoulos, H.; Tsiridis, E., Bone substitutes: an update. *Injury* **2005,** 36, (3), S20-S27.
4. Chen, Y.; Chen, S.; Kawazoe, N.; Chen, G., Promoted angiogenesis and osteogenesis by dexamethasone-loaded calcium phosphate nanoparticles/collagen composite scaffolds with microgroove networks. *Scientific reports* **2018,** 8, (1), 1-12.
5. Langer, R.; Vacanti, J., Tissue engineering, 1993. *Science* **1993,** 260, (5110).
6. Khademhosseini, A.; Vacanti, J. P.; Langer, R., Progress in tissue engineering. *Scientific American* **2009,** 300, (5), 64-71.
7. Sannino, A.; Madaghiele, M., Tuning the porosity of collagen-based scaffolds for use as nerve regenerative templates. *Journal of cellular plastics* **2009,** 45, (2), 137-155.
8. Cuadros, T. R.; Erices, A. A.; Aguilera, J. M., Porous matrix of calcium alginate/gelatin with enhanced properties as scaffold for cell culture. *Journal of the mechanical behavior of biomedical materials* **2015,** 46, 331-342.
9. Cho, S. H.; Oh, S. H.; Lee, J. H., Fabrication and characterization of porous alginate/polyvinyl alcohol hybrid scaffolds for 3D cell culture. *Journal of Biomaterials Science, Polymer Edition* **2005,** 16, (8), 933-947.
10. Ma, L.; Gao, C.; Mao, Z.; Zhou, J.; Shen, J.; Hu, X.; Han, C., Collagen/chitosan porous scaffolds with improved biostability for skin tissue engineering. *Biomaterials* **2003,** 24, (26), 4833-4841.
11. Vrana, N. E.; Builles, N.; Justin, V.; Bednarz, J.; Pellegrini, G.; Ferrari, B.; Damour, O.; Hulmes, D. J.; Hasirci, V., Development of a reconstructed cornea from collagen–chondroitin sulfate foams and human cell cultures. *Investigative ophthalmology & visual science* **2008,** 49, (12), 5325-5331.
12. Garcia-Fuentes, M.; Meinel, A. J.; Hilbe, M.; Meinel, L.; Merkle, H. P., Silk fibroin/hyaluronan scaffolds for human mesenchymal stem cell culture in tissue engineering. *Biomaterials* **2009,** 30, (28), 5068-5076.
13. Chen, C.; Zhao, M. l.; Zhang, R. k.; Lu, G.; Zhao, C. y.; Fu, F.; Sun, H. t.; Zhang, S.; Tu, Y.; Li, X. h., Collagen/heparin sulfate scaffolds fabricated by a 3D bioprinter improved mechanical properties and neurological function after spinal cord injury in rats. *Journal of Biomedical Materials Research Part A* **2017,** 105, (5), 1324-1332.
14. Thadavirul, N.; Pavasant, P.; Supaphol, P., Development of polycaprolactone porous scaffolds by combining solvent casting, particulate leaching, and polymer leaching techniques for bone tissue engineering. *Journal of Biomedical Materials Research Part A* **2014,** 102, (10), 3379-3392.
15. Barbanti, S.; Santos, A.; Zavaglia, C.; Duek, E., Porous and dense poly (L-lactic acid) and poly (D, L-lactic acid-co-glycolic acid) scaffolds: in vitro degradation in culture medium and

osteoblasts culture. *Journal of Materials Science: Materials in Medicine* **2004,** 15, (12), 1315-1321.
16. Arastouei, M.; Khodaei, M.; Atyabi, S. M.; Nodoushan, M. J., The in-vitro biological properties of 3D printed poly lactic acid/akermanite composite porous scaffold for bone tissue engineering. *Materials Today Communications* **2021,** 27, 102176.
17. Clar, C.; Cummins, E.; McIntyre, L.; Thomas, S.; Lamb, J.; Bain, L.; Jobanputra, P.; Waugh, N., Clinical and cost-effectiveness of autologous chondrocyte implantation for cartilage defects in knee joints: systematic review and economic evaluation. *NIHR Health Technology Assessment programme: Executive Summaries* **2005**.
18. MacNeil, S., Progress and opportunities for tissue-engineered skin. *Nature* **2007,** 445, (7130), 874-880.
19. Weinberg, C. B.; Bell, E., A blood vessel model constructed from collagen and cultured vascular cells. *Science* **1986,** 231, (4736), 397-400.
20. Paukshto, M. V.; Cooke, J. P.; Zaitseva, T. S.; Huang, N. F.; Fuller, G. G.; Martin, G. R. Graft for Directed Vascular and
Lymphatic Regeneration and
Methods to Guide Endothelial Cell Assembly. 1751-6161, 2014.
21. Katsumi Mochitate, T.-s. Method of preparing basement membrane, method of constructing basement membrane specimen, reconstituted artificial tissue using the basement membrane specimen and process for producing the same. US 2007.0122796A1 2007.
22. Vatine, G. D.; Barrile, R.; Workman, M. J.; Sances, S.; Barriga, B. K.; Rahnama, M.; Barthakur, S.; Kasendra, M.; Lucchesi, C.; Kerns, J., Human iPSC-derived blood-brain barrier chips enable disease modeling and personalized medicine applications. *Cell stem cell* **2019,** 24, (6), 995-1005. e6.
23. Zeng, J.; Sasaki, N.; Correia, C. R.; Mano, J. F.; Matsusaki, M., Fabrication of Artificial Nanobasement Membranes for Cell Compartmentalization in 3D Tissues. *Small* **2020,** 16, (24), 1907434.
24. Tasiopoulos, C. P.; Gustafsson, L.; van der Wijngaart, W.; Hedhammar, M., Fibrillar Nanomembranes of Recombinant Spider Silk Protein Support Cell Co-culture in an In Vitro Blood Vessel Wall Model. *ACS Biomaterials Science & Engineering* **2021,** 7, (7), 3332-3339.
25. Dohle, E.; Singh, S.; Nishigushi, A.; Fischer, T.; Wessling, M.; Möller, M.; Sader, R.; Kasper, J.; Ghanaati, S.; Kirkpatrick, C. J., Human Co-and triple-culture model of the alveolar-capillary barrier on a basement membrane mimic. *Tissue Engineering Part C: Methods* **2018,** 24, (9), 495-503.
26. Zeng, J.; Matsusaki, M., Analysis of Thickness and Roughness Effects of Artificial Basement Membranes on Endothelial Cell Functions. *Analytical Sciences* **2020**, 20SCP10.
27. Chen, S.; Kawazoe, N.; Chen, G., Biomimetic assembly of vascular endothelial cells and muscle cells in microgrooved collagen porous scaffolds. *Tissue Engineering Part C: Methods* **2017,** 23, (6), 367-376.
28. Yeong, W. Y.; Chua, C. K.; Leong, K. F.; Chandrasekaran, M.; Lee, M. W., Indirect fabrication of collagen scaffold based on inkjet printing technique. *Rapid Prototyping Journal* **2006**.
29. Versteegden, L. R.; Van Kampen, K. A.; Janke, H. P.; Tiemessen, D. M.; Hoogenkamp, H. R.; Hafmans, T. G.; Roozen, E. A.; Lomme, R. M.; van Goor, H.; Oosterwijk, E., Tubular

collagen scaffolds with radial elasticity for hollow organ regeneration. *Acta biomaterialia* **2017,** 52, 1-8.
30. Gleeson, J. P.; Levingstone, T. J.; O ' Brien, F. J. LAYERED COLLAGEN AND HA SCAFFOLD SUITABLE FOR OSTEOCHONDRAL REPAIR. US 10 , 052 , 407 B2, 2018.
31. Czernuszka, J. T.; Sachlos, E.; Derby, B.; Reis, N. A. E.; Ainsley, C. C. Tissue engineering scaffolds. US 2004/0258729 A1, 2004.
32. Neumann, T. Method for Creating Perfusable Microvessel Systems. 2008.
33. Zheng, Y.; Chen, J.; Craven, M.; Choi, N. W.; Totorica, S.; Diaz-Santana, A.; Kermani, P.; Hempstead, B.; Fischbach-Teschl, C.; López, J. A., In vitro microvessels for the study of angiogenesis and thrombosis. *Proceedings of the national academy of sciences* **2012,** 109, (24), 9342-9347.
34. Chrobak, K. M.; Potter, D. R.; Tien, J., Formation of perfused, functional microvascular tubes in vitro. *Microvascular research* **2006,** 71, (3), 185-196.
35. Romero-Ortega, M.; Galvan-Garcia, P., A biomimetic synthetic nerve implant. In Google Patents: 2007.
36. Chen, C. S.; Baranski, J. D.; Chaturvedi, R.; Yang, M. T.; Stevens, K.; Bhatia, S., Biomaterials for enhanced implant-host integration. In Google Patents: 2019.
37. Mao, J., Shape and dimension maintenance of soft tissue grafts by stem cells. In Google Patents: 2008.
38. Ingber, D. E.; Van der Meer, A.; Herland, A., Devices for simulating a function of a tissue and methods of use and manufacturing thereof. In Google Patents: 2018.
39. Li, G.; Han, Q.; Lu, P.; Zhang, L.; Zhang, Y.; Chen, S.; Zhang, P.; Zhang, L.; Cui, W.; Wang, H., Construction of dual-biofunctionalized chitosan/collagen scaffolds for simultaneous neovascularization and nerve regeneration. *Research* **2020,** 2020.
40. Sloviková, A.; Vojtová, L.; Jančař, J., Preparation and modification of collagen-based porous scaffold for tissue engineering. *Chemical Papers* **2008,** 62, (4), 417-422.
41. Haldar, S.; Sharma, A.; Gupta, S.; Chauhan, S.; Roy, P.; Lahiri, D., Bioengineered smart trilayer skin tissue substitute for efficient deep wound healing. *Materials Science and Engineering: C* **2019,** 105, 110140.
42. Frantz, C.; Stewart, K. M.; Weaver, V. M., The extracellular matrix at a glance. *Journal of cell science* **2010,** 123, (24), 4195-4200.
43. Rapoport, H. S.; Fish, J.; Basu, J.; Campbell, J.; Genheimer, C.; Payne, R.; Jain, D., Construction of a tubular scaffold that mimics J-shaped stress/strain mechanics using an innovative electrospinning technique. *Tissue Engineering Part C: Methods* **2012,** 18, (8), 567-574.
44. Laurila, P.; Leivo, I., Basement membrane and interstitial matrix components form separate matrices in heterokaryons of PYS-2 cells and fibroblasts. *Journal of cell science* **1993,** 104, (1), 59-68.
45. Alberts, B.; Johnson, A.; Lewis, J.; Raff, M.; Roberts, K.; Walter, P., Blood vessels and endothelial cells. In *Molecular Biology of the Cell. 4th edition*, Garland Science: 2002.
46. Nikolova, G.; Strilic, B.; Lammert, E., The vascular niche and its basement membrane. *Trends in cell biology* **2007,** 17, (1), 19-25.

47. Hallmann, R.; Hannocks, M.-J.; Song, J.; Zhang, X.; Di Russo, J.; Luik, A.-L.; Burmeister, M.; Gerwien, H.; Sorokin, L., The role of basement membrane laminins in vascular function. *The International Journal of Biochemistry & Cell Biology* **2020,** 127, 105823.
48. Brooke, B. S.; Karnik, S. K.; Li, D. Y., Extracellular matrix in vascular morphogenesis and disease: structure versus signal. *Trends in cell biology* **2003,** 13, (1), 51-56.
49. Wolf, K.; Alexander, S.; Schacht, V.; Coussens, L. M.; von Andrian, U. H.; van Rheenen, J.; Deryugina, E.; Friedl, P. In *Collagen-based cell migration models in vitro and in vivo*, Seminars in cell & developmental biology, 2009; Elsevier: 2009; pp 931-941.
50. Sun, B., The mechanics of fibrillar collagen extracellular matrix. *Cell Reports Physical Science* **2021,** 2, (8), 100515.
51. Oh, S. H.; Park, I. K.; Kim, J. M.; Lee, J. H., In vitro and in vivo characteristics of PCL scaffolds with pore size gradient fabricated by a centrifugation method. *Biomaterials* **2007,** 28, (9), 1664-1671.
52. Engler, A. J.; Sen, S.; Sweeney, H. L.; Discher, D. E., Matrix elasticity directs stem cell lineage specification. *Cell* **2006,** 126, (4), 677-689.
53. Sekiguchi, R.; Yamada, K. M., Basement membranes in development and disease. *Current topics in developmental biology* **2018,** 130, 143-191.
54. Jayadev, R.; Sherwood, D. R., Basement membranes. *Current Biology* **2017,** 27, (6), R207-R211.
55. Khoshnoodi, J.; Pedchenko, V.; Hudson, B. G., Mammalian collagen IV. *Microscopy research and technique* **2008,** 71, (5), 357-370.
56. Leclech, C.; Natale, C. F.; Barakat, A. I., The basement membrane as a structured surface–role in vascular health and disease. *Journal of Cell Science* **2020,** 133, (18), jcs239889.
57. Liliensiek, S. J.; Nealey, P.; Murphy, C. J., Characterization of endothelial basement membrane nanotopography in rhesus macaque as a guide for vessel tissue engineering. *Tissue Engineering Part A* **2009,** 15, (9), 2643-2651.
58. Cai, A.; Chatziantoniou, C.; Calmont, A., Vascular permeability: regulation pathways and role in kidney diseases. *Nephron* **2021,** 145, (3), 297-310.
59. Claesson-Welsh, L.; Dejana, E.; McDonald, D. M., Permeability of the endothelial barrier: identifying and reconciling controversies. *Trends in molecular medicine* **2021,** 27, (4), 314-331.
60. Wettschureck, N.; Strilic, B.; Offermanns, S., Passing the vascular barrier: endothelial signaling processes controlling extravasation. *Physiological reviews* **2019,** 99, (3), 1467-1525.
61. Brody, S.; Anilkumar, T.; Liliensiek, S.; Last, J. A.; Murphy, C. J.; Pandit, A., Characterizing nanoscale topography of the aortic heart valve basement membrane for tissue engineering heart valve scaffold design. *Tissue engineering* **2006,** 12, (2), 413-421.
62. Setyawati, M. I.; Tay, C. Y.; Docter, D.; Stauber, R. H.; Leong, D. T., Understanding and exploiting nanoparticles' intimacy with the blood vessel and blood. *Chemical Society Reviews* **2015,** 44, (22), 8174-8199.
63. Siperstein, M.; Unger, R. H.; Madison, L., Studies of muscle capillary basement membranes in normal subjects, diabetic, and prediabetic patients. *The Journal of clinical investigation* **1968,** 47, (9), 1973-1999.

64. FEINGOLD, K. R.; BROWNER, W. S.; SIPERSTEIN, M. D., Prospective studies of muscle capillary basement membrane width in prediabetics. *The Journal of Clinical Endocrinology & Metabolism* **1989,** 69, (4), 784-789.
65. Klein, R. F.; Feingold, K. R.; Morgan, C.; Stern, W. H.; Siperstein, M. P., Relationship of muscle capillary basement membrane thickness and diabetic retinopathy. *Diabetes Care* **1987,** 10, (2), 195-199.
66. Merimee, T. J.; Siperstein, M. D.; Hall, J. D.; Fineberg, S. E., Capillary basement membrane structure: a comparative study of diabetics and sexual ateliotic dwarfs. *The Journal of Clinical Investigation* **1970,** 49, (12), 2161-2164.
67. Begieneman, M. P.; Van De Goot, F. R.; Krijnen, P. A.; Fritz, J.; Paulus, W. J.; Spreeuwenberg, M. D.; Van Hinsbergh, V. W.; Niessen, H. W., The basement membrane of intramyocardial capillaries is thickened in patients with acute myocardial infarction. *Journal of vascular research* **2010,** 47, (1), 54-60.
68. Holm Nielsen, S.; Tengryd, C.; Edsfeldt, A.; Brix, S.; Genovese, F.; Bengtsson, E.; Karsdal, M.; Leeming, D. J.; Nilsson, J.; Goncalves, I., Markers of basement membrane remodeling are associated with higher mortality in patients with known atherosclerosis. *Journal of the American Heart Association* **2018,** 7, (21), e009193.
69. Perlmutter, L. S.; Chui, H. C., Microangiopathy, the vascular basement membrane and Alzheimer's disease: a review. *Brain research bulletin* **1990,** 24, (5), 677-686.
70. Buee, L.; Hof, P. R.; Delacourte, A., Brain microvascular changes in Alzheimer's disease and other dementias a. *Annals of the New York Academy of Sciences* **1997,** 826, (1), 7-24.
71. Little, K.; Llorián-Salvador, M.; Scullion, S.; Hernández, C.; Simó-Servat, O.; Del Marco, A.; Bosma, E.; Vargas-Soria, M.; Carranza-Naval, M. J.; Van Bergen, T., Common pathways in dementia and diabetic retinopathy: understanding the mechanisms of diabetes-related cognitive decline. *Trends in Endocrinology & Metabolism* **2022,** 33, (1), 50-71.
72. Xu, L.; Nirwane, A.; Yao, Y., Basement membrane and blood–brain barrier. *Stroke and vascular neurology* **2019,** 4, (2).
73. Iozzo, R. V., Basement membrane proteoglycans: from cellar to ceiling. *Nature reviews Molecular cell biology* **2005,** 6, (8), 646-656.
74. Savige, J.; Liu, J.; DeBuc, D. C.; Handa, J. T.; Hageman, G. S.; Wang, Y. Y.; Parkin, J. D.; Vote, B.; Fassett, R.; Sarks, S., Retinal basement membrane abnormalities and the retinopathy of Alport syndrome. *Investigative ophthalmology & visual science* **2010,** 51, (3), 1621-1627.
75. Kashtan, C. E.; Kleppel, M. M.; Butkowski, R. J.; Michael, A. F.; Fish, A. J., Alport syndrome, basement membranes and collagen. *Pediatric Nephrology* **1990,** 4, (5), 523-532.
76. Chakrabarti, S.; Cherian, P. V.; Sima, A. A., The effect of acarbose on diabetes-and age-related basement membrane thickening in retinal capillaries of the BBW-rat. *Diabetes research and clinical practice* **1993,** 20, (2), 123-128.
77. Brito, P. L.; Fioretto, P.; Drummond, K.; Kim, Y.; Steffes, M. W.; Basgen, J. M.; Sisson-Ross, S.; Mauer, M., Proximal tubular basement membrane width in insulin-dependent diabetes mellitus. *Kidney international* **1998,** 53, (3), 754-761.
78. Van Agtmael, T.; Bruckner-Tuderman, L., Basement membranes and human disease. *Cell and tissue research* **2010,** 339, (1), 167-188.

79. Passaro, D.; Di Tullio, A.; Abarrategi, A.; Rouault-Pierre, K.; Foster, K.; Ariza-McNaughton, L.; Montaner, B.; Chakravarty, P.; Bhaw, L.; Diana, G., Increased vascular permeability in the bone marrow microenvironment contributes to disease progression and drug response in acute myeloid leukemia. *Cancer cell* **2017,** 32, (3), 324-341. e6.
80. Novosel, E. C.; Kleinhans, C.; Kluger, P. J., Vascularization is the key challenge in tissue engineering. *Advanced drug delivery reviews* **2011,** 63, (4-5), 300-311.
81. Phelps, E. A.; García, A. J., Engineering more than a cell: vascularization strategies in tissue engineering. *Current opinion in biotechnology* **2010,** 21, (5), 704-709.
82. Burton, A. C., Relation of structure to function of the tissues of the wall of blood vessels. *Physiological reviews* **1954,** 34, (4), 619-642.
83. Koeppen, B. M.; Stanton, B. A., *Berne and levy physiology e-book*. Elsevier Health Sciences: 2017.
84. Schöneberg, J.; De Lorenzi, F.; Theek, B.; Blaeser, A.; Rommel, D.; Kuehne, A. J.; Kießling, F.; Fischer, H., Engineering biofunctional in vitro vessel models using a multilayer bioprinting technique. *Scientific reports* **2018,** 8, (1), 1-13.
85. Potente, M.; Gerhardt, H.; Carmeliet, P., Basic and therapeutic aspects of angiogenesis. *Cell* **2011,** 146, (6), 873-887.
86. Carmeliet, P., Mechanisms of angiogenesis and arteriogenesis. *Nature medicine* **2000,** 6, (4), 389-395.
87. Rouwkema, J.; Rivron, N. C.; van Blitterswijk, C. A., Vascularization in tissue engineering. *Trends in biotechnology* **2008,** 26, (8), 434-441.
88. Bridges, E.; Oon, C. E.; Harris, A., Notch regulation of tumor angiogenesis. *Future Oncology* **2011,** 7, (4), 569-588.
89. Sharma, A.; Brand, D.; Fairbank, J.; Ye, H.; Lavy, C.; Czernuszka, J., A self-organising biomimetic collagen/nano-hydroxyapatite-glycosaminoglycan scaffold for spinal fusion. *Journal of materials science* **2017,** 52, (21), 12574-12592.
90. Akhmanova, M.; Osidak, E.; Domogatsky, S.; Rodin, S.; Domogatskaya, A., Physical, spatial, and molecular aspects of extracellular matrix of in vivo niches and artificial scaffolds relevant to stem cells research. *Stem cells international* **2015,** 2015.
91. Hynes, R. O., Integrins: versatility, modulation, and signaling in cell adhesion. *Cell* **1992,** 69, (1), 11-25.
92. Meyer, M., Processing of collagen based biomaterials and the resulting materials properties. *Biomedical engineering online* **2019,** 18, (1), 1-74.
93. Heino, J., The collagen family members as cell adhesion proteins. *Bioessays* **2007,** 29, (10), 1001-1010.
94. Ferreira, A. M.; Gentile, P.; Chiono, V.; Ciardelli, G., Collagen for bone tissue regeneration. *Acta biomaterialia* **2012,** 8, (9), 3191-3200.
95. Jiang, S.; Lyu, C.; Zhao, P.; Li, W.; Kong, W.; Huang, C.; Genin, G. M.; Du, Y., Cryoprotectant enables structural control of porous scaffolds for exploration of cellular mechano-responsiveness in 3D. *Nature communications* **2019,** 10, (1), 1-14.
96. Costantini, M.; Barbetta, A., Gas foaming technologies for 3D scaffold engineering. In *Functional 3D Tissue Engineering Scaffolds*, Elsevier: 2018; pp 127-149.

97. Sin, D.; Miao, X.; Liu, G.; Wei, F.; Chadwick, G.; Yan, C.; Friis, T., Polyurethane (PU) scaffolds prepared by solvent casting/particulate leaching (SCPL) combined with centrifugation. *Materials Science and Engineering: C* **2010,** 30, (1), 78-85.
98. Matthews, J. A.; Boland, E. D.; Wnek, G. E.; Simpson, D. G.; Bowlin, G. L., Electrospinning of collagen type II: a feasibility study. *Journal of bioactive and compatible polymers* **2003,** 18, (2), 125-134.
99. Boland, E. D.; Matthews, J. A.; Pawlowski, K. J.; Simpson, D. G.; Wnek, G. E.; Bowlin, G. L., Electrospinning collagen and elastin: preliminary vascular tissue engineering. *Front Biosci* **2004,** 9, (1422), e32.
100. O'Brien, F. J.; Harley, B. A.; Yannas, I. V.; Gibson, L., Influence of freezing rate on pore structure in freeze-dried collagen-GAG scaffolds. *Biomaterials* **2004,** 25, (6), 1077-1086.
101. Haugh, M. G.; Murphy, C. M.; O'Brien, F. J., Novel freeze-drying methods to produce a range of collagen–glycosaminoglycan scaffolds with tailored mean pore sizes. *Tissue Engineering Part C: Methods* **2010,** 16, (5), 887-894.
102. Tierney, C. M.; Haugh, M. G.; Liedl, J.; Mulcahy, F.; Hayes, B.; O'Brien, F. J., The effects of collagen concentration and crosslink density on the biological, structural and mechanical properties of collagen-GAG scaffolds for bone tissue engineering. *Journal of the mechanical behavior of biomedical materials* **2009,** 2, (2), 202-209.
103. Loh, Q. L.; Choong, C., Three-dimensional scaffolds for tissue engineering applications: role of porosity and pore size. **2013**.
104. Suesca, E.; Dias, A.; Braga, M.; De Sousa, H.; Fontanilla, M., Multifactor analysis on the effect of collagen concentration, cross-linking and fiber/pore orientation on chemical, microstructural, mechanical and biological properties of collagen type I scaffolds. *Materials Science and Engineering: C* **2017,** 77, 333-341.
105. Jeong, L.; Yeo, I.-S.; Kim, H. N.; Yoon, Y. I.; Jung, S. Y.; Min, B.-M.; Park, W. H., Plasma-treated silk fibroin nanofibers for skin regeneration. *International journal of biological macromolecules* **2009,** 44, (3), 222-228.
106. Unger, R. E.; Wolf, M.; Peters, K.; Motta, A.; Migliaresi, C.; Kirkpatrick, C. J., Growth of human cells on a non-woven silk fibroin net: a potential for use in tissue engineering. *Biomaterials* **2004,** 25, (6), 1069-1075.
107. Wray, L.; Rnjak-Kovacina, J.; Kaplan, D. L., Silk-based scaffold platform for engineering tissue constructs. In Google Patents: 2018.
108. Form, D.; Pratt, B.; Madri, J., Endothelial cell proliferation during angiogenesis. In vitro modulation by basement membrane components. *Laboratory investigation; a journal of technical methods and pathology* **1986,** 55, (5), 521-530.
109. Grant, D.; Kibbey, M.; Kinsella, J.; Cid, M.; Kleinman, H., The role of basement membrane in angiogenesis and tumor growth. *Pathology-Research and Practice* **1994,** 190, (9-10), 854-863.
110. Zhang, J.; Hernandez-Gordillo, V.; Trapecar, M.; Wright, C.; Taketani, M.; Schneider, K.; Chen, W. L. K.; Stas, E.; Breault, D. T.; Carrier, R. L., Coculture of primary human colon monolayer with human gut bacteria. *Nature Protocols* **2021,** 16, (8), 3874-3900.
111. Le Visage, C.; Dunham, B.; Flint, P.; Leong, K. W., Coculture of mesenchymal stem cells and respiratory epithelial cells to engineer a human composite respiratory mucosa. *Tissue engineering* **2004,** 10, (9-10), 1426-1435.

112. Gonzales, G. B.; Van Camp, J.; Vissenaekens, H.; Raes, K.; Smagghe, G.; Grootaert, C., Review on the Use of Cell Cultures to Study Metabolism, Transport, and Accumulation of Flavonoids: From Mono-Cultures to Co-Culture Systems. *Comprehensive reviews in food science and food safety* **2015,** 14, (6), 741-754.
113. Chang, Y.-H.; Kumar, V. B.; Wen, Y.-T.; Huang, C.-Y.; Tsai, R.-K.; Ding, D.-C., Induction of Human Umbilical Mesenchymal Stem Cell Differentiation Into Retinal Pigment Epithelial Cells Using a Transwell-Based Co-culture System. *Cell Transplantation* **2022,** 31, 09636897221085901.
114. Demircan, P. C.; Sariboyaci, A. E.; Unal, Z. S.; Gacar, G.; Subasi, C.; Karaoz, E., Immunoregulatory effects of human dental pulp-derived stem cells on T cells: comparison of transwell co-culture and mixed lymphocyte reaction systems. *Cytotherapy* **2011,** 13, (10), 1205-1220.
115. Rennert, K.; Steinborn, S.; Gröger, M.; Ungerböck, B.; Jank, A.-M.; Ehgartner, J.; Nietzsche, S.; Dinger, J.; Kiehntopf, M.; Funke, H., A microfluidically perfused three dimensional human liver model. *Biomaterials* **2015,** 71, 119-131.
116. Ramadan, Q.; Jing, L., Characterization of tight junction disruption and immune response modulation in a miniaturized Caco-2/U937 coculture-based in vitro model of the human intestinal barrier. *Biomedical microdevices* **2016,** 18, (1), 1-9.
117. Richardson, L.; Kim, S.; Menon, R.; Han, A., Organ-on-chip technology: the future of feto-maternal interface research? *Frontiers in Physiology* **2020,** 11, 715.
118. Yang, H.; Borg, T. K.; Ma, Z.; Xu, M.; Wetzel, G.; Saraf, L. V.; Markwald, R.; Runyan, R. B.; Gao, B. Z., Biochip-based study of unidirectional mitochondrial transfer from stem cells to myocytes via tunneling nanotubes. *Biofabrication* **2016,** 8, (1), 015012.
119. Neto, E.; Alves, C. J.; Sousa, D. M.; Alencastre, I. S.; Lourenço, A. H.; Leitão, L.; Ryu, H. R.; Jeon, N. L.; Fernandes, R.; Aguiar, P., Sensory neurons and osteoblasts: close partners in a microfluidic platform. *Integrative Biology* **2014,** 6, (6), 586-595.
120. Jeon, J. S.; Bersini, S.; Whisler, J. A.; Chen, M. B.; Dubini, G.; Charest, J. L.; Moretti, M.; Kamm, R. D., Generation of 3D functional microvascular networks with human mesenchymal stem cells in microfluidic systems. *Integrative Biology* **2014,** 6, (5), 555-563.
121. Siddique, A.; Meckel, T.; Stark, R. W.; Narayan, S., Improved cell adhesion under shear stress in PDMS microfluidic devices. *Colloids and Surfaces B: Biointerfaces* **2017,** 150, 456-464.
122. Zervantonakis, I. K.; Hughes-Alford, S. K.; Charest, J. L.; Condeelis, J. S.; Gertler, F. B.; Kamm, R. D., Three-dimensional microfluidic model for tumor cell intravasation and endothelial barrier function. *Proceedings of the National Academy of Sciences* **2012,** 109, (34), 13515-13520.
123. Bersini, S.; Jeon, J. S.; Dubini, G.; Arrigoni, C.; Chung, S.; Charest, J. L.; Moretti, M.; Kamm, R. D., A microfluidic 3D in vitro model for specificity of breast cancer metastasis to bone. *Biomaterials* **2014,** 35, (8), 2454-2461.
124. Ahn, C. B.; Son, K. H.; Yu, Y. S.; Kim, T. H.; Lee, J. I.; Lee, J. W., Development of a flexible 3D printed scaffold with a cell-adhesive surface for artificial trachea. *Biomedical Materials* **2019,** 14, (5), 055001.
125. Wong, K. H.; Chan, J. M.; Kamm, R. D.; Tien, J., Microfluidic models of vascular functions. *Annual review of biomedical engineering* **2012,** 14, (1), 205-230.

126. Lee, N.; Park, J. W.; Kim, H. J.; Yeon, J. H.; Kwon, J.; Ko, J. J.; Oh, S.-H.; Kim, H. S.; Kim, A.; Han, B. S., Monitoring the differentiation and migration patterns of neural cells derived from human embryonic stem cells using a microfluidic culture system. *Molecules and cells* **2014,** 37, (6), 497.
127. Ahn, J.; Lim, J.; Jusoh, N.; Lee, J.; Park, T.-E.; Kim, Y.; Kim, J.; Jeon, N. L., 3D microfluidic bone tumor microenvironment comprised of hydroxyapatite/fibrin composite. *Frontiers in bioengineering and biotechnology* **2019**, 168.
128. Pins, G. D.; Toner, M.; MORGAN, J. R., Microfabrication of an analog of the basal lamina: biocompatible membranes with complex topographies. *the FASEB Journal* **2000,** 14, (3), 593-602.
129. Downing, B. R.; Cornwell, K.; Toner, M.; Pins, G. D., The influence of microtextured basal lamina analog topography on keratinocyte function and epidermal organization. *Journal of Biomedical Materials Research Part A: An Official Journal of The Society for Biomaterials, The Japanese Society for Biomaterials, and The Australian Society for Biomaterials and the Korean Society for Biomaterials* **2005,** 72, (1), 47-56.
130. Lammers, G.; Roth, G.; Heck, M.; Zengerle, R.; Tjabringa, G. S.; Versteeg, E. M.; Hafmans, T.; Wismans, R.; Reinhardt, D. P.; Verwiel, E. T., Construction of a microstructured collagen membrane mimicking the papillary dermis architecture and guiding keratinocyte morphology and gene expression. *Macromolecular bioscience* **2012,** 12, (5), 675-691.
131. Klassen, C. C., Thin film interposition of basement membrane scaffolds. In Google Patents: 2019.
132. Tozzi, L.; Laurent, P.-A.; Di Buduo, C. A.; Mu, X.; Massaro, A.; Bretherton, R.; Stoppel, W.; Kaplan, D. L.; Balduini, A., Multi-channel silk sponge mimicking bone marrow vascular niche for platelet production. *Biomaterials* **2018,** 178, 122-133.
133. Di Buduo, C. A.; Wray, L. S.; Tozzi, L.; Malara, A.; Chen, Y.; Ghezzi, C. E.; Smoot, D.; Sfara, C.; Antonelli, A.; Spedden, E., Programmable 3D silk bone marrow niche for platelet generation ex vivo and modeling of megakaryopoiesis pathologies. *Blood, The Journal of the American Society of Hematology* **2015,** 125, (14), 2254-2264.
134. Frueh, F. S.; Menger, M. D.; Lindenblatt, N.; Giovanoli, P.; Laschke, M. W., Current and emerging vascularization strategies in skin tissue engineering. *Critical reviews in biotechnology* **2016**.
135. Naughton, G. K.; Mansbridge, J. N., Human-based tissue-engineered implants for plastic and reconstructive surgery. *Clinics in plastic surgery* **1999,** 26, (4), 579-586.
136. Santos, M. I.; Reis, R. L., Vascularization in bone tissue engineering: physiology, current strategies, major hurdles and future challenges. *Macromolecular bioscience* **2010,** 10, (1), 12-27.
137. Rouwkema, J.; Khademhosseini, A., Vascularization and angiogenesis in tissue engineering: beyond creating static networks. *Trends in biotechnology* **2016,** 34, (9), 733-745.
138. Zhang, X.; Karim, M.; Hasan, M. M.; Hooper, J.; Wahab, R.; Roy, S.; Al-Hilal, T. A., Cancer-on-a-Chip: Models for Studying Metastasis. *Cancers* **2022,** 14, (3), 648.
139. Ghanaati, S.; Unger, R. E.; Webber, M. J.; Barbeck, M.; Orth, C.; Kirkpatrick, J. A.; Booms, P.; Motta, A.; Migliaresi, C.; Sader, R. A., Scaffold vascularization in vivo driven by primary human osteoblasts in concert with host inflammatory cells. *Biomaterials* **2011,** 32, (32), 8150-8160.

140. LiáJeon, N., Microfluidic vascularized bone tissue model with hydroxyapatite-incorporated extracellular matrix. *Lab on a Chip* **2015,** 15, (20), 3984-3988.
141. Chan, E. C.; Kuo, S.-M.; Kong, A. M.; Morrison, W. A.; Dusting, G. J.; Mitchell, G. M.; Lim, S. Y.; Liu, G.-S., Three dimensional collagen scaffold promotes intrinsic vascularisation for tissue engineering applications. *PloS one* **2016,** 11, (2), e0149799.
142. Min, S.; Cleveland, D.; Ko, I. K.; Kim, J. H.; Yang, H. J.; Atala, A.; Yoo, J. J., Accelerating neovascularization and kidney tissue formation with a 3D vascular scaffold capturing native vascular structure. *Acta Biomaterialia* **2021,** 124, 233-243.
143. Bischel, L. L.; Young, E. W.; Mader, B. R.; Beebe, D. J., Tubeless microfluidic angiogenesis assay with three-dimensional endothelial-lined microvessels. *Biomaterials* **2013,** 34, (5), 1471-1477.
144. Li, T.; Peng, M.; Yang, Z.; Zhou, X.; Deng, Y.; Jiang, C.; Xiao, M.; Wang, J., 3D-printed IFN-γ-loading calcium silicate-β-tricalcium phosphate scaffold sequentially activates M1 and M2 polarization of macrophages to promote vascularization of tissue engineering bone. *Acta biomaterialia* **2018,** 71, 96-107.
145. Liu, L. X.; Lu, H.; Luo, Y.; Date, T.; Belanger, A. J.; Vincent, K. A.; Akita, G. Y.; Goldberg, M.; Cheng, S. H.; Gregory, R. J., Stabilization of vascular endothelial growth factor mRNA by hypoxia-inducible factor 1. *Biochemical and biophysical research communications* **2002,** 291, (4), 908-914.
146. Xie, A. W.; Murphy, W. L., Engineered biomaterials to mitigate growth factor cost in cell biomanufacturing. *Current Opinion in Biomedical Engineering* **2019,** 10, 1-10.
147. Damon, D. H.; Lobb, R. R.; D'Amore, P. A.; Wagner, J. A., Heparin potentiates the action of acidic fibroblast growth factor by prolonging its biological half-life. *Journal of cellular physiology* **1989,** 138, (2), 221-226.
148. Oka, N.; Soeda, A.; Inagaki, A.; Onodera, M.; Maruyama, H.; Hara, A.; Kunisada, T.; Mori, H.; Iwama, T., VEGF promotes tumorigenesis and angiogenesis of human glioblastoma stem cells. *Biochemical and biophysical research communications* **2007,** 360, (3), 553-559.
149. Schmitt, T.; Kajave, N.; Cai, H. H.; Gu, L.; Albanna, M.; Kishore, V., In vitro characterization of xeno-free clinically relevant human collagen and its applicability in cell-laden 3D bioprinting. *Journal of Biomaterials Applications* **2021,** 35, (8), 912-923.
150. Pagella, P.; Neto, E.; Lamghari, M.; Mitsiadis, T. A., Investigation of orofacial stem cell niches and their innervation through microfluidic devices. *European Cells and Materials (ECM)* **2015,** 29, 213-23.
151. Wevers, N. R.; van Vught, R.; Wilschut, K. J.; Nicolas, A.; Chiang, C.; Lanz, H. L.; Trietsch, S. J.; Joore, J.; Vulto, P., High-throughput compound evaluation on 3D networks of neurons and glia in a microfluidic platform. *Scientific reports* **2016,** 6, (1), 1-10.
152. Millet, L. J.; Gillette, M. U., New perspectives on neuronal development via microfluidic environments. *Trends in neurosciences* **2012,** 35, (12), 752-761.
153. Borenstein, J. T.; Charest, J. L.; Jeon, J. S.; Kamm, R. D.; Chung, S.; Zervantonakis, I.; Vickerman, V., Three-dimensional microfluidic platforms and methods of use and manufacture thereof. In Google Patents: 2011.
154. G., P. J. B.; P., B. R. J. Cell Culture Device. WO2012104087A2.
155. Daniele, M.; Young, A. T., Two-dimensional (2d) models of tissue barriers, methods of making and using the same. In Google Patents: 2021.

156. Vacanti, J. P.; Borenstein, J. T.; Weinberg, E. Microfabricated compositions and processes for engineering tissues containing multiple cell types. US 7,960,166 B2, 2011.
157. Kamm, R. D.; Chung, S.; Vickerman-Kelley, V. V., Three-dimensional microfluidic platforms and methods of use thereof. In Google Patents: 2015.
158. Kamm, R. D.; Asada, H. H.; Farahat, W. A.; Zervantonakis, I. K.; Wood, L. B.; Kothapalli, C.; Chung, S.; Macklis, J. D.; Tharin, S.; Varner, J., Device for high throughput investigations of multi-cellular interactions. In Google Patents: 2016.
159. Zhang, W.; Choi, D. S.; Nguyen, Y. H.; Chang, J.; Qin, L., Studying cancer stem cell dynamics on PDMS surfaces for microfluidics device design. *Scientific reports* **2013,** 3, (1), 1-8.
160. Liu, Y.; Sun, S.; Singha, S.; Cho, M. R.; Gordon, R. J., 3D femtosecond laser patterning of collagen for directed cell attachment. *Biomaterials* **2005,** 26, (22), 4597-4605.
161. Fang, Y.; Zhang, T.; Zhang, L.; Gong, W.; Sun, W., Biomimetic design and fabrication of scaffolds integrating oriented micro-pores with branched channel networks for myocardial tissue engineering. *Biofabrication* **2019,** 11, (3), 035004.
162. Golden, A. P.; Tien, J., Fabrication of microfluidic hydrogels using molded gelatin as a sacrificial element. *Lab on a Chip* **2007,** 7, (6), 720-725.
163. Yeong, W. Y.; Chua, C. K.; Leong, K. F.; Chandrasekaran, M.; Lee, M. W., Comparison of drying methods in the fabrication of collagen scaffold via indirect rapid prototyping. *Journal of Biomedical Materials Research Part B: Applied Biomaterials* **2007,** 82, (1), 260-266.
164. Rieu, C.; Parisi, C.; Mosser, G.; Haye, B.; Coradin, T.; Fernandes, F. M.; Trichet, L., Topotactic fibrillogenesis of freeze-cast microridged collagen scaffolds for 3D cell culture. *ACS applied materials & interfaces* **2019,** 11, (16), 14672-14683.
165. Jiménez-Torres, J. A.; Peery, S. L.; Sung, K. E.; Beebe, D. J., LumeNEXT: a practical method to pattern luminal structures in ECM gels. *Advanced healthcare materials* **2016,** 5, (2), 198-204.
166. Mansoorifar, A.; Subbiah, R.; de Souza Balbinot, G.; Parthiban, S. P.; Bertassoni, L. E., Embedding cells within nanoscale, rapidly mineralizing hydrogels: A new paradigm to engineer cell-laden bone-like tissue. *Journal of Structural Biology* **2020,** 212, (3), 107636.
167. Hribar, K. C.; Meggs, K.; Liu, J.; Zhu, W.; Qu, X.; Chen, S., Three-dimensional direct cell patterning in collagen hydrogels with near-infrared femtosecond laser. *Scientific reports* **2015,** 5, (1), 1-7.
168. Rnjak-Kovacina, J.; Gerrand, Y. w.; Wray, L. S.; Tan, B.; Joukhdar, H.; Kaplan, D. L.; Morrison, W. A.; Mitchell, G. M., Vascular pedicle and microchannels: simple methods toward effective in vivo vascularization of 3D scaffolds. *Advanced Healthcare Materials* **2019,** 8, (24), 1901106.
169. Kotha, S. S.; Hayes, B. J.; Phong, K. T.; Redd, M. A.; Bomsztyk, K.; Ramakrishnan, A.; Torok-Storb, B.; Zheng, Y., Engineering a multicellular vascular niche to model hematopoietic cell trafficking. *Stem cell research & therapy* **2018,** 9, (1), 1-14.
170. Deng, K.; Liu, Z.; Luo, F.; Xie, R.; He, X.-H.; Jiang, M.-Y.; Ju, X.-J.; Wang, W.; Chu, L.-Y., Controllable fabrication of polyethersulfone hollow fiber membranes with a facile double co-axial microfluidic device. *Journal of Membrane Science* **2017,** 526, 9-17.
171. Iijima, K.; Ichikawa, S.; Ishikawa, S.; Matsukuma, D.; Yataka, Y.; Otsuka, H.; Hashizume, M., Preparation of Cell-Paved and-Incorporated Polysaccharide Hollow Fibers

Using a Microfluidic Device. *ACS Biomaterials Science & Engineering* **2019,** 5, (11), 5688-5697.
172. Dikici, S.; Claeyssens, F.; MacNeil, S., Bioengineering vascular networks to study angiogenesis and vascularization of physiologically relevant tissue models in vitro. *ACS Biomaterials Science & Engineering* **2020,** 6, (6), 3513-3528.
173. Bettinger, C. J.; Cyr, K. M.; Matsumoto, A.; Langer, R.; Borenstein, J. T.; Kaplan, D. L., Silk fibroin microfluidic devices. *Advanced Materials* **2007,** 19, (19), 2847-2850.
174. Hölzl, K.; Lin, S.; Tytgat, L.; Van Vlierberghe, S.; Gu, L.; Ovsianikov, A., Bioink properties before, during and after 3D bioprinting. *Biofabrication* **2016,** 8, (3), 032002.
175. Wenz, A.; Borchers, K.; Tovar, G. E.; Kluger, P. J., Bone matrix production in hydroxyapatite-modified hydrogels suitable for bone bioprinting. *Biofabrication* **2017,** 9, (4), 044103.
176. Cui, X.; Boland, T., Human microvasculature fabrication using thermal inkjet printing technology. *Biomaterials* **2009,** 30, (31), 6221-6227.
177. Shim, K.-Y.; Lee, D.; Han, J.; Nguyen, N.-T.; Park, S.; Sung, J. H., Microfluidic gut-on-a-chip with three-dimensional villi structure. *Biomedical microdevices* **2017,** 19, (2), 1-10.
178. Suzuki, A.; Kato, H.; Kawakami, T.; Kodama, Y.; Shiozawa, M.; Kuwae, H.; Miwa, K.; Hoshikawa, E.; Haga, K.; Shiomi, A., Development of microstructured fish scale collagen scaffolds to manufacture a tissue-engineered oral mucosa equivalent. *Journal of Biomaterials Science, Polymer Edition* **2020,** 31, (5), 578-600.
179. Jonelle, Z. Y.; Korkmaz, E.; Berg, M. I.; LeDuc, P. R.; Ozdoganlar, O. B., Biomimetic scaffolds with three-dimensional undulated microtopographies. *Biomaterials* **2017,** 128, 109-120.
180. Bush, K. A.; Pins, G. D., Development of microfabricated dermal epidermal regenerative matrices to evaluate the role of cellular microenvironments on epidermal morphogenesis. *Tissue engineering Part A* **2012,** 18, (21-22), 2343-2353.
181. Chen, S.; Nakamoto, T.; Kawazoe, N.; Chen, G., Engineering multi-layered skeletal muscle tissue by using 3D microgrooved collagen scaffolds. *Biomaterials* **2015,** 73, 23-31.
182. Price, G. M.; Chu, K. K.; Truslow, J. G.; Tang-Schomer, M. D.; Golden, A. P.; Mertz, J.; Tien, J., Bonding of macromolecular hydrogels using perturbants. *Journal of the American Chemical Society* **2008,** 130, (21), 6664-6665.
183. Kelman, C. D.; DeVore, D. P., Collagen-based adhesives and sealants and methods of preparation and use thereof. In Google Patents: 1993.
184. Kew, S.; Mead, T.; Rushton, N., Collagen gel for bonding porous collagen-based materials with non-porous collagen-based materials. In Google Patents: 2016.
185. Yannas, I. V.; Harley, B.; Zagorski, C. J.; Reddy, H. K., Gradient Template for Angiogensis During Large Organ Regeneration. In Google Patents: 2010.
186. Rabbani, A.; Salehi, S., Dynamic modeling of the formation damage and mud cake deposition using filtration theories coupled with SEM image processing. *Journal of Natural Gas Science and Engineering* **2017,** 42, 157-168.
187. Moore Jr, J. E.; Maier, S. E.; Ku, D. N.; Boesiger, P., Hemodynamics in the abdominal aorta: a comparison of in vitro and in vivo measurements. *Journal of Applied Physiology* **1994,** 76, (4), 1520-1527.

188. Faraj, K. A.; Van Kuppevelt, T. H.; Daamen, W. F., Construction of collagen scaffolds that mimic the three-dimensional architecture of specific tissues. *Tissue engineering* **2007,** 13, (10), 2387-2394.
189. Bružauskaitė, I.; Bironaitė, D.; Bagdonas, E.; Bernotienė, E., Scaffolds and cells for tissue regeneration: different scaffold pore sizes—different cell effects. *Cytotechnology* **2016,** 68, (3), 355-369.
190. Wahl, D. A.; Sachlos, E.; Liu, C.; Czernuszka, J. T., Controlling the processing of collagen-hydroxyapatite scaffolds for bone tissue engineering. *Journal of Materials Science: Materials in Medicine* **2007,** 18, (2), 201-209.
191. Bose, S.; Li, S.; Mele, E.; Silberschmidt, V. V., Dry vs. wet: Properties and performance of collagen films. Part I. Mechanical behaviour and strain-rate effect. *Journal of the Mechanical Behavior of Biomedical Materials* **2020,** 111, 103983.
192. Ryan, A. J.; O'Brien, F. J., Insoluble elastin reduces collagen scaffold stiffness, improves viscoelastic properties, and induces a contractile phenotype in smooth muscle cells. *Biomaterials* **2015,** 73, 296-307.
193. Ferrara, M.; Lugano, G.; Sandinha, M. T.; Kearns, V. R.; Geraghty, B.; Steel, D. H., Biomechanical properties of retina and choroid: a comprehensive review of techniques and translational relevance. *Eye* **2021,** 35, (7), 1818-1832.
194. Varley, M.; Neelakantan, S.; Clyne, T.; Dean, J.; Brooks, R.; Markaki, A., Cell structure, stiffness and permeability of freeze-dried collagen scaffolds in dry and hydrated states. *Acta biomaterialia* **2016,** 33, 166-175.
195. Liu, C.-K.; Latona, N.; Taylor, M.; Aldema-Ramos, M., Biobased films prepared from collagen solutions derived from un-tanned hides. *Journal of the American Leather Chemists Association* **2015,** 110, (02), 25-32.
196. Wolf, K.; Sobral, P.; Telis, V., Physicochemical characterization of collagen fibers and collagen powder for self-composite film production. *Food Hydrocolloids* **2009,** 23, (7), 1886-1894.
197. Welling, L. W.; Zupka, M. T.; Welling, D. J., Mechanical properties of basement membrane. *Physiology* **1995,** 10, (1), 30-35.
198. Aizawa, M.; Nakamura, H.; Matsumoto, K.; Oguma, T.; Shishido, A., Oriented collagen films with high Young's modulus by self-assembly on micrometer grooved polydimethylsiloxane. *Materials Advances* **2021,** 2, (21), 6984-6987.
199. Chen, X.; Zhou, L.; Xu, H.; Yamamoto, M.; Shinoda, M.; Kishimoto, M.; Tanaka, T.; Yamane, H., Effect of the Application of a Dehydrothermal Treatment on the Structure and the Mechanical Properties of Collagen Film. *Materials* **2020,** 13, (2), 377.
200. Lucotte, B. M.; Powell, C.; Knutson, J. R.; Combs, C. A.; Malide, D.; Yu, Z.-X.; Knepper, M.; Patel, K. D.; Pielach, A.; Johnson, E., Direct visualization of the arterial wall water permeability barrier using CARS microscopy. *Proceedings of the National Academy of Sciences* **2017,** 114, (18), 4805-4810.
201. Sachlos, E.; Reis, N.; Ainsley, C.; Derby, B.; Czernuszka, J., Novel collagen scaffolds with predefined internal morphology made by solid freeform fabrication. *Biomaterials* **2003,** 24, (8), 1487-1497.
202. Jayalalitha, G.; Deviha, V. S.; Uthayakumar, R., Fractal model for blood flow in cardiovascular system. *Computers in Biology and Medicine* **2008,** 38, (6), 684-693.

203. Ostadfar, A., Chapter 3—Macrocirculation System. *In Biofluid Mechanics; Academic Press: Cambridge, MA, USA* **2016**, 87-109.